NASA Technical Memorandum 86219

Research Review—1984

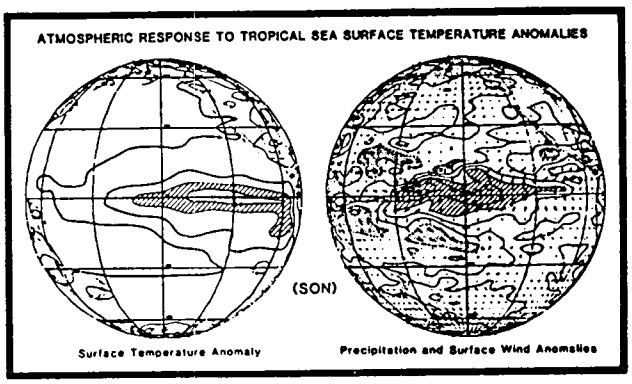

Staff
Global Modeling and Simulation Branch
Laboratory for Atmospheres

FEBRUARY 1986

NASA

NASA Technical Memorandum 86219

Research Review—1984

Staff
Global Modeling and Simulation Branch
Laboratory for Atmospheres
Goddard Space Flight Center
Greenbelt, Maryland

National Aeronautics
and Space Administration

**Scientific and Technical
Information Branch**

1986

TABLE OF CONTENTS

P R E F A C E

The Global Modeling and Simulation Branch (GMSB) of the Laboratory for Atmospheres (GLA) is engaged in general circulation modeling studies related to global atmospheric and oceanographic research. The research activities are organized into two disciplines: Global Weather/Observing Systems and Climate/Ocean-Air Interactions.

During the past year, a very large number of research projects have been completed as indicated by the list of refereed papers included at the end of this publication. The purpose of the review is to present a brief overview of this research, and to document the status of other projects currently underway. In addition, abstracts of the 1984 Summer Lecture Series jointly sponsored by the Global Modeling and Simulation Branch and the University of Maryland are also included.

I. GLOBAL WEATHER/OBSERVING SYSTEMS

A. ANALYSIS AND FORECAST STUDIES

Analysis of Ocean Surface Wind Fields Using Seasat-A Scatterometer Data

E. Kalnay and R. Atlas

In addition to the Seasat forecast impact studies previously conducted with the GLA model, a study was also made of the global analyses of surface wind stress, wind stress curl, and surface sensible and latent heat fluxes, which are generated as a by-product of the assimilation process. Both instantaneous analyses of these quantities and 15-day averages of each of these fields were found to be in good qualitative agreement with published fields.

Examples of Synoptic (Instantaneous) Analyses

Fig. 1 presents the GLA surface wind streamline analysis for 00 GMT 15 September 1978. All the meteorological features described by Peteherych et al. (1984), are also present in the GLA analysis. Among these note the two typhoons off the coast of Japan, southwesterly monsoon flow on the coast of equatorial West Africa and the Indian subcontinent, the cyclones and anticyclones in the Northern and Southern Hemispheres, the strong westerlies that drive the Antartic circumpolar Ocean current, and the trade winds from the Northern and Southern Hemispheres meeting in the ITCZ at about 10°N, and others. In addition, a weak cyclone at 45°N, was detected in the GLA analysis and not in the hand analysis because it is in a region where no SASS data was available due to the SEASAT orbital configuration.

Fig. 2 presents the instantaneous wind stress field for the same date. The most notable feature is the intense stress associated with the enormous Southern Hemisphere-cyclone pointed out by Peteherych et al. and centered at 32°S and 135°W.

15 Day Averaged Surface Wind and Wind Stress Fields

Fig. 3a, b presents a comparison of the long term mean vector surface winds in the GATE area during September adapted by Burpee and Reed (1981), and our GLA analysis surface wind for the 15 day period 6-20 September 1978. There is very good agreement between these fields, with a col at about 10°N and 27°W. West of this col the trade winds converge into the ITCZ which is located at about 10°N. East of the col, the winds are towards the east, converging towards a broad cyclonic circulation located over the maximum surface temperature at about 20°N and 10°W. The cyclone center in our analysis is displaced towards the Greenwich meridian. The mean (vector) wind speeds are also in reasonable agreement, with the larger values in the GLA analysis probably due to the short averaging period.

REFERENCES

Kalnay, E. and R. Atlas, 1985: Global analysis of ocean surface wind and wind stress using the GLAS GCM and Seasat scatterometer winds. Accepted by J. Geophys. Res.

Burpee, R. W. and R. J. Reed, 1981: Chapter 4, "Synoptic Scale Motions". NSF GATE Report.

Peteherych, S., M. G. Wurtele, P. M. Woiceshyn, D. H. Boggs, and R. Atlas, 1984: First global analysis of Seasat scatterometer winds and potential for meteorological research. Frontiers of Remote Sensing of the Oceans and Troposphere from Air and Space Platforms, 575-586.

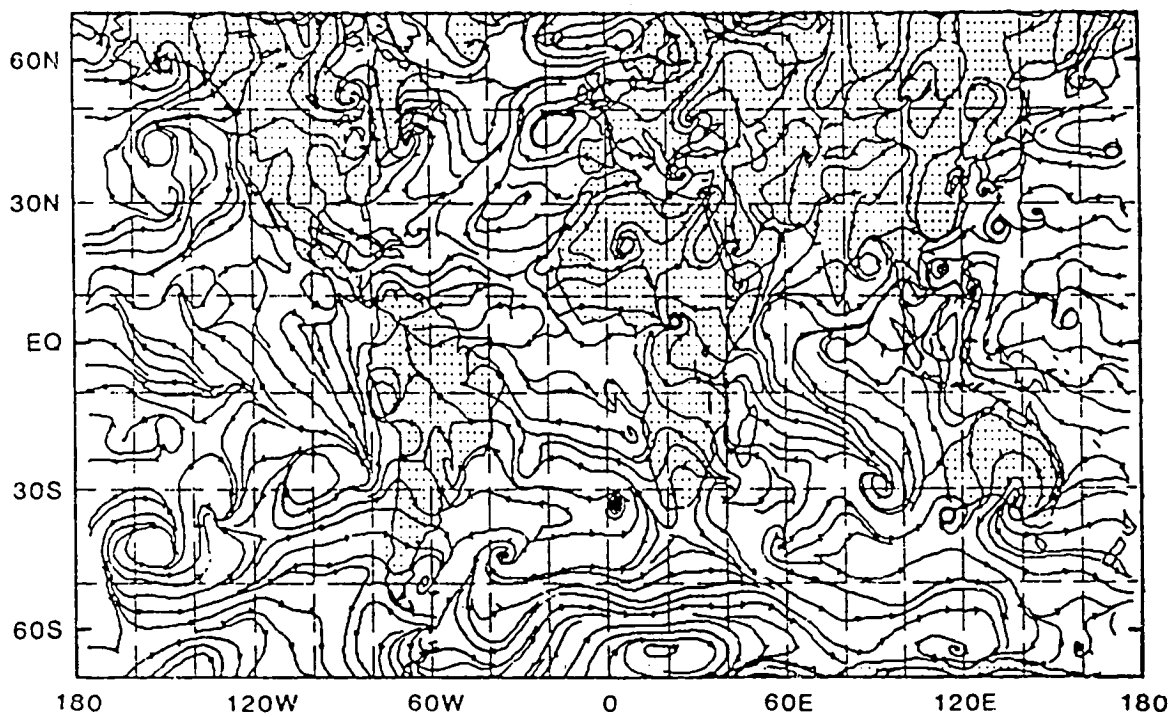

Fig.1 GLA surface streamline analysis for 00 GMT 15 September 1978.

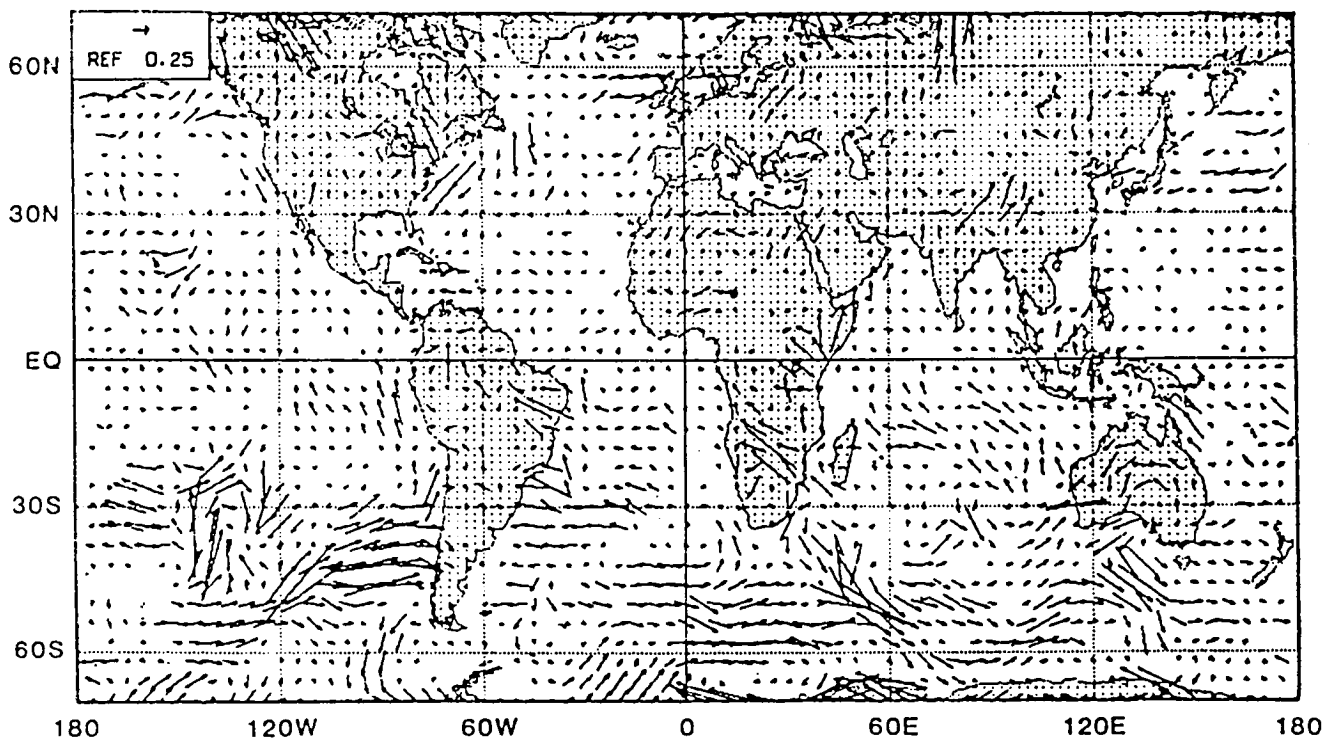

Fig.2 GLA surface wind stress (Nm^{-2}) for 00 GMT 15 September 1978.

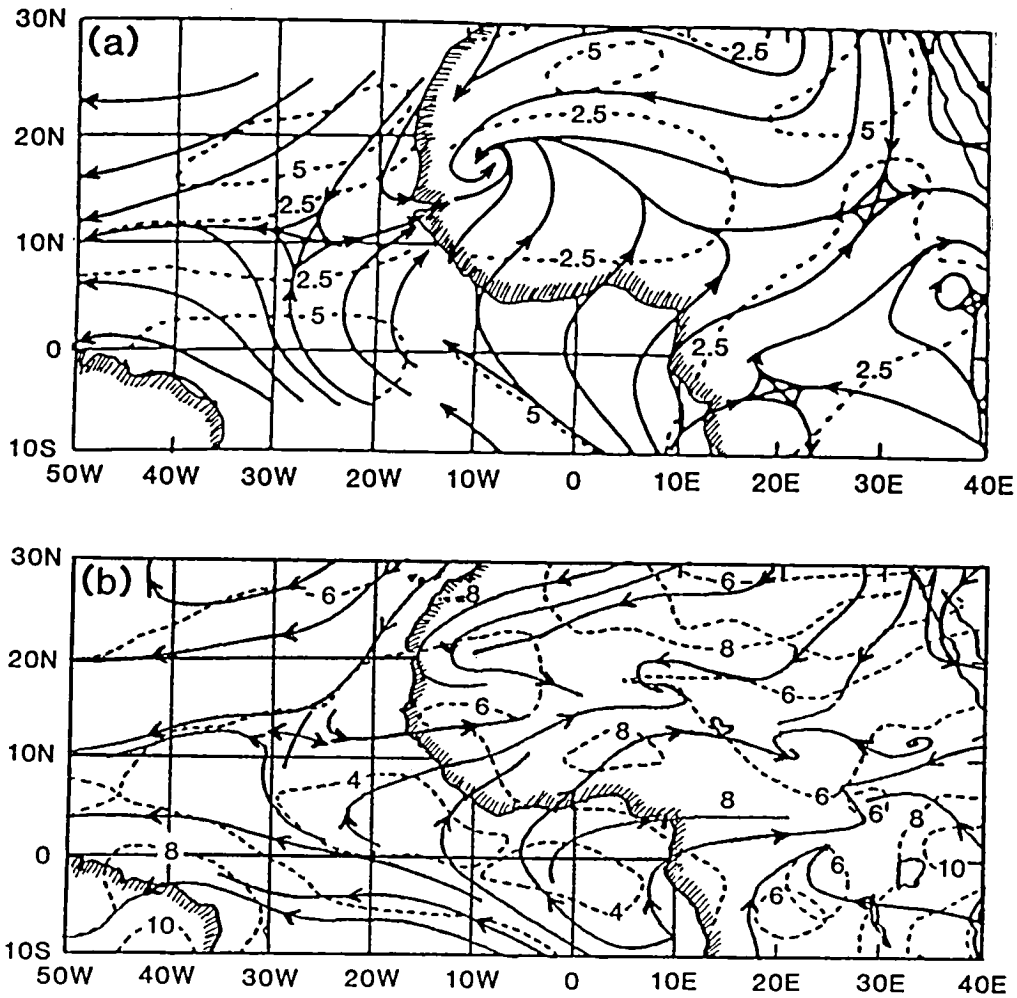

Fig.3 Mean surface winds in the GATE area during September (a) adapted from Burpee and Reed (1981), (b) 15 day average from GLA analyses for 6-20 September 1978.

Forecast Impact Simulation Studies

R. Atlas, E. Kalnay, W. E. Baker, J. Susskind, D. Reuter, and M. Halem
Laboratory for Atmospheres, NASA/Goddard Space Flight Center
Greenbelt, MD 20771

A series of simulation experiments is being conducted as a cooperative effort between the European Centre for Medium Range Weather Forecasts (ECMWF), the National Meteorological Center (NMC) and the Goddard Laboratory for Atmospheres (GLA), to provide a quantitative assessment of the potential impact of proposed observing systems on large scale numerical weather prediction. For these studies an advanced analysis/forecast simulation system has been developed which provides for a more realistic assessment of the impact of proposed observing systems than was possible in earlier studies. This system consists of four elements: 1) An atmospheric model integration to provide a complete record of the "true" state of the atmosphere (called nature). This record is then used to fabricate observational reports and to evaluate analyses and forecasts. 2) A conventional data assimilation cycle that is used as the "control experiment." The control experiment is like an operational analysis/forecast cycle based on conventional observations, except that it makes use of fabricated conventional data obtained from the nature run to produce the analyzed fields. 3) A satellite data assimilation that differs from the control in also including fabricated satellite data incorporated in the forecast-analysis cycle. 4) Forecasts produced from both control and satellite initial conditions. Comparison of these forecasts with nature provides an assessment of the impact of satellite data.

Previous simulation studies have been characterized by the use of the same model to simulate "nature" and observations and to produce forecasts. This "identical twin" problem can distort the conclusions derived from such studies. In the present study, we attempt to avoid these limitations by designing a more realistic simulation system and calibrating its results by comparison with real data experiments performed with a similar system, and by simulating the expected accuracy and characteristics of observational systems. In order to avoid the "identical twin" character of previous studies, the high resolution (1.875° x 1.875° x 15 levels) ECMWF model is used as nature, and the 4° x 5° x 9 level GLAS model is used as the assimilation and forecast model.

For all of the experiments which have been completed to date, the nature run is a twenty-day integration from 0000 GMT 10 November 1979 using the ECMWF model. All types of FGGE and conventional data were simulated by NMC by interpolating the nature fields to observation locations and adding assumed random or systematic errors to the interpolated values. Only satellite temperature soundings were assumed to have systematic errors. LIDAR wind profiles were simulated at the TIROS observational locations with 1-3m sec^{-1} accuracy. Wind profiles were not generated at levels below which the integrated cloud amount exceeded 90%.

Experiments have been conducted to calibrate the simulation system and determine its realism, and to begin to assess the relative impact of temperature and wind profile observing systems. To this end, two real data assimilation cycles, a control (which included only conventional data) and FGGE (which included conventional data plus satellite temperature soundings, cloud-track winds and drifting buoys and were performed for the period 0000 GMT 10 November to 0000 GMT 25 November 1979. Six simulated data assimilation cycles, control, FGGE, control plus TIROS temperature soundings, control plus perfect temperatures, control plus cloud-track winds, and control plus wind profiles were then generated for the same period.

The NMC analysis for 0000 GMT 10 November was used as initial conditions for the real data assimilation cycles. Initial conditions for the simulated data assimilations were provided by a real data control assimilation from 0000 GMT 4 November to 0000 GMT 10 November. Eight five-day forecasts were generated from each assimilation at 48 h intervals beginning on 11 November.

The results from these experiments indicate that 3-dimensional wind profile data are more effective than temperature data in controlling analysis errors. If the proposed accuracies and coverage for LIDAR wind profiles can be achieved, the experiments show that a very significant improvement in Southern Hemisphere forecast skill will result. In the Northern Hemisphere, the impact is smaller but still significant: a case study showed a major improvement in the prediciton of a storm over the United States, which was poorly forecasted with the simulated current system. The use of either perfect temperature soundings or wind profile data resulted in an improved cyclone forecast.

Further experiments with this system will be used to assess the degree of forecast improvement that might result from different configurations of Lidar observing systems. Improved methods for assimilating future observations will also be studied with the simulation system.

The Impact of Scatterometer Data on Limited-Area Model Predictions of the QE II Storm

D. Duffy and R. Atlas

Experiments have been conducted to assess the impact of Seasat-A scatterometer (SASS) data on high resolution model predictions of the QEII storm and to explore different approaches for utilizing SASS data. For all of the experiments, the model used is the limited-area model described by Duffy (1981) with a horizontal resolution of 100 km.

Numerical weather forecasts were made from initial conditions which included and excluded SASS data. The initial condition for the control run was the global analysis from the National Meteorological Center (NMC) which we had archived at the resolution of 4° latitude and 5° longitude. This field was bilinearly interpolated to the model's 100 km by 100 km grid. For the SASS experiments, the 1000 mb winds were replaced by subjectively dealiased SASS winds wherever they were available. Furthermore, SASS winds were allowed to influence the upper-level winds through the use of a vertical correlation function (Yu and McPherson (1984)). If the upper-level winds were not modified, the effects from the upper levels soon overwhelmed the corrections that we had made at the surface.

In Fig. 1, we present the sea-level pressure and 1000-500 mb thickness at the initial time of the experiments, 12 GMT 9 September 1978. We were primarily interested in the evolution of the nascent low located just off Nova Scotia.

The results from the two different numerical forecasts are presented in Figs. 2 and 3. In both cases the low located just off Nova Scotia has moved out into the open waters of the North Atlantic Ocean. In the case of the control, the low has intensified only slightly. The central pressure contour at 36 hrs is 1000 mb with peak winds of 21 m/sec. These results are slightly better than those given by the operational limited-area, fine-mesh model run at the NMC and the Navy's operational model.

From Fig. 3 we see that the inclusion of SEASAT data has had a dramatic effect on the cyclogenesis. The central pressure contour at 36 h is now 988 mb and the peak winds are 37 m/sec. A study of the results indicates that the deepening of the low occurs because of larger amounts of convective precipitation in the SEASAT experiment than the control.

In Fig. 4 we show the observed NMC hand analysis of the QEII, valid at 00 GMT 11 September 1978. From this figure we see that the forecast with SEASAT data is closer to the observed storm than the control. However, there is still a considerable position error.

These results show that scatterometer data can be important in defining the initial conditions that result in rapid maritime cyclogenesis. Currently, work is under way to determine improved ways to couple the surface winds to the upper levels in global atmospheric models.

References

Duffy, D., 1981: A split explicit reformation on the regional numerical weather prediction model of the Japan Meteorological Agency. Mon. Wea. Rev., 109, 931-945.

Yu, T.-W., and R. D. McPherson, 1984: Global data assimilaion experiments with scatterometer winds from SEASAT-A. Mon. Wea Rev., 112, 368-376.

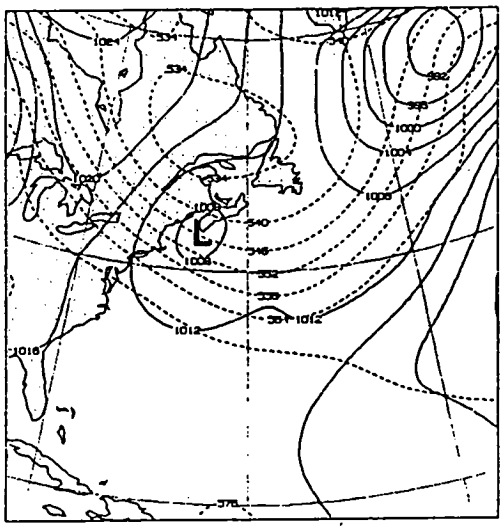

Fig. 1. The initial sea-level pressure and 1000-500 thickness (dashed lines) for 12 UT 9 September 1978.

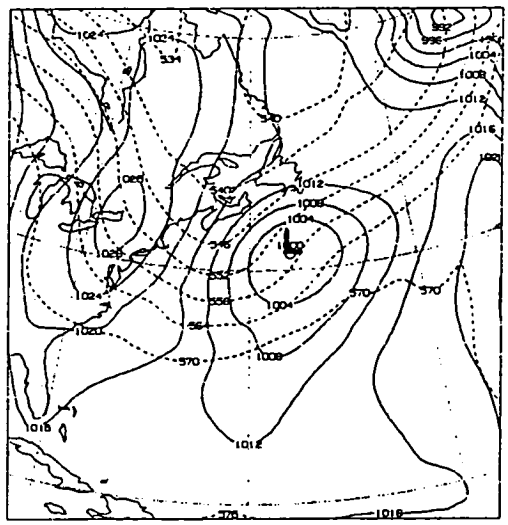

Fig. 2. The 36 h predicted sea-level and 1000-500 thickness (dashed lines) field for the control experiment.

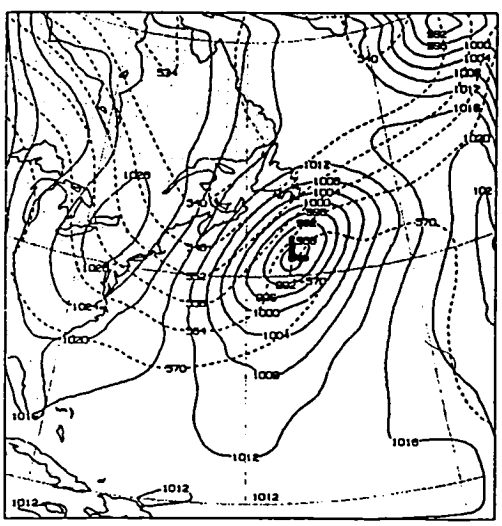

Fig. 3. Same as Fig. 2 except for SEASAT experiment.

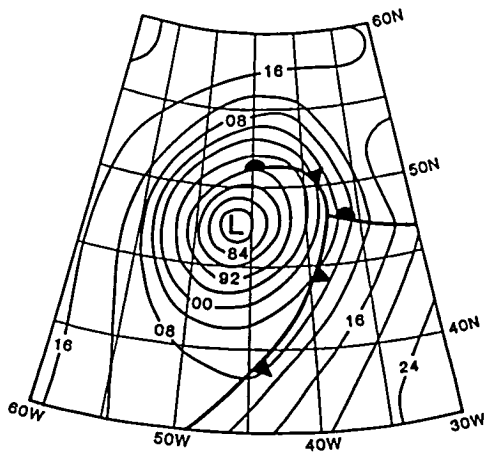

Fig. 4. NMC hand analysis of the QEII storm at 00 UT 11 September 1978.

Objective Determination of Heat Wave Patterns

N. Wolfson and R. Atlas

A simple index was developed in order to objectively characterize a heat wave pattern in either analyses or forecasts of 500 mb height. 500 mb height was chosen because this parameter is usually among the most accurate fields predicted by numerical models. In addition, it is highly correlated with the surface air temperature on many time scales.

The heat index IN is designed to be applied to any region of interest and to be used for any objectively analyzed data and specifically those of NWP models. IN is given by

$$IN = \frac{1}{S \cdot T} \int_T \int_S H_{500}(\ell,t) - \overline{H}_{500}(\ell)\, ds\, dt \qquad (1)$$

where H_{500} is the 500 mb height

$\overline{H}_{500}$ is the 500 mb climatological value of H_{500}
ℓ, t are location and time
ds is an area element (represented by a grid box for an NWP model)
S is the total area of interest
T is the period under study

The index can be calculated for any time period, day, month or season with usage of the corresponding $\overline{H}_{500}(\ell)$. It can be used to study results of NWP models by substituting forecasted values of $H_{500}(\ell,t)$ into (1) or to diagnose observations by using objectively analyzed values of $H_{500}(\ell,t)$.

In formulating the index, it was assumed that point values of height are representative of field values in an area element. The height field spatial autocorrelations at 500 mb are very high for distances of ~ 250 km (Buell, 1972). Thus for the distances involved here, within an area element, point values can be considered to be highly representative for the areas involved.

The first integration over the area transfers the local anomalies to an areal measure. It enables the determination of whether a distinct geographical region is experiencing a heat wave or whether there is simply a local event. The second integration in time assesses the temporal average anomaly of the event.

To evaluate the seasonal representiveness of the index for the summer season, June-September seasonal values for the years 1963-1977 were correlated with average seasonal temperatures for the northern and southern Plains of the U.S. The index was calculated from the U.S. National Meteorological Center (NMC) 500 mb analysis after interpolation to the GLA grid. Average seasonal temperatures were calculated by averaging monthly average temperature which were taken from U.S. Dept. of Commerce (1981). The correlation coefficients were .85 and .82 for the North and South Plains respectively.

Figure 1, which presents the daily variation of the heat wave index for the North and South Plains, clearly shows the different nature of the heat wave in these two regions. The horizontal lines are the seasonal threshold values, i.e. higher values indicate a heat wave. The heat wave in the southern plains was rather continuous with short breaks, the northern plains experienced numerous spells of hot weather which were shorter than the southern spells.

As the area integral in (1) is reduced to one grid point one obtains the measure for the local heat wave. A grid point by grid point calculation of monthly values enables the monitoring of the local monthly variability. In order to assess the severity of the heat wave at a local grid point ℓ a "t" measure has been applied thus

$$t(\ell) = \frac{IN(\ell)}{\sigma_E(\ell)} \qquad (2)$$

where $IN(\ell)$ is the monthly index at location ℓ.
σ_E is the monthly standard error of IN.

IN and σ_E are calculated from the same data, which can be observations or forecasts. As both are in meters $t(\ell)$ is dimensionless.

The numerator in (2) gives the temporal average anomaly. This information is not enough to decide whether the heat wave was characterized by a series of events with high anomalous values with frequent in between breaks or by a persistant anomaly with no breaks. Dividing by the standard error allows us to give weight to the heat wave character (small standard errors are indicative of persistant $H(\ell,t) - H(\ell,t)$ values during the time perids under consideration).

This concept is close to the "t" student test checking the null hypothesis that $IN(\ell)$ equals zero. Interpretations of $t(\ell)$ as "t" student test values is very complicated due to the difficulties in determining the effective number of degrees of freedom and other statistical constraints. However, it is obvious that higher $t(\ell)$ values are indicative of a stronger heat wave as a combination of the two factors of intensity and persistence.

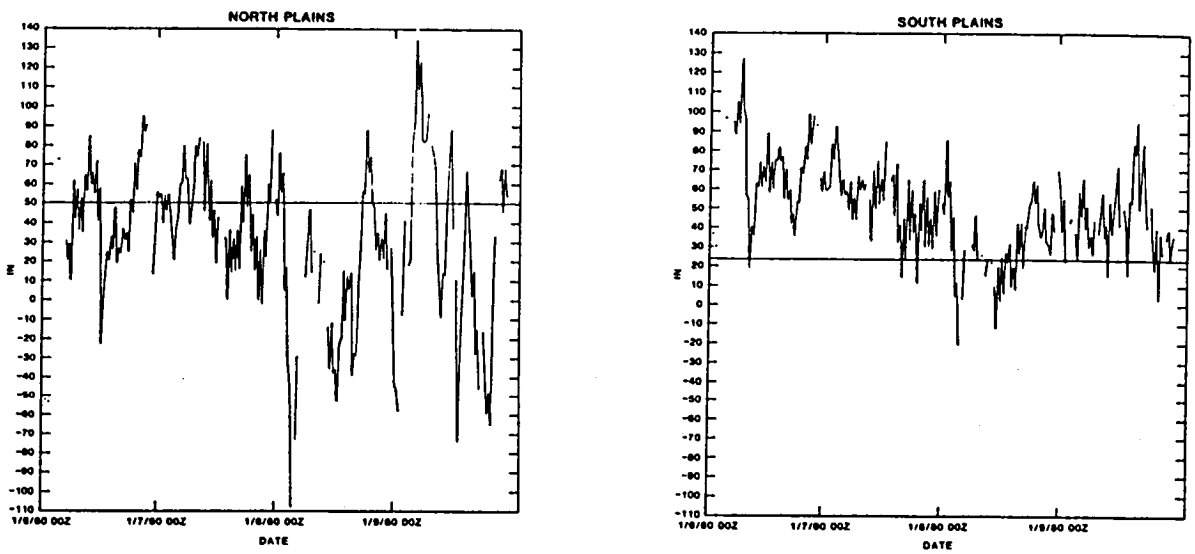

Fig. 1. Daily changes of the heat wave index in the North and South Plains. Threshold values for the heat wave are shown as horizontal lines (gaps indicate missing data).

Wave Structure Associated with the Summer 1980 Heat Wave and Drought

N. Wolfson and R. Atlas

A study has been made of the wave structure associated with the summer 1980 heat wave and drought in relation to other years. This study was performed for the 500 mb level for the months of June-Sept. 1963-1977 and 1980. The data was obtained from the National Meteorological Center (NMC) final analysis interpolated to the GLA 4° latitude x 5° longitude grid. For each year the 500 mb height was spectrally decomposed. Then waves 1-3 and 4-7 were combined. The decompositions were carried out for latitudes 30°N to 54°N every 4°. Fig. 1a presents the longitudinal location of the ridge lines for waves 1-3 for the period June-Sept. of 1963-1977, 1967 and 1980. One may see that there are three ridge lines, one over Tibet and central Asia and the other two over the central U.S. and eastern Atlantic. The ridge over the U.S. is very stable and does not change much from year to year. This is indicated by the bar line on Fig. 1a which indicates one standard deviation in the yearly location. The deviation from the mean is usually smaller than 20° longitude.

As indicated by Fig. 1a the summer of 1980 has a different pattern and shows large deviations from climatology. The ridge over the central U.S. north of 38° shifted by 10°-20° eastward. This shift is more apparent in the northern latitudes and is larger than the standard deviation.

The ridge lines of waves 4-7 are presented in Fig. 1b. Ridges are observed near main mountain chains i.e. the Alps, Caucasus, Tibet and the Rockies, indicating the importance of these ranges in influencing the summer circulation. One may note that over the central U.S. the planetary waves 1-3 and the shorter 4-7 waves support each other, with both contributing to the standing wave. The ridge line follows the eastward slope of the longitude of the Continental Divide supporting Wallace's (1983) hypothesis of the effect of orography on the summer circulation. It is evident that summer 1980 was highly anomalous in that the ridge north of 35°N shifted eastward by ~ 15° longitude, while the climatological standard deviation is only 5°-12° longitude.

Further evidence of the relationship between the location of the planetary waves and average seasonal temperature is gained by analyzing the wave structure for 1967, which was the coldest summer of the 15 years analyzed in the northern plains. North of 38N, waves 1-3 were shifted westward (Fig. 1a) by 15°-25° longitude, while waves 4-7 showed a 10° average shift from the climatological location in the same direction. Furthermore, the 1967 summer was the warmest year on record between 1963-1977 in the pacific region.

In order to study the relative importance of the 1-3 and 4-7 waves during the heat wave episode we have plotted their amplitude for the period June through September 1980.

95°W is a representative longitude for the Great Plains. At 30°N,95°W the main contribution of the heat wave is from waves 1-3 whose amplitude is almost always larger than those of waves 4-7. However, both of these wave bands had positive amplitudes and supported each other during this period. This is similar at 34°N but the contribution of waves 4-7 was more important for the maintenance during June and the second part of August. At 38°N the combination of 1-7 is

mostly positive but it is the 4-7 band that is primarily responsible for the anomaly.

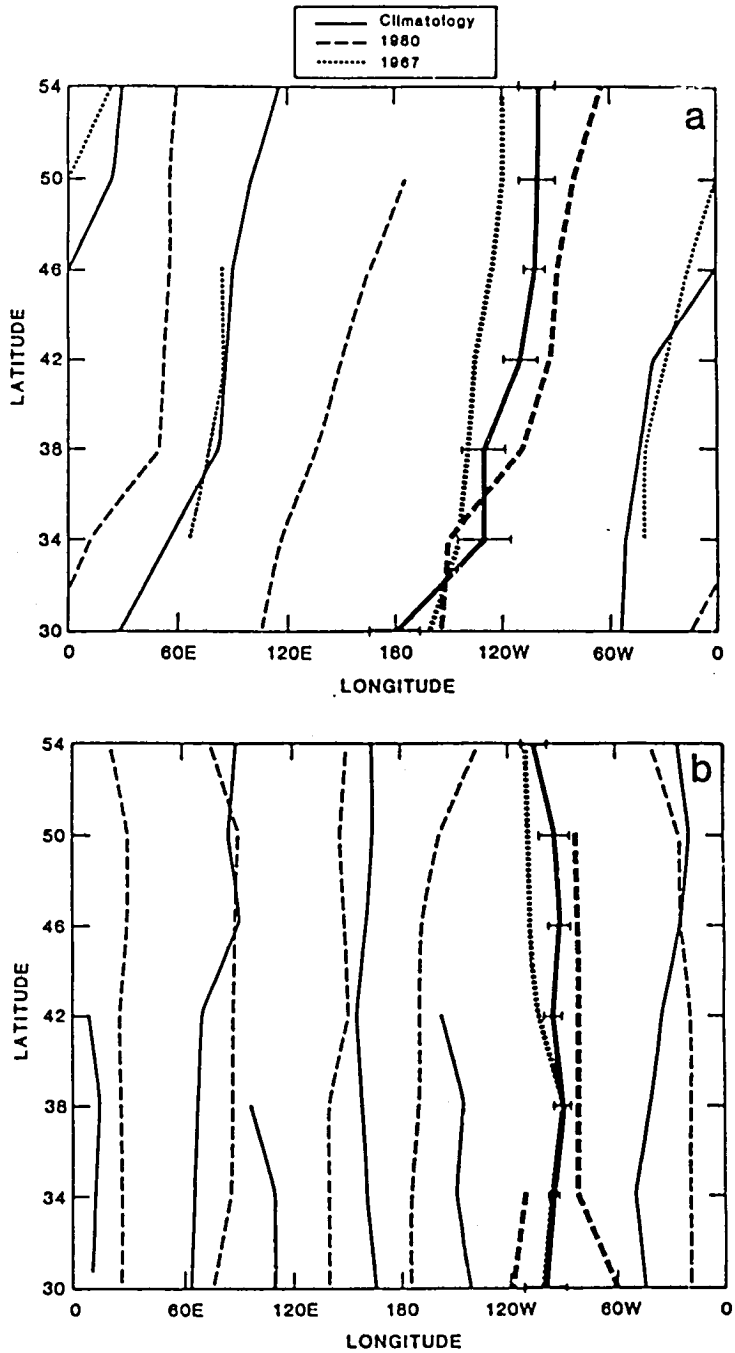

Fig. 1. Longitudinal ridge positions for waves 1-3 (a) and 4-7 (b) as a function of latitude.

Preliminary Results from Numerical Experiments on the Summer 1980 Heat Wave and Drought

N. Wolfson, R. Atlas, and Y. Sud

During the summer of 1980, a prolonged heat wave and drought affected the United States. The heat wave began in the southern Great Plains in June extended northward and westward in July and then in August and September weakened and retreated to the Southeast.

A preliminary set of experiments has been conducted to study the effect of varying boundary conditions on the GLA model simulation of the heat wave. Five 10-day numerical integrations with three different specifications of boundary conditions were carried out: a "control" experiment which utilized climatological boundary conditions, an "SST" experiment which utilized summer 1980 sea-surface temperatures in the North Pacific but climatological values elsewhere, and a "Soil Moisture" experiment which utilized the values of Mintz-Serafini for the summer 1980. The starting dates for the five forecasts were 11 June, 7 July, 21 July, 22 August, and 6 September of 1980. These dates were specifically chosen as days when a heat wave was already established in order to investigate the effect of soil moistures or North Pacific sea-surface temperatures on the model's ability to maintain the heat wave pattern. The experiments were evaluated in terms of the heat wave index (Wolfson and Atlas, 1985) for the South Plains, North Plains, Great Plains and the entire U.S. In addition a subjective comparison of map patterns has been performed.

Table 1 presents the average ten day index values for the four regions. The differences between the various experiments are very small at the beginning of the integration (not shown), and usually develop after the fourth or fifth day. One may note that the SST influence has been usually to decrease the index value. This might be due to the cold ocean temperatures prevailing in 1980. One may place confidence in these SST fields only for short-range forecasting because a longer period of integration would demand global SST distribution to be introduced. On the other hand, introduction of 1980 real soil moisture values over the U.S. has enhanced the heat wave. This effect is much more prominent over the northern plains than over the southern plains.

Table 2 summarized the impact of boundary conditions on the heat wave index. In addition, "t" student test values are shown to indicate the significance of the results.

Additional model experiments are being conducted to study the initiation and breakdown of the heat wave and the effect of global sea-surface temperatures.

REFERENCE

Wolfson, N. and R. Atlas, 1985: Objective determination of heat wave patterns. (This issue).

Table 1: Average ten day index values

Experiment	Control	SST	Soil Moisture
South Plains			
6/11	56.06	52.38	55.16
7/07	58.8	57.69	62.38
7/21	46.7	45.55	44.56
8/22	64.52	55.72	58.88
9/06	60.70	58.33	64.23
North Plains			
6/04	3.59	-1.68	4.50
7/07	50.8	47.18	54.30
7/21	50.99	52.26	54.15
8/22	47.0	44.18	53.71
9/06	54.0	47.76	58.81
Great Plains			
6/11	26.2	21.69	27.54
7/07	54.3	51.73	57.79
7/21	49.1	49.36	50.00
8/22	54.58	49.17	55.95
9/06	56.90	52.33	58.93
U.S.			
6/11	9.20	7.56	9.44
7/07	10.60	13/21	14.08
7/21	43.01	43.49	42.08
8/22	17.71	14.80	20.79
9/06	40.08	38.72	44.63

Table 2: Impact of boundary conditions on heat wave index (significant values are underlined) with "t" value in lower right side.

Region	Average control value	Impact of SST	Impact of Soil Moisture
South Plains	57.36	-3.42 2.68	.31 1.17
North Plains	41.28	-3.34 3.30	3.42 4.05
Great Plains	48.22	-3.36 3.71	1.83 4.54

B. SATELLITE OBSERVING SYSTEMS

Improved Cloud and Surface Fields Derived from HIRS2/MSU

J. Susskind and D. Reuter

The methods to retrieve cloud parameters from HIRS2/MSU data, described in Susskind et al., (1984), have been shown to produce qualitatively reasonable cloud fields but to underestimate cloud amount. Improvements have been made to the cloud algorithm which allow for better determination of low clouds. These improvements involve retrieving cloud fields at a higher spatial resolution, which decreases the problems arising from multiple layer clouds, and increasing the number of channels used to determine the cloud parameters from 2 15 μm lower tropospheric sounding channels to 5 channels, including the 11 μm window and 2 15 μm mid and upper tropospheric sounding channels. The use of the 11 μm window channel was very important in identifying low level clouds.

Another way of checking for the existence of low clouds, at least over the open ocean during the day, is by looking at the reflected solar radiation in HIRS2 channel 20, sensing the near IR and red regions. Channel 20 was not used in the cloud algorithm because of the desirability to use the same algorithms day and night in order to generate meaningful statistics of day-night cloud differences.

Global one day cloud fractions and cloud top pressure fields have been derived from the HIRS2/MSU data. These fields are completely consistent with visible and infra-red imagery taken the same time from AVHRR but contain considerably more information than the AVHRR images. In addition to cloud height information, which is not apparent from the imagery, there is also good cloud information at high latitudes where the visible imagery on AVHRR sees either no signal (perpetual night) or shows reduced contrast because of background ice and snow cover, and the 11 μm imagery on AVHRR is hampered because of the low thermal contrast between the clouds, which are usually low, and the cold surface.

Monthly mean fields of cloud fraction, cloud top pressure, and cloud top temperature, for both day clouds (3 PM) and night clouds (3 AM), and their differences, have been prepared for a number of months. Average monthly mean cloud fractions obtained in this fashion are about 40%, with 3 AM fields being about 5% more cloudy than 3 PM fields. These cloud fractions are effective, because the clouds have have been treated as black. They represent the product of the cloud fraction and the cloud emissivity, which averages about .7 in the 15 μm region (Paltridge and Platt, 1976).

Monthly mean "albedo" (actually per cent reflected solar radiation at a specific angle in a specific wavelength interval) fields have also been prepared by averaging the observations in HIRS channel 20, divided by the cosine of the solar zenith angle. These fields show excellent agreement with the day-time cloud fields, indicating most clouds which are apparent in visible imagery are also found by the infra-red algorithms. The albedo fields also show features attributable to deserts and ice and snow, though it is difficult to distinguish the ice and snow from the cloudy regions around them from the visible imagery directly.

The cloud algorithm, which does not use the visible data, provides the ability to select scenes which are clear or cloudy. Monthly mean fields of "cloud free albedo" were generated by eliminating all scenes from the instanteous albedo field considered to be cloudy and averaging the albedo only for cloud free scenes.

This procedure serves two purposes. First, it checks the extent that the cloud algorithm may have missed clouds apparent in the visible, and second, if successful, it provides a reasonable estimate of surface albedo once atmospheric corrections can be made. The "cloud free albedo" fields indeed showed only slight trace of low cloud contamination, whose sources we have identified and are correcting. In addition, desert features were readily apparent and clear indications of ice and snow fields emerged from the cloudy mid-latitude and polar regions. These ice and snow fields were quite consistent with those derived from the surface-emissivity at 50.3 GHz (channel 1 of the MSU, which has a surface transmittance of .7) and the retrieved ground temperature. The agreement of these ice and snow fields, neither of which could have been derived by single spectral region sounding, shows the power of a combined infra-red, microwave, and visible monitoring system.

Another extremely important parameter derived from the HIRS2/MSU soundings is the monthly mean difference of the 3 PM and 3 AM ground temperatures. This difference is related to the forcing function, given by incoming solar radiation, and the response function, given by the thermal inertia of the ground, which depends on soil moisture and evapotranspiration rate. Clouds affect the day-night temperature difference in two ways. The direct effect of clouds is to block incoming solar radiation during day, which slows daytime warming, and reflect upwelling longwave radiation back to the surface at night, slowing nocturnal cooling. The indirect effect of clouds is to cause rain, which increases soil mosture and again decreases the diurnal surface temperature variation. Indeed, the day-night surface temperature difference fields are quite consistent with the retrieved cloud cover fields for all the months processed, especially in the regions of convective cloudiness.

The effects of clouds on incoming and outgoing radiation are, to first order, not a factor in the day-night ground temperature fields because retrievals are not performed under full overcast conditions and retrievals are performed only in the clear portions of partially cloudy scenes as a result of the cloud correction algorithm. The day-night temperature difference fields then should be a measure of rainfall and soil moisture. Mintz et al. (1985) have developed an energy balance model relating the monthly mean day-night ground temperature field derived from HIRS2/MSU to soil miosture and evapotranspiration and have derived reasonable monthly mean fields for these parameters.

In summary, HIRS2/MSU data provides the possiblity of obtaining accurate fields of a number of important climate parameters, all derived together in a consistent fashion. This system, launched at the end of 1978, will be in place through the 80's. The opportunity exists to develop a 10 year climate data set from similar instrumentation. Our immediate plans are to process all of 1979 with a slightly improved version of the current system and possibly process all data up to 1984.

REFERENCES

Mintz, Y., J. Susskind, and J. Dorman, 1985: Large scale evapotranspiration and soil mositure from satellite observations. In preparation.

Paltridge, G. W., and C. H. R. Platt, 1976: Radiative processes in Meteorology and Climatology, Elsevier, New York.

Susskind, J., J. Rosenfield, D. Reuter, and M. T. Chahine, 1984: Remote sensing of weather and climate parameters from HIRS2/MSU on TIROS-N. J. Geophys. Res 89, 4677-4697.

Intercomparison of Sea-surface Temperature Anomaly Fields

J. Susskind and D. Reuter

Sea-surface temperature anomaly fields produced from analysis of HIRS2/MSU data at GLAS for the months November 1979, December 1981, March 1982, and July 1982 were compared to those produced from data from ships, AVHRR, and SMMR in a series of NASA sponsored sea-surface temperature workshops. The methods used by GLAS to analyze the HIRS2/MSU data were similar to those in Susskind et al., (1984), but improvements were made to the algorithm used to retrieve sea and land surface temperatures and in the cloud filtering algorithm. One of the improvements involved generating weights for a given sounding, which decreased with increasing cloudiness and increasing humidity. These weights should be used in generating monthly mean fields. The workshop generated statistics for the weighted HIRS2/MSU field only for the month of July 1982.

Statistics generated by the workshop for the last two months, in which the latest improved algorithm (called HIRS version 2 in the workshop) was used to process the HIRS/MSU data, are shown in Tables 1 and 2. Climatology is also treated as a sensor for comparison. The values given are C, the correlation coefficient, B, the bias (sensor-ship), S, standard deviation, and N, the number of grid points sampled (2° x 2° grid) comparing fields from a number of sensors with ship fields. Statistics are given for global colocations and also for those in the North Pacific and North Atlantic Oceans. Results are given for the unsmoothed field, and also for 9 point smoothed fields, in which case, both the ship field and retrieved field were smoothed and compared to each other.

To interpret the significance of the standard deviation from ships, an anomaly field produced by a sensor can be considered skillful if its standard deviation from ships is at least as low as that of climatology, which is representative of the ocean signal. A better indicator of skill is the correlation of the sensor anomaly field with that of ships. Climatology, by definition, has zero correlation and zero skill.

As seen in Tables 1 and 2, smoothing has reduced the noise and increased the correlation coefficients for all cases. Part of this is due to random noise reduction in the ship field and part due to noise reduction in the field being compared to ships. The AVHRR field in March 1982 shows marginal skill in the standard deviation sense and good skill in the correlation sense in the unsmoothed fields. Statistics for the unsmoothed March HIRS field were not generated at the workshop.

In the smoothed fields, AVHRR shows increased skill in both categories. The statistics for the smoothed HIRS fields are almost as good as those of AVHRR with regard to standard deviation but the correlations are considerably lower. It should be noted that these statistics are for the unweighted HIRS2 field. The weighted field provides better visual agreement with the ship field but statistics were not computed in the workshop using the weighted field. The SMMR field is much more noisy but shows some correlation skill in the North Pacific Ocean. An additional field produced using both SMMR data and ship data shows good agreement in the vicinity of ships as expected. Surprisingly, the statistics are only marginally better than those of AVHRR and HIRS which did not have the benefit of including the ship data used to verify the solutions.

When one looks at the actual anomaly fields for March 1982 (not shown), it is apparent that March 1982 was indeed very close to climatology, expecially in the North Atlantic Ocean. In the North Pacific Ocean, there are small cold anomalies centered at about 160° W, 35° N and 175° E, 28° N and a small warm anomaly about 115° W, 20° N. The weighted HIRS2/MSU field likewise shows small anomalies in the North Pacific ocean, of the correct sign, centered at the appropriate locations. The small anomalies in the Atlantic Ocean are in almost perfect agreement with those in the ship field. The AVHRR field, on the other hand, is shown to indicate extensive areas of cold anomaly in both the North Atlantic and Pacific Ocean, sometimes exceeding 1.5° in magnitude. This feature is consistent with the cold bias of .3° to .5°C indicated in Table 1 for AVHRR. The AVHRR field also has a very large spurious warm anomaly in the region along the equator from 75° E to 155° E. Agreement of all fields in the southern hemisphere is reasonable, but the AVHRR warm anomalies are larger than those indicated by HIRS2/MSU or the ships. The unweighted HIRS field is somewhat warmer than the weighted field and has essentially no anomalies in the North Pacific Ocean. It is not surprising that small correlation coefficients were found in the North Pacific Ocean for the unweighted HIRS Version 2 field.

Statistics for July 1982 are shown in Table 2. For this month, statistics were generated for both the weighted and unweighted HIRS version 2 fields. As observed from looking at the statistics comparing climatology with ships, July 1982 was much more anomalous than other months in the workship with a standard deviation of about .6°C about a cold bias (ships-climatology) of .96°C in the North Pacific Ocean and .4°C in the North Atlantic Ocean. Therefore signals are large and one expects larger correlations between retrieved anomaly fields and ship fields. Correlations for AVHRR are similar to those of March 1982 but the standard deviations are considerably larger than in the other months. HIRS statistics show improved correlation over March 1982, as expected, with standard deviations slightly degraded over those of March 1982. Statistics for the weighted HIRS field, relative to the unweighted field, show the soundings have become colder on the average by about .35°. Results have improved somewhat in the Atlantic Ocean and degraded somewhat in the Pacific Ocean. SMMR results have improved over previous months, both in the standard deviation sense and in the sense of error correlation. The SMMR/Ship field shows good agreement with the ships used to produce the field and shows more of an improvement with regard to standard deviation over the HIRS2 field, which did not have the benefit of including ships, than in March.

The detailed anomaly fields for this month show that HIRS again gives very good agreement with the ship anomaly fields, which this time are quite large and extensive in both the North Atlantic and North Pacific Oceans. The HIRS field does have a few areas of spurious cold anomaly in July, located mainly within a thin latitude band running from about 15° N - 25° N over most of the ocean, and off the west coast of South American from 15° S to about the equator. These spurious anomalies, which are mostly of the order .5° - 1°C, may well be due to the effects of aerosols put into the atmosphere by the El Chichon eruption. The errors are amplified in the weighted field, which is in general colder. The effects of this eruption on derived sea-surface temperatures are much more evident in the AVHRR anomaly pattern which shows a large block of spurious cold anomaly from 10° N - 35° N running across the entire oceanic area, with magnitudes of the order of 2°C.

In summary, the HIRS2 sea-surface temperature fields are statistically comparable to those produced from AVHRR, but the errors tend to be spatially

random while the AVHRR errors are more spatially coherent. The effect of the El Chichon eruption on derived HIRS sea-surface temperatures appear to be considerably less than on those retrieved from AVHRR.

Table 1
Comparison of Monthly Mean Anomaly Fields
With Ships > 5/Cell
March 1982

		UNSMOOTHED			SMOOTHED		
		GLOBAL	N. PAC.	N. ATL.	GLOBAL	N. PAC.	N. ATL.
AVHRR	C	.67	.52	.67	.77	.58	.80
	B	-.36	-.50	-.29	-.44	-.54	-.30
	S	.51	.48	.42	.29	.29	.21
	N	795	434	267	368	210	153
HIRS2 VERSION 2	C				.55	.30	.66
	B				.29	.36	.21
	S				.31	.34	.22
	N				368	210	153
SMMR NIGHT	C	.24	.37	-.05	.15	.54	-.09
	B	-.21	.05	-.76	-.17	.13	-.77
	S	1.11	.99	1.19	.79	.67	.69
	N	690	392	213	300	200	95
SMMR/SHIP COMPOSITE	C	.58	.57		.75	.75	
	B	.04	.03		.07	.07	
	S	.47	.46		.25	.25	
	N	438	394		207	203	
VAS	C	.40		.50	.79		.79
	B	.90		.89	.91		.91
	S	.56		.52	.26		.26
	N	109		106	51		51
XBT	C	.39	.38		.70	.70	
	B	-.27	-.29		-.47	-.47	
	S	.89	.91		.35	.35	
	N	242	227		18	18	
CLIM	C	.00	.00	.00	.00	.00	.00
	B	.09	.27	-.05	.13	.29	-.10
	S	.52	.48	.42	.35	.32	.27
	N	795	434	267	368	210	153

Table 2
Comparison of Monthly Mean Anomaly Fields
With Ships > 5/Cell
July 1982

		UNSMOOTHED			SMOOTHED		
		GLOBAL	N. PAC.	N. ATL.	GLOBAL	N. PAC.	N. ATL.
AVHRR	C	.62	.59	.66	.70	.63	.84
	B	-.48	-.37	-.57	-.35	-.17	-.48
	S	.79	.93	.60	.52	.62	.37
	N	644	320	258	274	117	157
HIRS2 VERSION 2	C	.49	.43	.51	.78	.52	.85
	B	-.07	.01	-.08	.09	.14	.04
	S	.69	.72	.62	.38	.39	.36
	N	662	337	259	327	170	157
HIRS2 VERSION 2 WEIGHTED	C	.52	.45	.56	.79	.45	.88
	B	-.37	-.31	-.37	-.25	-.23	-.27
	S	.69	.74	.61	.38	.43	.30
	N	662	337	259	327	170	157
SMMR NIGHT	C	.46	.54	.32	.55	.62	.66
	B	-.43	-.22	-.88	-.69	-.39	-1.07
	S	.97	.87	.93	.60	.48	.51
	N	522	278	193	230	127	103
SMMR/SHIP	C	.76	.74		.86	.86	
	B	-.04	-.06		-.10	-.10	
	S	.53	.54		.27	.27	
	N	316	282		137	137	
VAS	C	.49		.46	.42		.42
	B	.48		.50	.55		.55
	S	.46		.45	.22		.22
	N	92		88	38		38
XBT	C	.58	.55				
	B	-.22	-.23				
	S	.94	.96				
	N	154	146				
CLIM	C		.00	.00	.00	.00	.00
	B		.67	.26	.70	.96	.40
	S		.73	.69	.63	.50	.64
	N		338	259	336	179	157

REFERENCE

Susskind, J., J. Rosenfield, D. Reuter, and M. T. Chahine, 1984: Remote Sensing of Weather and Climate parameters of HIRS2/MSU on TIROS-N. J. Geophys. Res., 89, 4677-4697.

Experiments on the Assimilation of Patches of Data Using a Barotropic Model

F.H.M. Semazzi

Experiments are performed to examine the impact of adopting various procedures in the assimilation of patches of data during the progress of a numerical forecast. A barotropic model described by Takacs and Balgovind, 1983 is used for the experiments. The model is global and its discretization is similar to the GLA Fourth Order GCM. The effect of orography is included in the model.

The experiments are of an "identical twin" kind. The "nature" run starts from global fields of wind (u and v) and height (h) at 300 mb. They are real data of January 1979 00Z which were interpolated from the adjacent sigma levels of the GLA GCM and then balanced by the bounded derivative method (Browning et al., 1980, Semazzi, 1985). From this initial state a 6 day forecast is performed. At intervals of 3 hours this information is saved over sectors of 60° width in longitude, from the south pole to the north pole, to simulate data coverage and observational frequency of a polar orbiting satellite.

The initial wind field of the assimilation experiment is constructed from simple zonal averages of the u-component of the initial state for the "nature" run. The corresponding zonally averaged height field is determined from the geostrophic relationship. Every 3 hours the forecast in the assimilation experiment is interrupted and data is inserted over the appropriate sector region from the "nature" run.

The evaluation of the assimilation proccess is based on the global RMS of the difference in height between the "nature" run and the assimilation forecast. Fig. 1 displays the limiting case when all the three prognostic variables, namely, u,v and h are simultaneously inserted. The two runs become identical in about a day when the earth makes a complete rotation. Fig. 2 shows that the direct insertion of heights has only a small impact. Fig. 3 indicates that the insertion of winds only is far more effective than the height (Fig. 2). Finally, Fig. 4 displays the impact of making geostrophic wind correction in addition to the insertion of height. The improvement over the results shown in Fig. 2 is dramatic.

We are presently exploring the prospect of accelerating the assimilation by using a combination of the bounded derivative method and the estimation theory of stochastic-dynamic systems suggested in Bengtsson et al. (1981).

References

Bengtsson, L., M. Ghil and E. Kallen (eds.), 1981: Dynamic Meteorology: Data Assimilation Methods. Springer-Verlag, New York/Heidelberg/Berlin, 330 pp.

Browning, G., A. Kasahara and H. O. Kreiss, 1980: Initialization of the primitive equations by the bounded derivative method. J. Atmos. Sci., 37, 1424-1436.

Takacs, L. L., and R. C. Balgovind, 1983: High latitude filtering in grid point models. Mon. Wea. Rev., 111, 2005-2015.

Semazzi, H. F. M., 1985: On the investigation of the equatorial orographic dynamic mechanism. To appear in January issue of J. Atmos. Sci.

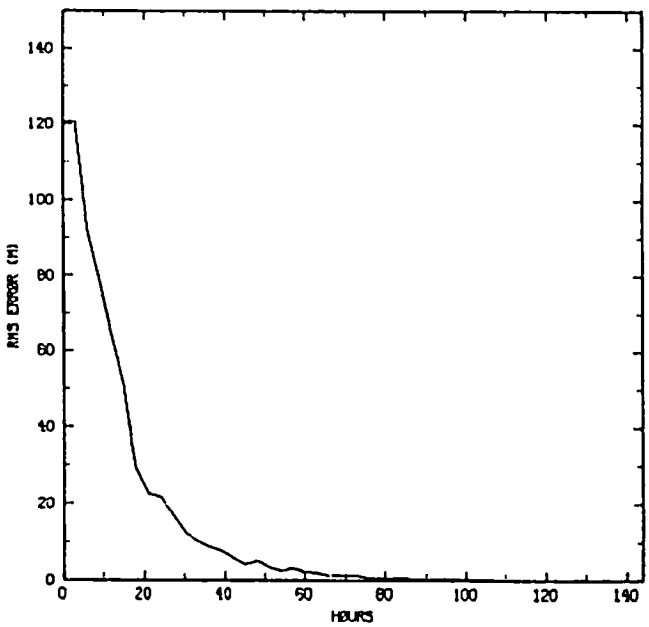

Fig. 1

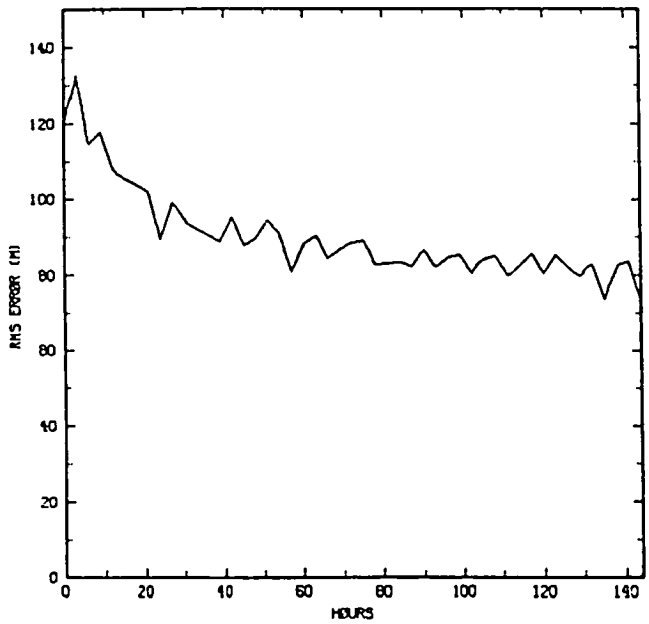

Fig. 2

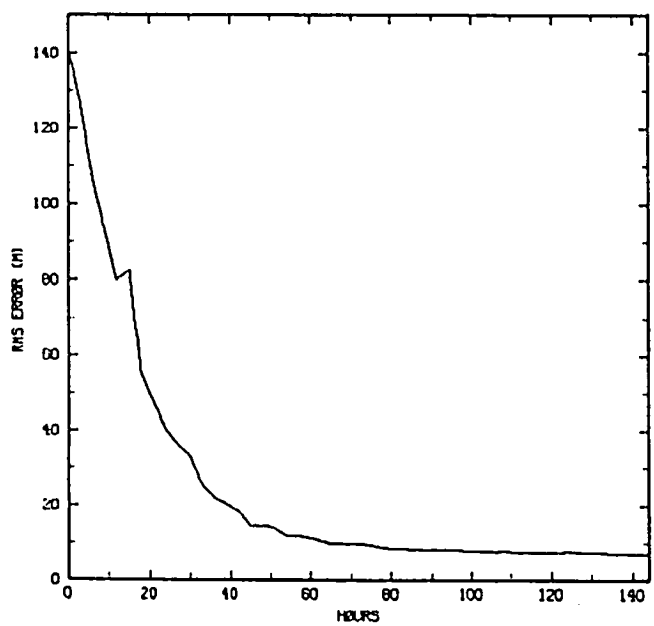

Fig. 3

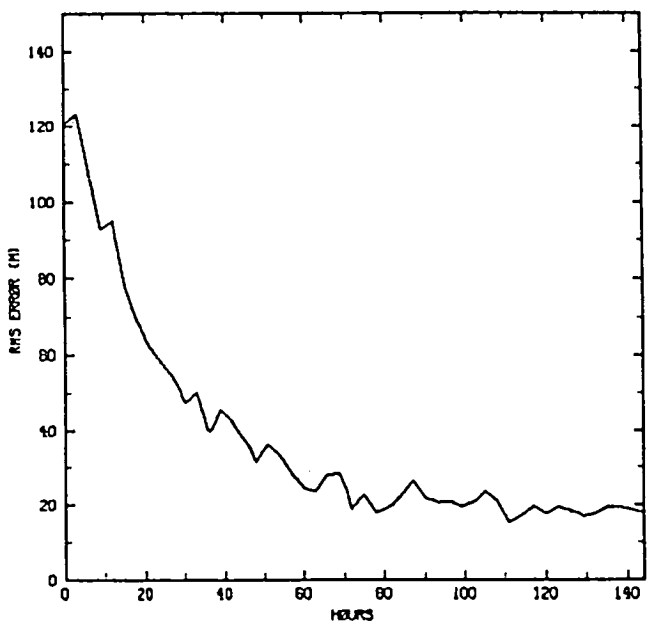

Fig. 4

High-Latitude Filtering in a Global Grid-Point Model Using Model Normal Modes

L. L. Takacs, I. M. Navon, and E. Kalnay

1. Introduction

The aim of high-latitude filtering in the vicinity of the poles is to avoid the excessively short time steps imposed on an explicit time-differencing scheme by linear stability due to fast moving inertia-gravity waves near the poles. In this paper we apply the model normal mode expansion toward the problem of high-latitude filtering in a global shallow water model using the same philosophy as that used by Daley (1980) for the problem for large timesteps in P.E. models with explicit time integration schemes.

2. Computational Procedure

Starting from a non-linear normal mode initialized state, we transformed forward at each timestep n the dependent variables $(u, v, h)^n$ given to us by the model, thus producing a normal mode coefficient set. The model used a conventional explicit Matsuno time-integration scheme. To obtain the projection onto the fast modes, we simply back transformed only those modes whose eigenfrequency was greater than the maximum allowed derived from timestep considerations. This produced Δu, Δv, and Δh, which were then subtracted from the current fields to produce "filtered" new values of those variables. A new integration step was then carried out.

3. Experimental results

Figs. 1 and 2 show difference plots after 3 days of the height and wind field between three filtering techniques and a control run using no high-latitude filter and a small timestep (60 seconds). The three filtering techniques are 1) the norm mode filter (NMF), 2) the prognostic field filter (UVH), and 3) the time-tendency filter (DOT). The control run is considered as "truth" in these experiments.

From these figures we see that the NMF filter has the best simulation of the control run, producing very little differences in high latitudes. The DOT filter is not much worse. The UVH filter, however, shows major differences in high latitudes and begins to spread its influence to lower latitudes as well.

4) Conclusions

A methodology has been developed in which fast-moving inertia-gravity waves are transformed to normal mode space in order to perform a "surgical" high-latitude filter required in global grid-point models. In contrast to other high latitude filtering techniques, the new approach leaves the model's Rossby modes intact, and is shown to best simulate a control, no-filter run.

Reference

Daley, R., 1980: The development of efficient time integration schemes using model normal modes. Mon. Wea. Rev., 108, 110-110.

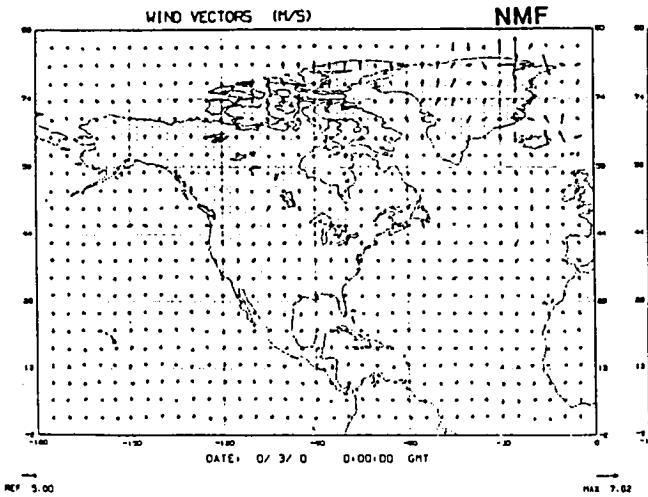
WIND VECTORS (M/S)
NMF
DATE: 0/ 3/ 0 0:00:00 GMT

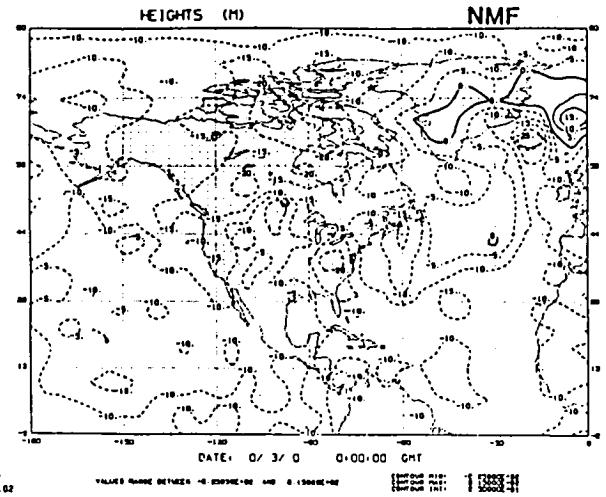
HEIGHTS (M)
NMF
DATE: 0/ 3/ 0 0:00:00 GMT

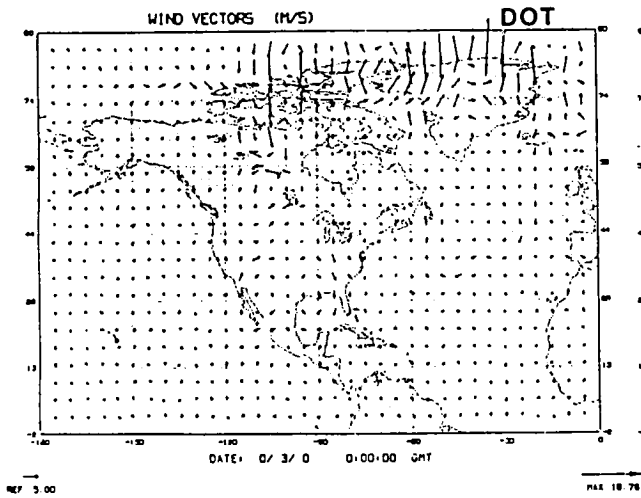
WIND VECTORS (M/S)
DOT
DATE: 0/ 3/ 0 0:00:00 GMT

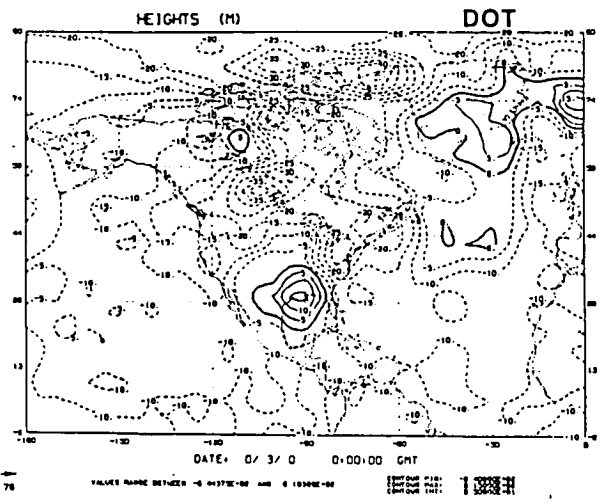
HEIGHTS (M)
DOT
DATE: 0/ 3/ 0 0:00:00 GMT

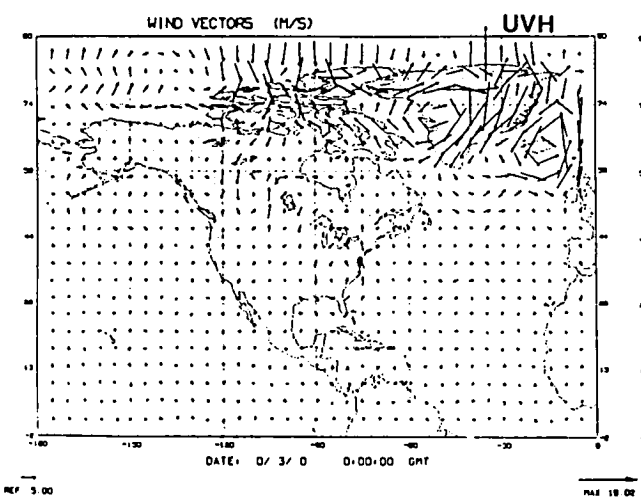
WIND VECTORS (M/S)
UVH
DATE: 0/ 3/ 0 0:00:00 GMT

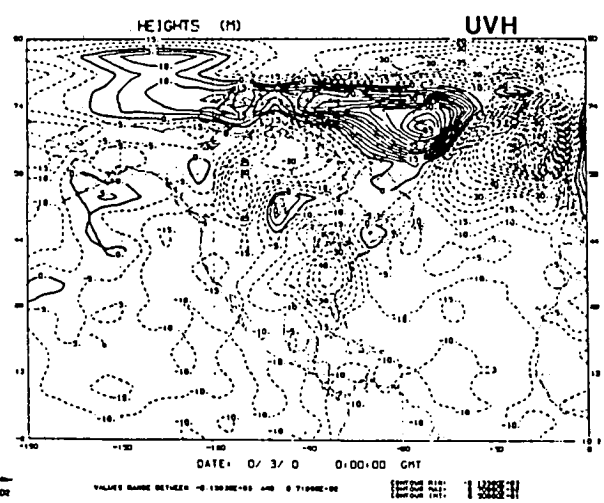
HEIGHTS (M)
UVH
DATE: 0/ 3/ 0 0:00:00 GMT

Fig. 1

Fig. 2

On the Improvement of Satellite Temperature Retrievals by Means of Boundary Layer Models

R. Boers

A simulation study was conducted to determine whether boundary layer models could be used to improve the accuracy of the satellite temperature retrievals close to the earth's surface. We used the simplest type of boundary layer models that only consider time changes in the mean boundary layer quantities such as equivalent potential temperature and specific humidity, but neglect the details of the turbulent structure in the interior of the layer. They can be run with relatively few externally specified parameters: surface wind speed and divergence rate. Extensive theoretical development of boundary layer models can be found in the literature over the last 20 years (Tennekes, 1973, Stage and Businger, 1981 and many others). Model verification studies (Boers et al., 1984 and others) show that under certain conditions the mean atmospheric structure can be simulated very well.

The following process was carried out to study the impact of boundary layer models on the retrieval accuracy.

a) A set of randomly distributed wind speed and divergence rates was assigned to a randomly distributed set of oceanic temperature and humidity profiles.

b) Boundary layer model runs (Stage et al., 1981) were performed on these profiles until a stationary solution was found in boundary layer height and temperature. These modified profiles were called the truth.

c) Brightness temperature (AMTS, HIRS) were computed for the truth and temperature and humidity retrievals were performed using these brightness temperatures.

d) Boundary layer model runs were performed on the retrievals until a stationary solution of boundary layer parameters was obtained. The solution was called the modified retrieval.

e) RMS errors of the retrievals and the modified retrieval with respect to the truth were computed.

Tests included simulations whereby all externally specified parameters at step (d) were left the same as those used in generating the "truth", and simulations whereby each one was perturbed to study the influence of the uncertainty of those parameters on the mixed layer solution. Early sensitivity tests indicated that in order to acquire meaningful results an accurate scheme was needed to compute the radiative sky temperature in case clouds developed at the top of the boundary layer. We used the scheme of Harshvardhan et al. (1984) to obtain the radiative sky temperature for both the truth and the modified retrievals. We can draw the following conclusion from this study:

a) If wind speed and divergence rate are known exactly for computation of the modified retrievals, the modified retrievals are more accurate than the retrievals in representing the truth by .2° C to .8° C in the lowest 200 mb.

b) Typical perturbations of the wind speed by 30-60% do not significantly affect these results.

c) Typical perturbations of divergence by 50-100% decrease the accuracy of the modified retrieval to that of the retrieval.

d) The combined effect of b and c is of no improvement of the modified retrieval over the retrieval.

e) We can significantly improve on the disappointing results of b and c by selecting those cases where the truth and the modified retrieval both contain clouds, or both contain no clouds, excluding all other results. For these cases the modified retrieval is more accurate than the retrieval by .4 to .6° C in the lowest 200 mb.

To illustrate some of our results we consider Figure 1. The four lines represent RMS errors in temperature of 1 HIRS-retrieval, 2 HIRS-modified retrieval, 3 AMTS-retrieval, 4 AMTS-modified retrieval. Excluded are all non-matching cloud - no cloud pairs in the truth and the modified retrieval. RMS-errors of retrievals and modified retrievals are between .8 and 1.8°C. AMTS retrievals are more accurate than the HIRS-retrievals by .2°C except close to the surface. The modified retrievals for both HIRS and AMTS improve on the retrievals by up to .8°C close to the surface.

References

Boers, R., E. W. Eloranta, R. L. Coulter, 1984: Lidar Observations of Mixed Layer Dynamics: Tests of Parameterized Entrainment Models of Mixed Layer Growth Rate. J. Clim. Appl. Meteor., 23, 247-266.

Harshvandhan, T. G. Corsetti, 1984: Longwave Radiation Parameterization for the UCLA/GLAS GCM. NASA Tech. Mem. 86072.

Stage, S. A., J. A. Businger, 1981: A model for entrainment into a cloud topped marine boundary Layer Part I. J. Atmos. Sci., 38, 2213-2229.

Tennekes, H., 1973: A model for the Dynamics of the Inversion Above a Convective Boundary Layer. J. Atmos. Sci., 30, 558-567.

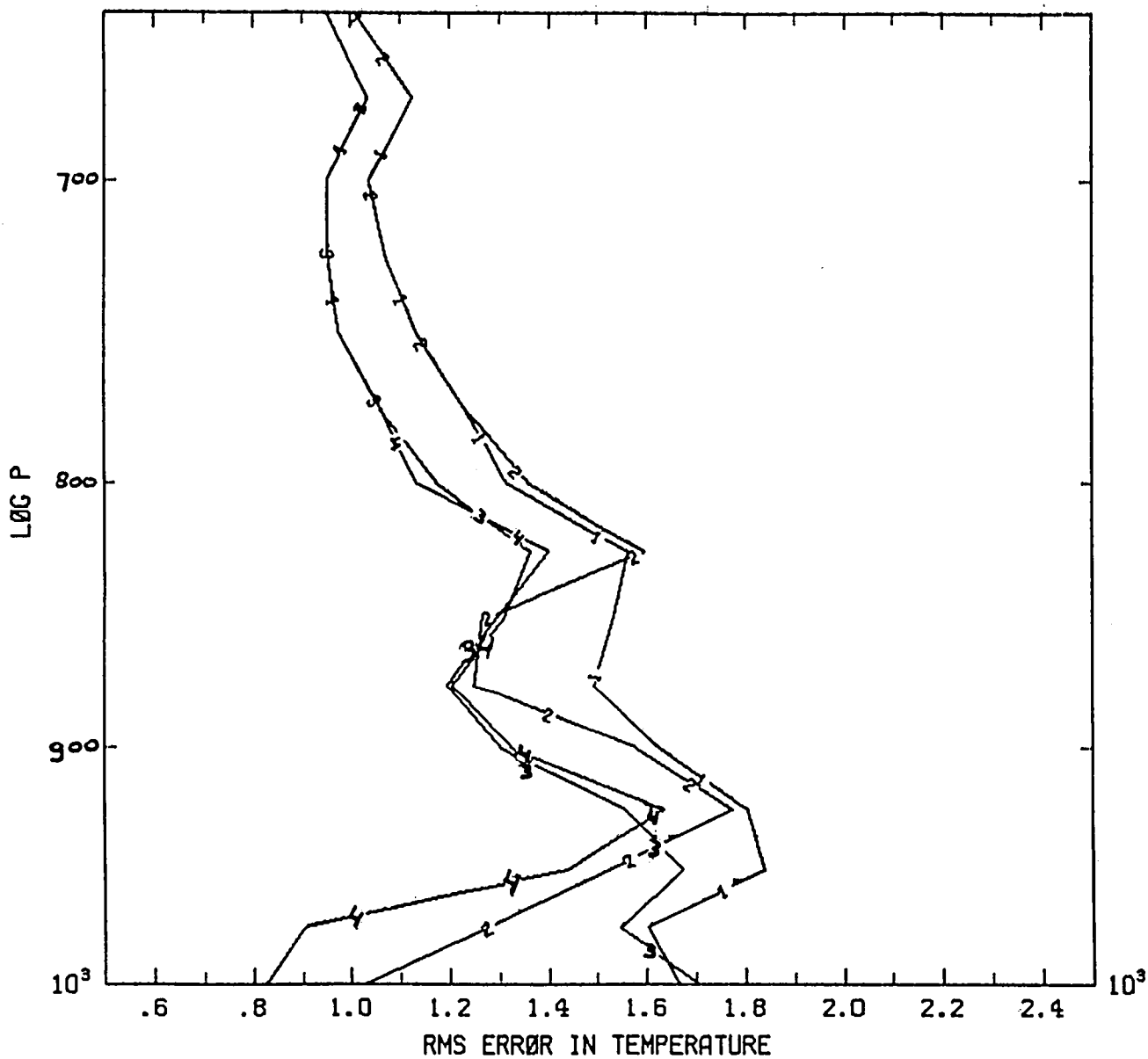
LØG P
700
800
900
10³
.6
.8
1.0
1.2
1.4
1.6
1.8
2.0
2.2
2.4
10³
RMS ERRØR IN TEMPERATURE

Figure 1

Applications of Fuzzy Clustering Techniques to Stratified by Tropopause MSU Temperature Retrievals

By

Marie-Jeanne Munteanu and Paul Piraino

The purpose of this paper is to apply the method studied in a previous paper (Munteanu [1]) for the three and four microwave channels which exist on TIROS-N. The context is exactly the same as in that paper, namely, the data used and the definition of the control experiment are identical.

In the earlier paper we used 8 channels, 3 MSU and 5 IR. The reason for using only microwave channels in this paper is that the infrared channels used in the previous paper are affected by clouds in the case of real data. That study only dealt with simulated data, an idealized case.

The results of the previous paper will have to be changed in a major way in order to be used on real data. We have applied the method of fuzzy partitioned clustering to predict tropopause height only using microwave information with an eye towards using it on real data under cloudy conditions. After this, in the second stage, we have developed stratified by tropopause regression temperature retrievals using only the three or four microwave channels for each 40 mb range.

The data used are the 1575 radiosondes collected by N. Phyllips and their corresponding simulated microwave brightness temperatures.

The first step in the experiment is the fuzzy partitioned clustering of the microwave brightness temperatures. This method is a combination of standard hard clustering and discriminant analysis. The new so called "fuzzy partitioned clustering" uses all the generated probabilities of membership of each pattern vector in any of the given clusters. These probabilities are generated by discriminant analysis in order to locate the correct cluster.

The ultimate goal of standard discriminant analysis is to provide the unique (correct) cluster to which the pattern vector belongs. That means it takes into account only the maximum of all the generated probabilities and discards the rest of them.

In our method we use all the probabilities and weight the regressions generated within each cluster. These regression formulas predict the tropopause height from the microwave brightness temperatures. With the standard method of hard clustering and discriminant analysis the overall r.m.s. error for prediction of the tropopause height is 42 mb for the summer and 49 mb for the winter. Using fuzzy partitioned clustering the overall r.m.s. error for prediction is 35 mb for the summer and 45 mb for the winter.

In the second step of the experiment we have stratified the microwave regression temperature retrievals by tropopause height every 40 mb. The control experiment is defined as in the prior paper, namely, the data is stratified by land/ocean, summer/winter, and latitude bands.

A table with total r.m.s. errors for the stratified microwave temperature retrievals and the control experiment is displayed for three and four microwave channels. Significant improvement is obtained at most of the mandatory levels where we have satellite information using our method.

Reference:

1. Munteanu M. J., 1984: "The prediction of tropopause height from clusters of brightness temperatures and its applications in stratified regression temperature retrievals using microwave and infrared satellite measurements", (Proceedings of the Workshop on Advances in Remote Sensing Retrieval Methods, Williamsburg Nov.), submitted for publication at JCAM.

Comparison of R.M.S Retrieved Temperature Errors Stratified by Tropopause

Pressure	Control Experiment 4 MSU	Stratified Regression 4 MSU (40 mb)	Control Experiment 3 MSU	Stratified Regression 3 MSU (40 mb)
30 mb	2.12	1.74	2.11	1.78
50 mb	2.21	1.55	2.23	1.63
70 mb	2.02	1.51	2.09	1.55
100 mb	1.94	1.65	1.92	1.69
150 mb	2.25	1.60	2.41	1.73
200 mb	3.00	2.74	3.13	2.77
250 mb	2.69	2.52	2.77	2.60
300 mb	2.69	2.21	2.76	2.26
400 mb	2.91	2.25	2.90	2.25
500 mb	2.75	2.43	2.73	2.43
700 mb	2.31	2.10	2.51	2.51
850 mb	3.28	3.14	3.33	3.14
1000 mb	2.84	2.92	3.73	3.33
Total	2.57	2.19	2.70	2.35

Applications of Fuzzy Set Theory to Satellite Soundings

Marie - Jeanne Munteanu

Cao Hongxing and Chen Guofan have used fuzzy partitions based on imprecise relations to partition weather processes [1]. These authors have applied the principles of fuzzy similiarity to the partition of daily circulation processes during winter-spring of 1972.

The objective of their study has been to group all circulations into different patterns that possess clear features in order to provide a basis for weather forecasting based on principles of fuzzy relations and cluster analysis.

The purpose of this paper is to propose, first, the introduction of an appropriate fuzzy setting for satellite soundings and then, with this setting in mind, to apply it to clustering methods via unimodal fuzzy sets in the future. Methods of hard clustering analysis and fuzzy partitioned clustering have been applied by the author on simulated data with very encouraging results [3].

The new methodology proposed here is meant to apply to real data. We will start with a discussion of the clustering technique proposed. The notion of a unimodal fuzzy set has been chosen to represent the partition of a data set for two reasons. First, it is capable of detecting all the locations in the vector space where there exist highly concentrated clusters of points, since these will appear as modes according to some measure of "cohesiveness." Second, the notion is general enough to represent clusters that exhibit quite general distributions of points.

The technique is optimal in the sense that it detects all of the existing unimodal fuzzy sets and realizes the maximum separation among them. It is economical in memory space and computational time requirements and also detects groups that are fairly generally distributed in the feature space. The algorithm is a systematic procedure instead of iterative in nature. Most of the other algorithms are not capable of detecting categories with complicated distributions in the feature space and a great many are not applicable to large data sets.

An important distinction between the clustering unimodal fuzzy algorithm and other clustering algorithms is that the latter use a distance measure as the only means of clustering. In [2] Gitman and Levine have introduced another "dimension", the dimension of the order of importance of every point, as an aid in the clustering process. This is accomplished by associating with every point in the set a grade of membership or characteristic value. Thus, the order of the points according to their grade of membership as well as their order according to distance are used in the technique. The order of importance is introduced via the grade of membership notion which, in turn, is introduced via the fuzzy set setting. This latter partitions the sample from a multimodal fuzzy set into unimodal fuzzy sets. This is a very important step since any inversion method will perform considerably better once we divide the multimodal data sets into

ones that are unimodal in nature. The motivation behind this new methodology is the fact that our satellite data as well as our ultimate goal, the set of temperature profiles, are multimodal in nature.

Now we will present the fuzzy sets setting which we propose for the satellite soundings, a setting which has merits by itself and which will also provide the context for the unimodal fuzzy clustering method proposed.

Fuzzy Sets

The theory of fuzzy sets has been invented with the idea of introducing a multivalued logic which could possibly simulate some processes of the human brain. It is well known that the human brain performs much better than any computer in the world in the field of pattern recognition (and many other subtle qualitative decision-making processes).

Experts in artificial intelligence have only begun to use fuzzy sets. This context seems appropriate for satellite sounding because of the nature of the information being associated with a specific weighting function.

Consider the weighting functions as membership functions and form pairs of the soundings and their corresponding membership functions. There are two very interesting cases. First, take the satellite information at the peak of the weighting functions or as representing the information at the peak of the weighting fuctions. In terms of fuzzy sets this represents reducing or approximating the weighting function by one point, namely its peak. The second important case is the mean layer case. We take slices of the weighting functions contained within the layer. There it is possible to define how to extract the optimal information within a layer as well as intermediary steps of approximations. In this way we can define maximum information within a layer and eliminate redundancy by the nature of operations in the fuzzy sets context.

This new context has the potential of providing solutions for the optimal distribution of channels in order to solve important structure of the temperature profile and optimal ways of scanning given certain constraints. For this, methods of optimization theory (among them dynamic programming) should be used.

For the first case, when information from a given channel is considered at one point, classification of sounding data has been proposed with hard clustering and fuzzy partitioned clustering on simulated data. These techniques have been the object of two papers published by the author in the Williamsburg 1984 proceedings.

Further generalizations

If we consider the N-tuple element containing the satellite measurements from one given channel and its varying membership function (with the angle, the angle time, and any other important quantities) in the general context of distributive lattices, then we can define different optimal methods of

extracting information from our satellite data.

For these more complicated assumptions we have to generalize fuzzy sets theory to fit our needs while keeping the same basic assumptions. Specifically, we have to consider fuzzy sets in the framework of distributive lattices. Once the optimal information is derived from satellite data, different methods of inversion could be applied. We also can have an estimate of the error by taking different degrees of approximation of the given satellite data.

Another important point is that combining data optimally could lead to new inversion methods. For example, if we take besides the satellite data, its membership function as a function of angle and the angle itself we can conceive an arrangement of data containing optimal information leading naturally to the use of the computerized tomography method (used by H. Flemming).

One new important approach would be to arrange data optimally for different two dimensional retrievals. We may take information at grid points or along a satellite track.

In more dimensions we may have a two dimensional field such as total ozone which, for example, we want to integrate in the general scheme as a constraint. Taking such surface constraints would represent an optimal approximation in three dimensions while taking information at a point would represent a minimal approximation. Taking data along satellite tracks or other curves in space would be an intermediate approximation for a three-dimensional solution.

In the last part of the abstract a few definitions of fuzzy sets theory are presented.

The theory of fuzzy sets

By fuzziness we mean a type of imprecision which is associated with indistinct sets, that is, classes in which there are no sharp boundaries and no sharp distinction between membership and nonmembership.

Definition: Let $X = \{x\}$ denote a collection of objects (points) x. Then a fuzzy set A in X is a set of ordered pairs

$$A = \{(x, \mu_A(x)): x \in X\}$$

where $\mu_A(x)$ is termed the grade of membership of x in A and $\mu_A: X \to M$ is a function from X to a space M called the membership space.

The choice of M

1. We can assume M as the interval [0,1] with 0 and 1 representing respectively the lowest and the highest grades of membership.

2. More generally, M can be a partially ordered set or more particularly a lattice (which has a maximal and minimal element).

Thus our basic assumption is that a fuzzy set, despite the unsharpness of its boundaries, can be defined precisely by associating with each object x a number between 0 and 1 which represents its grade of membership in A.

Definitions

Normality: A fuzzy set A is normal iff

$$\text{Sup}_X \mu_A(x) = 1.$$

Equality: Two fuzzy sets A and B are equal iff $\mu_A = \mu_B$ that is

$$\mu_A(x) = \mu_B(x)$$

for all $x \in X$.

Containment: A fuzzy set A is contained in or is a subset of a fuzzy set B, $A \subset B$ iff

$$\mu_A \leq \mu_B.$$

Complementation: A' is said to be the complement of A iff

$$\mu_{A'} = 1 - \mu_A.$$

Intersection: $A \cap B$ is said to be the intersection of A and B iff

$$\mu_{A \cap B}(x) = \text{Min}(\mu_A(x), \mu_B(x))$$

for all $x \in X$.

Union: $A \cup B$ is said to be the union of A and B iff

$$\mu_{A \cup B}(x) = \text{Max}(\mu_A(x), \mu_B(x))$$

for all $x \in X$.

Union and intersection are associative, they distribute over each other and satisfy De Morgan's laws. It is easy to verify that

$$\mu_{A' \cup B'} = \mu_{(A \cap B)'}$$

$$\mu_{A' \cap B'} = \mu_{(A \cup B)'}$$

Algebraic Product:

AB is said to be the algebraic product of A and B iff

$$\mu_{AB}(x) = \mu_A(x) \cdot \mu_B(x)$$

for all $x \in X$.

Algebraic Sum:

A + B is said to be the algebraic sum of A and B iff

$$\mu_{A+B}(x) = \mu_A(x) + \mu_B(x) - \mu_A(x) \cdot \mu_B(x)$$

for all $x \in X$.

The algebraic sum and product are associative, but do not distribute over each other. They satisfy a form of De Morgan's laws. It is easy to verify

$(A + B)' = (A'B')'$.

The fuzzy sets as described here as well as the unimodal fuzzy clustering are introduced with an eye towards developing an expert system for the processing and interpretation of real satellite data.

References:

1. Cao, H. and G. Chen, 1980: Fuzzy Partition of Weather Processes, Kexue Tonghao, 25.

2. Gitman, I. and M. D. Levine, 1970: An Algorithm for Detecting Unimodal Fuzzy Sets and its Application as a Clustering Technique, IEEE Trans. Comput., C-19, 583-593.

3. Munteanu, M. J., O. Jakubowicz, E. Kalnay, P. Piraino, 1984: "Applications of Cluster Analysis to Satellite Soundings", Proceedings of the Workshop on Advances in Remote Sensing, November, Williamsburg, Va.

4. Zadeh, L. A., Fuzzy Sets, 1965: Inf. Control, 8, 338-353.

Applications of Some Artificial Intelligence Methods to Satellite Soundings

Marie-Jeanne Munteanu and Oleg Jakubowicz

In this paper we continue the research started in a previous paper Munteanu et. al.[1] The new element is the use of fuzzy partitioned clustering instead of hard clustering for temperature profiles.

We use exactly the same setting, namely, 1575 radiosondes collected by N. Phyllips and the corresponding simulated satellite measurements. The control experiment is formulated in exactly the same way, namely, the usual concept of regression used by NMC based on stratification by land, ocean, summer, winter and latitude bands.

In the first paper we used hard clustering of temperature profiles and discriminant analysis to locate the correct cluster from satellite measurements. In the second step we developed regression temperature retrievals within each cluster and compared the total r.m.s. errors against the control experiment. Excellent results have been obtained, namely, improvements of more than 1° appeared at all of the mandatory levels where we had satellite information.

In this paper our aim was to refine this method using the probabilities of membership of each pattern vector in each of the clusters derived with discriminant analysis.

In hard clustering one takes the maximum probability and considers the corresponding cluster as the correct cluster discarding the rest of the probabilities. In fuzzy partitioned clustering we keep these probabilities and the final regression retrieval is a weighted regression retrieval of several clusters. We have used this method in the clustering of brightness temperatures where the purpose was to predict tropopause height. (See [2]).

This is only the first step towards a fuzzy clustering where we minimize more qualitative functionals than just the euclidean distance. A further refinement in this work is the division of temperature profiles into three major regions for classification purposes.

The results are summarized in the tables where we display total r.m.s. errors. It seems that an approach based on fuzzy logic which is intimately related to artificial intelligence methods holds promise. Larger improvements than in the case of hard clustering are obtained at most of the levels.

References:

1. Munteanu, M. J., Jakubowicz, O., Kalnay E., and Piraino P., 1984: "Applications of Cluster Analysis to Satellite Soundings". (Proceedings of the Workshop on Advances in Remote Sensing Retrieval Methods, Williamsburg, Va. Nov.), submitted for publication at JCAM.

2. Munteanu, M. J., 1984: "The prediction of tropopause height from clusters of brightness temperatures and its applications in the stratified regression temperature retrievals using microwave and infrared satellite measurements", (Proceedings of the Workshop on the Advances in Remote Sensing, Williamsburg, Va., Nov.).

Comparison of RMS Temperature Retrievals (Summer) 5IR & 3 MSU

Pressure	Control Experiment	Clusters of Temperature	Fuzzy Partitioned Clusters of Temperatures
30 mb	2.00	1.92	1.90
50 mb	1.88	1.76	1.69
70 mb	1.69	1.59	1.39
100 mb	1.66	1.52	1.41
150 mb	1.93	1.69	1.40
200 mb	2.51	1.87	1.68
250 mb	2.36	1.80	1.59
300 mb	2.03	1.59	1.39
400 mb	1.80	1.37	1.24
500 mb	1.63	1.28	1.09
700 mb	1.84	1.51	1.39
850 mb	2.29	1.86	1.85
1000 mb	2.29	2.16	2.16

Figure 1

Comparison of RMS Temperature Retrievals (Winter) 5IR & 3 MSU

Pressure	Control Experiment	Clusters of Temperature	Fuzzy Partitioned Clusters of Temperatures
30 mb	4.71	4.19	4.09
50 mb	2.88	2.43	2.35
70 mb	1.89	1.74	1.70
100 mb	2.31	1.94	1.89
150 mb	2.15	1.97	1.88
200 mb	2.36	2.16	1.70
250 mb	2.43	1.86	1.80
300 mb	2.53	1.81	1.69
400 mb	2.40	1.73	1.51
500 mb	2.62	1.77	1.63
700 mb	2.57	1.86	1.69
850 mb	2.75	2.18	2.01
1000 mb	2.72	2.30	2.10

Figure 2

C. ANALYSIS AND FORECAST MODEL DEVELOPMENT

A Factored Implicit Scheme for Numerical Weather Prediction with Small Factorization Error

J. M. Augenbaum, S. E. Cohn[1], and D. Marchesin[2]

The time step used in current models for integrating the global baroclinic primitive equations is limited by the Courant-Friedrich-Lewy (CFL) stability criterion. In schemes based on explicit time discretization, for example, whether finite-difference, pseudospectral or finite element in space, the time step cannot exceed the quotient of the smallest spatial interval and the maximum phase speed. This is a severe restriction first of all because the fastest waves propagate roughly ten times faster then the waves which carry most of the atmosphere's synoptic scale energy. Second, on a uniform latitude-longitude grid the mesh spacing becomes very small near the poles. As a consequence the time discretization error of explicit schemes is much smaller than the spatial discretization error, especially in middle and low latitudes.

By using a scheme with more desirable stability properties, it is possible to increase the time step without effecting overall forecast accuracy, thereby increasing computational efficiency. Recently, Cohn et al. (1985) have introduced a fully implicit scheme for the barotropic primitive equations based on the work of Beam and Warming (hereafter referred to as B-W). The B-W scheme is unconditionally linearly stable and allows use of a large time step, whose size is determined solely by accuracy requirements. The method is based on a spatial factorization of the implicit operator into one-dimensional operators, and yields second order accuracy in time and fourth order accuracy in space. The scheme is efficient because it only requires the solution of one-dimensional block-tridiagonal linear systems. In an effort to analyze the accuracy of the B-W scheme, for meteorological applications, we have carried out an analysis of the factorization error for a linear shallow water system on a tangent plane. By discretizing the equations only in the time domain, while assuming a spatial variation of the form $\hat{W}^n = \hat{W}^n e^{i(kx + ly)}$ we can derive analytic expressions for the amplification matrix, F(k,l), in terms of the wave number (k,l) i.e.

$$\hat{W}^{n+1} = F(k,l)\, \hat{W}^n$$

The eigenvalues of F, for a given set of wave numbers, can then be used to find amplitudes and periods of the various wave components of the solution. This method can also be used to find the periods and amplitudes of the various modes for the unfactored Crank-Nicolson scheme (referred to as C-N) and, with a slight modification, the continuous (true) solution (referred to as CONT).

Numerical results (presented in table 1) show that, for large time steps, the factorization error can be significant, even for the slowly propagating Rossby modes. We have formulated a new scheme based on a more accurate factorization of the equations. By grouping separately the terms of the equations which give rise to the fast and slow motion, the equations are factored

[1] Courant Institute of Mathematical Sciences, New York University
New York, N. Y. 10012

[2] Department of Mathematics, Pontificia Universidade Católica do Rio de Janiero, Rio de Janeiro-RJ, CEP22453, Brazil

in a more accurate way. The fast-slow factorization completely eliminates the factorization error. If each of the fast and slow factors are now factored again, this time according to spatial components, the resulting scheme only involves the solution of one-dimensional linear systems, and is computationally efficient. We have shown that the factorization error for the slow mode component of the solution is negligible for this new scheme (which we refer to as F-S).

In table 1 we present a comparison of several implicit schemes (including the semi-implicit scheme, which we refer to as SIMP) for a Rossby wave with wavenumber 16,8 in x,y directions.

The results of table 1 show that the fast-slow scheme is accurate, even for large time steps, for middle and low latitudes.

We are currently conducting numerical experiments to compare the various schemes for the full nonlinear barotropic shallow water equations.

Table 1

Period (in hours) for the Rossby wave component of a 16 x 8 wave with Δt = 30, 60, 120 min. at lat θ = 0°, 45°.

	Lat = 0°			Lat = 45°		
Δt(min) / scheme	30	60	120	30	60	120
CONT	27.82	27.82	27.82	20.90	20.90	20.90
C-N	27.85	27.94	28.30	20.94	21.08	21.59
B-W	30.70	39.35	74.01	23.60	31.73	64.43
F-S	27.84	27.89	28.07	20.93	21.01	21.33
SIMP	27.76	27.58	26.81	20.81	20.53	19.25

References

1. J. M. Augenbaum, S. E. Cohn, D. P. Dee, E. Isaacson, and D. Marchesin; "A fully implicit scheme for global numerical weather prediction." To appear in preprint Volume, 7th Conf. on Numerical Weather Prediction, June 17-20, 1985, Montreal, Canada. American Meteorological Society, Boston, Mass.

2. S. E. Cohn, D. Dee, E. Isaacson, D. Marchesin, and G. Zwas; "A fully implicit scheme for the bartropic primitive equations" to appear in Mon. Wea. Review (1985).

Comparison of Optimum Interpolation and Cressman Analyses

W. E. Baker, S. C. Bloom, and M. S. Nestler

The objective of this investigation is to develop a state-of-the art optimum interpolation (O/I) objective analysis procedure for use in numerical weather prediction studies. A three-dimensional multivariate O/I analysis scheme has been developed for the purpose. Some characteristics of the GLAS O/I compared with those of the NMC and ECMWF systems are summarized in Table 1. Some recent enhancements of the GLAS scheme include a univariate analysis of water vapor mixing ratio, a geographically dependent model prediction error correlation function and a multivariate oceanic surface analysis (Bloom et al., 1984).

Figure 1 compares the 24 h and 48 h forecasts from 0000 GMT 13 January 1979 initial conditions provided by the O/I analysis scheme with forecasts from a successive correction method (SCM) of analysis developed earlier. As may be seen in Fig. 1, the forecast of the intensity and position of the cyclone which moves northeastward across the United States as well as the ridging which follows, is more accurate with the O/I than with the SCM.

Future work includes completing vectorization of the O/I on the Cyber 205, a detailed comparison with the SCM, real and simulated data impact studies and experiments with normal mode initialization.

Reference

Bloom, S. C., W. E. Baker and M. S. Nestler, 1984: Multivariate optimum interpolation of surface pressure and winds over oceans. Preprints Tenth Conf. on Weather Forecasting and Analysis, 25-29 June, Amer. Meteor. Soc., Clearwater, Florida, 106-108.

TABLE 1. Characteristics of the GLAS OI compared with those of other systems.

SALIENT FEATURES	GLAS	NMC	ECMWF
APPROACH	3-D; MULTIVARIATE IN Z,U,V UNIVARIATE IN W	3-D; MULTIVARIATE IN Z,U,V UNIVARIATE IN RH	3-D; MULTIVARIATE IN Z,U,V UNIVARIATE IN Q
RESOLUTION	18 LEVELS; 4° x 5° (2-D) 12 LEVELS; 4° x 5° (3-D)	12 LEVELS; 3.75° UPPER AIR, 2.5° SURFACE	15 LEVELS; 1.875°
AUTOCORRELATION FUNCTION	DAMPED COSINE FOR Z DAMPED EXPONENTIAL FOR W	GAUSSIAN	BESSEL
CROSS-CORRELATION MODEL	GEOSTROPHIC (SCALED TO 0.0 AT EQUATOR)	SAME	SAME
ASSUMPTION OF ISOTROPY	Z (YES); U,V (NO)	SAME	SAME
GEOGRAPHICALLY DEPENDENT μ	YES	NO	YES (LATITUDINALLY DEPENDENT)
MULTIVARIATE SURFACE ANALYSIS	YES (EKMAN BALANCE)	YES (GEOSTROPHIC)	YES (GEOSTROPHIC AT 1000 MB)

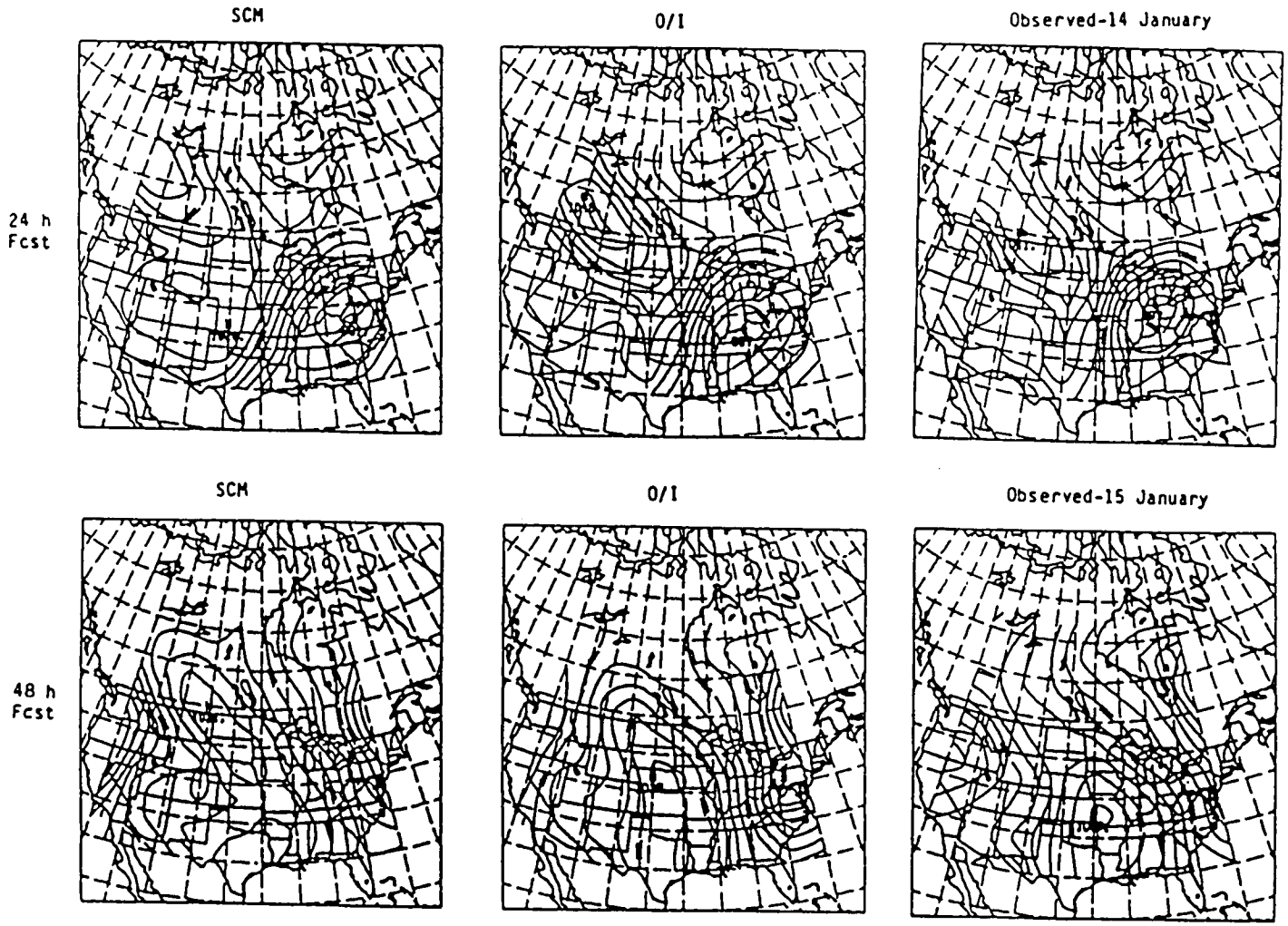

Fig. 1. OI and SCM forecasts from 0000 GMT 13 January 1979.

Derivation of Model Topography

R. C. Balgovind

In the GLA Fourth-Order model it is necessary to represent the topography. In doing so one has to address the problem of the representation of the topography at grid points. Topographies we prepared were for the 4° x 5° and 2° x 2.5° forecast models. The tabulated source data came from the Navy Fleet Numerical Oceanography Center at Monterey. This source has the global elevation given at every 10 minutes in latitude and longitude. The accompanying figures show six examples of different topographys [O1, S1, S23, S3, Q3 and T1] for the 4° x 5° model derived from the source data.

We first attempted to derive an envelope topography. An example of this is the T1 obtained by taking local mean plus one standard deviation at each grid point and sigma filtering it. We found this method to be greatly influenced by large standard deviations at steep mountains.

The O1 topography is just the local mean. The S1 is obtained by Sigma* filtering in both latitude and longitude the mean O1. S2 is when the operation is applied twice and S3 thrice. Q3 is the sigma filtered local mean of the upper third quantile of the source data - that is the mean of the one third of the largest source data.

Presently experiments are underway to determine which is the best topography for the Fourth-Order model. Preliminary results indicate a close contest between Q3 and S1.

* For Sigma FIlter see paper by that name in this review.

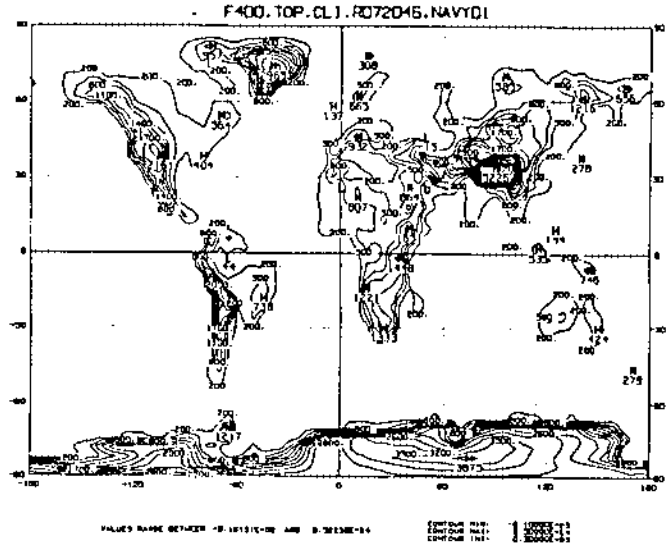
F400.TOP.CLI.R072046.NAVY01

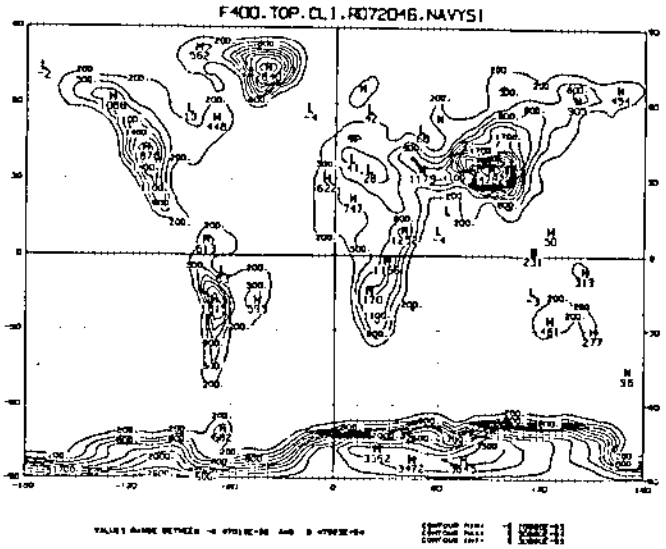
F400.TOP.CLI.R072046.NAVYS1

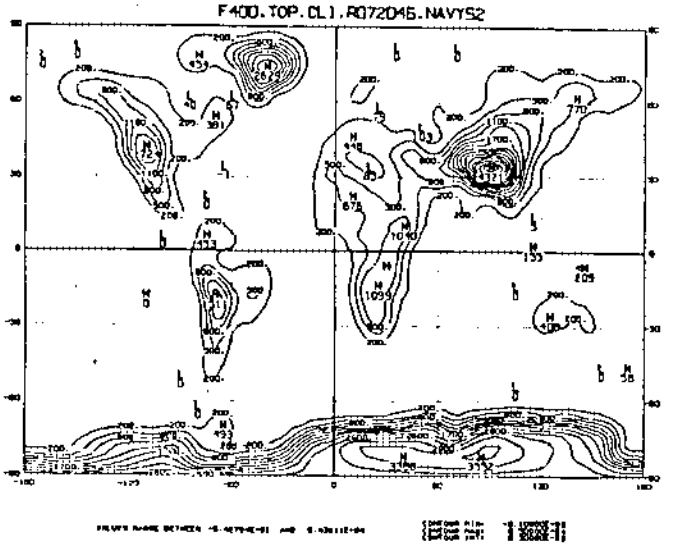
F400.TOP.CLI.R072046.NAVYS2

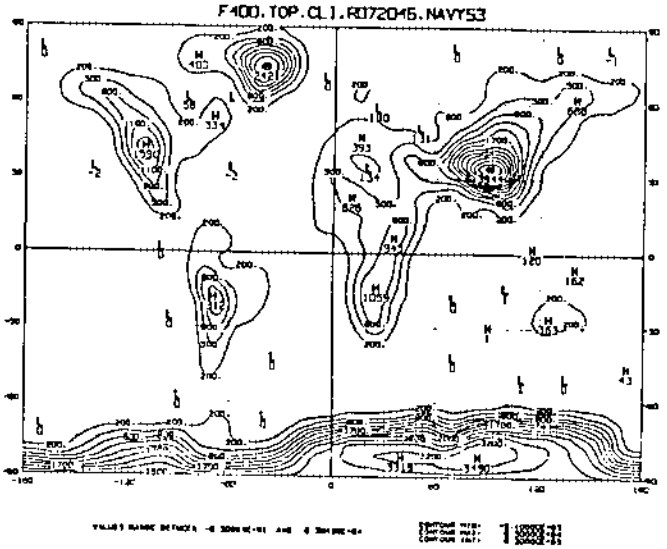
F400.TOP.CLI.R072046.NAVYS3

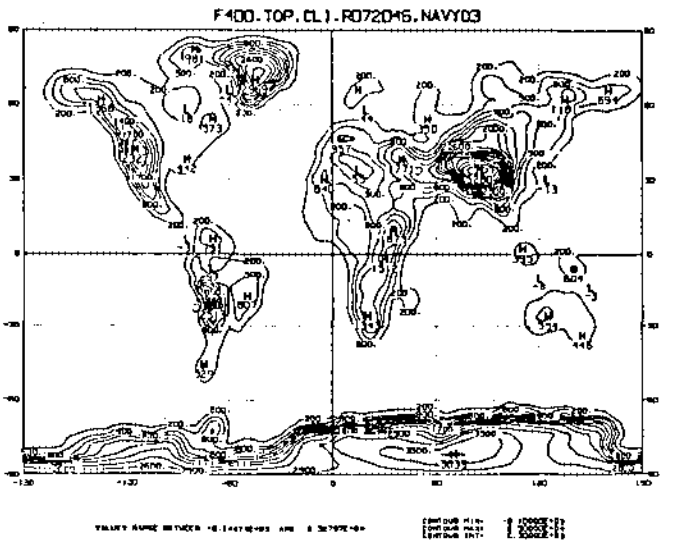
F400.TOP.CLI.R072046.NAVY03

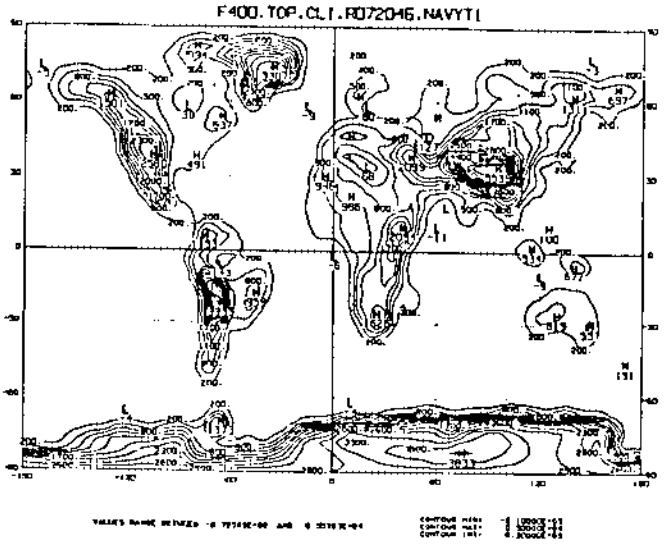
F400.TOP.CLI.R072046.NAVYTI

Sigma Filter

R. C. Balgovind

In deriving the topography for the GLA Fourth-Order model we needed to smooth the topography. This is in order to remove the Gibbs phenomenon. The Gibbs phenomenon occurs whenever we truncate a Fourier Series.

Sigma filtering is smoothing using Sigma factors. Cornelius Lanczos (1966) introduced the Sigma factors for the purpose of reducing the Gibbs phenomenon. The idea is that for a given Fourier Series

$$f_N(t) = a_o/2 + \sum_{k=1}^{N} [a_k \cos kt + b_k \sin kt]$$

we apply the averaging operator

$$\frac{N}{2\Pi} \int_{t - t/N}^{t + t/N} f_N(x)dx$$

The result of this is a smooth field

$$f_n(t) = \frac{a_o}{2} + \sum_{k=1}^{N} \sigma_k [a_k \cos kt + b_k \sin kt]$$

where

$$\sigma k = \begin{cases} 1 & k = 0 \\ \dfrac{\sin(\frac{k\pi}{N})}{k\pi/N} & \text{otherwise} \\ 0 & k = N \end{cases}$$

That is the smooth Fourier series is nothing but the orginal Fourier series with its coefficients multiplied by corresponding sigma factors.

This operator can be applied many times to obtain high order sigma filtered field and is easily applicable using FFT. We found this filter beneficial in deriving the topography.

Reference

Lanczos, C., 1966: Discourse on Fourier Series, Hafner Publishing, New York.

Recent Developments in Nonlinear Normal Mode Initialization

S. Bloom

In order to assess the importance of a balanced initial condition upon GLAS GCM forecasts and assimilation cycles, an effort to combine previous work on normal mode initilization at GLA (Bloom, 1982, 1983; Navon et al., 1983) is currently underway with the goal of developing an initialization process for the production version of the GLAS 4th order GCM. The major aspects of this work fall into two parts: vectorization of the linear projector code (Bloom, 1983), and the insertion of the mode projector and Machenhauer iteration algorithm into the full GLAS GCM.

Memory and paging constraints place restrictions on the number of horizontal modes stored for initialization purposes, as well as on the manner in which they are stored. Only the first five vertical structures of the gravity modes are used; these account for only 40% of the total set of the model's normal modes. One source of difficulty encountered in moving the projector code to the CYBER 205 lay in the use of different FFT packages on the two machines (NCAR on the Amdahl, Temperton on the Cyber). Differing phase and normalization conventions provided many elusive coding errors.

For the preliminary studies, a Machenhauer nonlinear normal mode initialization technique (Williamson and Temperton, 1981) is used. This method entails the insertion of a modified version of the mode projector into the full GCM, and the modification of the GCM to allow for iterative calls to the projector. The main difficulties encountered with inserting the projector code have been in obtaining the correct communication among the various model and projector commons, and in performing the update to the correct variables within the projector. The GCM is integrated for one time step in order to estimate the time tendencies of the 'fast' gravity mode coefficients; however proper care must be taken to save the original set of fields since the 'slow' coefficients are never computed. If the original fields are not saved, the iterative process diverges. This result is due to the 'slow' coefficients evolving in time away from the adjusted 'fast' coefficients; the resulting unbalanced fields quickly develop unrealistic winds. The GLAS GCM also has a special treatment of the fields at the poles (using subroutines POLINP and POLOUT); if this is ignored during the iterations, wildly unrealistic winds and pressures ensue. Finally, if a timestep is chosen too small (for the model integration to estimate time tendencies), then truncation error will cause the iterations to diverge.

The initialization process is still undergoing testing. Preliminary results do show the Machenhauer process to be convergent over 4 iterations if only the external vertical structure is initialized. However, tests initializing the first two vertical structures diverge after the second iteration. Currently, a shallow water version of the GCM (the same one as used in Navon et al., 1983) is being used to test various parts of the initialization algorithm.

References

Bloom, S. C., 1983: Normal Modes of the GLAS 4th Order Model. Research Review - 1982, NASA Tech. Memo. 84983, 99-103.

Bloom, S. C., 1984: Design of a Linear Projector for Use with the Normal Modes of the GLAS 4th Order GCM. Research Review - 1983, NASA Tech. Memo. 86053, 101-105.

Navon, I. M., S. Bloom and L. Takacs, 1984: Computational Aspects of the Nonlinear Normal Mode Initialization of the GLAS 4th Order GCM. Research Review - 1983, NASA Tech. Memo. 86053, 106-112.

Williamson, D. L., and C. Temperton, 1981: Normal Mode Initialization for the Multilevel Grid-Point Model. Part II: Nonlinear Aspects. Mon. Wea. Rev., 109, 744-757.

Comparison of Two Orographical Data Sets for the GLAS Fourth Order GCM

H. M. Helfand, R. Balgovind, R. Dlouhy, J. Pfaendtner

The development of a 2° latitude by 2.5° longitude version of the GLAS Fourth Order General Circulation Model has necessitated the specification of a correspondingly fine horizontal resolution orographic data set to act as a lower boundary condition for the GCM. Elsewhere in this volume, R. Balgovind has described the development of two such fine resolution orographic data sets which he has labeled the S1 and the Q3 topographies. These differ from one another primarily in their respective height specifications over rugged terrain. The S1 topography attempts to relate the mean areally-averged height of such terrain while the Q3 topography emphasizes the effect of the flow of the tallest peaks in such regions by specifying an exaggerated "significant height" as described by Balgovind.

In order to assess the relative merits of these two orographic data sets, we have initiated a series of tests to evaluate the comparative weather forecasting and climate simulation skills of the GLAS Fourth Order GCM when the S1 and Q3 topographies are applied to the lower boundary. These tests were carried out at both 2° x 2.5° and 4° x 5° horizontal resolutions.

Three sets of Northern Hemispheric winter forecasts at the 2° x 2.5° resolution indicate that the Q3 topography gives slightly better results over the Northern Hemisphere than does the S1 topography. The improvement did not occur until after 4 days for Skill Score 1 and after 2 to 3 days for root mean square error. Fig. 1 illustrates a typical example of this improvement. There were no significant trends for forecasts over the Southern Hemisphere on tropical regions. No forecasts were available at this resolution for the summer season.

The results of the 4° x 5° forecasts were mixed. For the first 3 to 4 days, sea level pressure forecasts for the Northern Hemisphere were better with the Q3 topography for a period of time. After this time, there were no consistent trends.

In the Southern Hemisphere, forecasts with the Q3 topography were slightly better than those with S1 topography but not until after 3 to 6 days. In the tropics, a June forecast was substantially better with the S1 topography while the (Northern Hemisphere) winter forecasts favored the Q3 topography at sea level and were mixed at 500 mb.

It is apparent that more forecasts will be necesary at both horizontal resolutions before any definitive conclusions can be made regarding the choice of an optimal orographic data set.

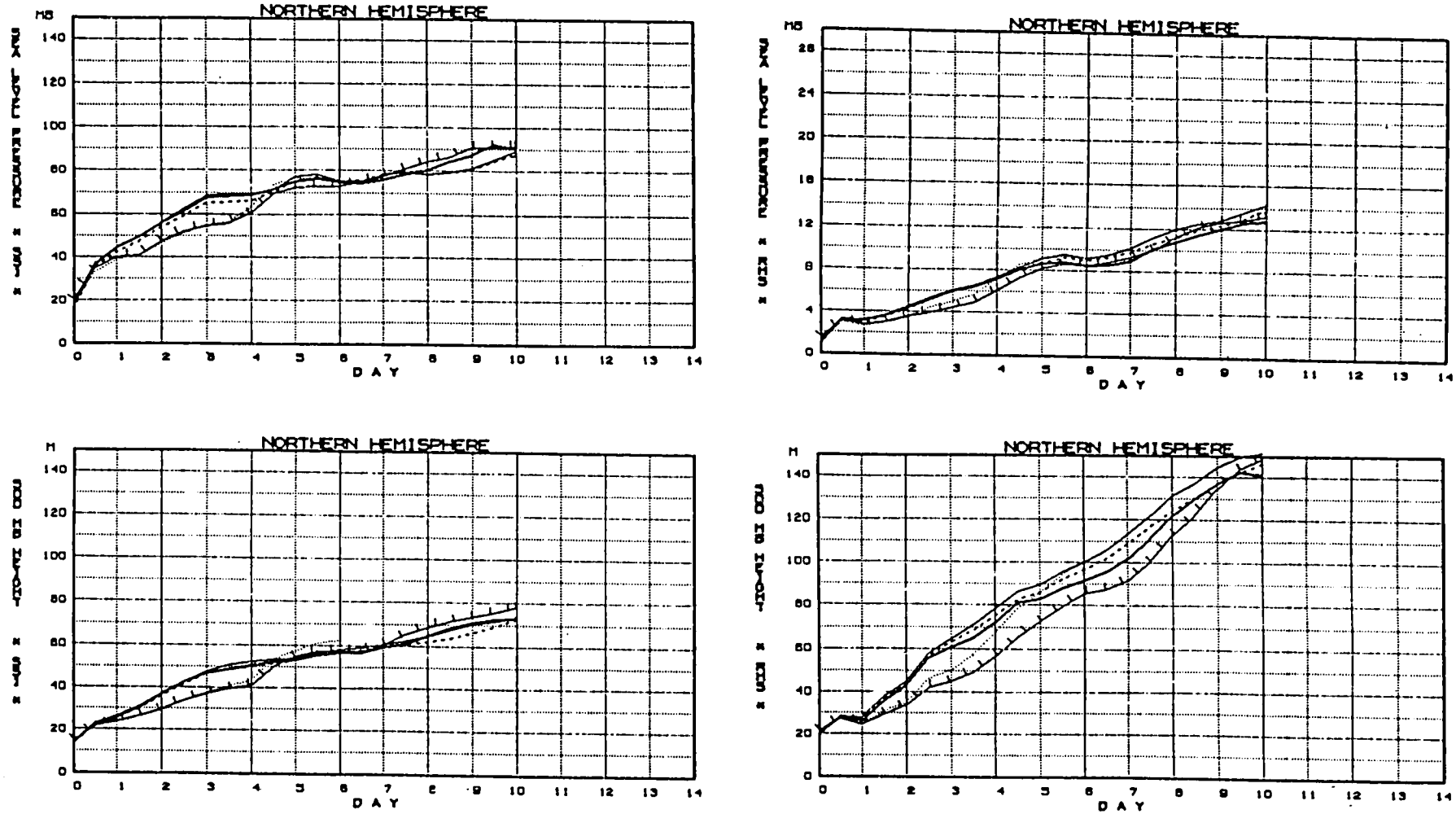

Dotted = 2° x 2.5° with S1 topography
Ticked = 2° x 2.5° with Q3 topography
Dashed = 4° x 5° with S1 topography
Heavy = 4° x 5° with Q3 topography
Solid = 4° x 5° with old topography

Fig. 1 Forecast skill for the Northern Hemisphere for a forecast beginning on Jan. 5, 1979. The top panels represent sea level pressure scores, while the bottom panels represent 500 mb heights. Skill score 1 is shown in the left panels, and root mean square error on the right.

Development and Testing of the Variable Vertical Resolution Fourth Order GCM

H. M. Helfand, R. Dlouhy, J. Pfaendtner, L. L. Takacs

The vertical coordinate of the Fourth Order Model has been generalized so that the model can now run with an arbitrary number of vertical layers and so that the thicknesses of these layers can be arbitrarily specified (in the σ-coordinate). This Variable Vertical Resolution (VVR) version of the Fourth Order Model will soon replace the current production model although it will probably still be run with 9 equally spaced layers when used for production purposes.

In addition to the generalization of vertical interpolation and quadrature calculation and of vertical array dimensioning, the VVR model contains the following changes:

i) The strapping scheme for cumulus convection has been generalized from the current 2-2-2 scheme to a three-layer scheme whose strapping parameters can be arbitrarily specified through namelist parameters.

ii) The redistribution of convective heating is now specified by a conserving quadratic interpolation scheme and the scheme for the redistribution of convection moistening has been generalized.

iii) A relative humidity criterion for the onset of cumulus convection (Helfand, 1981) has been specified as a namelist option.

iv) Subroutine COMP3 has been fully modularized for ease of testing and development of new physical parameterization schemes.

v) The computation of large-scale precipitation has been improved by limiting the evaporation of falling rainwater to the amount which can be held by the receiving atmospheric layer as is computed by linearization about the state of that layer before such evaporation occurs.

vi) Optical thicknesses of clouds are computed to reflect changes in the vertical grid and in the strapping parameters for convective clouds.

vii) Planetary Boundary Layer (PBL) parameters are computed in the basis of the depth of the lowest model layer.

Presently physical parameterization schemes are being developed so that the vertical structure of the PBL can be explicitly resolved in the VVR model but this work is currently to be regarded only as experimental.

To assess the skill of the VVR model, it has been run with 9 equally spaced layers and compared with the current production model. In two Northern Hemispheric winter cases and one summer case, the two models were virtually identical in forecast skill for 6 to 7 days. After that the VVR model was slightly better in the winter cases and the production model was slightly better in the summer case. The only exception to this was that after 2 days the production model gave slightly more skillful 500 mb forecasts in the tropics for the summer case.

Surprisingly, there were substantial differences in the climatologies produced by the two models. The mean January 500 mb height fields for simulations initialized at 0Z, 15 December 1978, for example (see figure 1), were markedly different in the location and shape of a North Atlantic ridge, in the location of a trough over central Europe, in the shape and westward extent of the Siberian low, and in the zonality of the Southern Hemispheric and mid-latitude westerlies.

The simulation by the VVR model seems to be more in accord with mean observations for January 1979 which suggests that the VVR model might give better extended range weather forecasts. The simulation by the production model, on the other hand, appears to be in better agreement with the climatological mean with the exception of European trough. Obviously, the comparison of the two models warrants further study.

References

Helfand, H. M., 1981: Dependence of tropospheric temperatures on the parameterization of cumulus convection in the GLAS model of the general circulation. Mon. Wea. Rev., 109, 65-76.

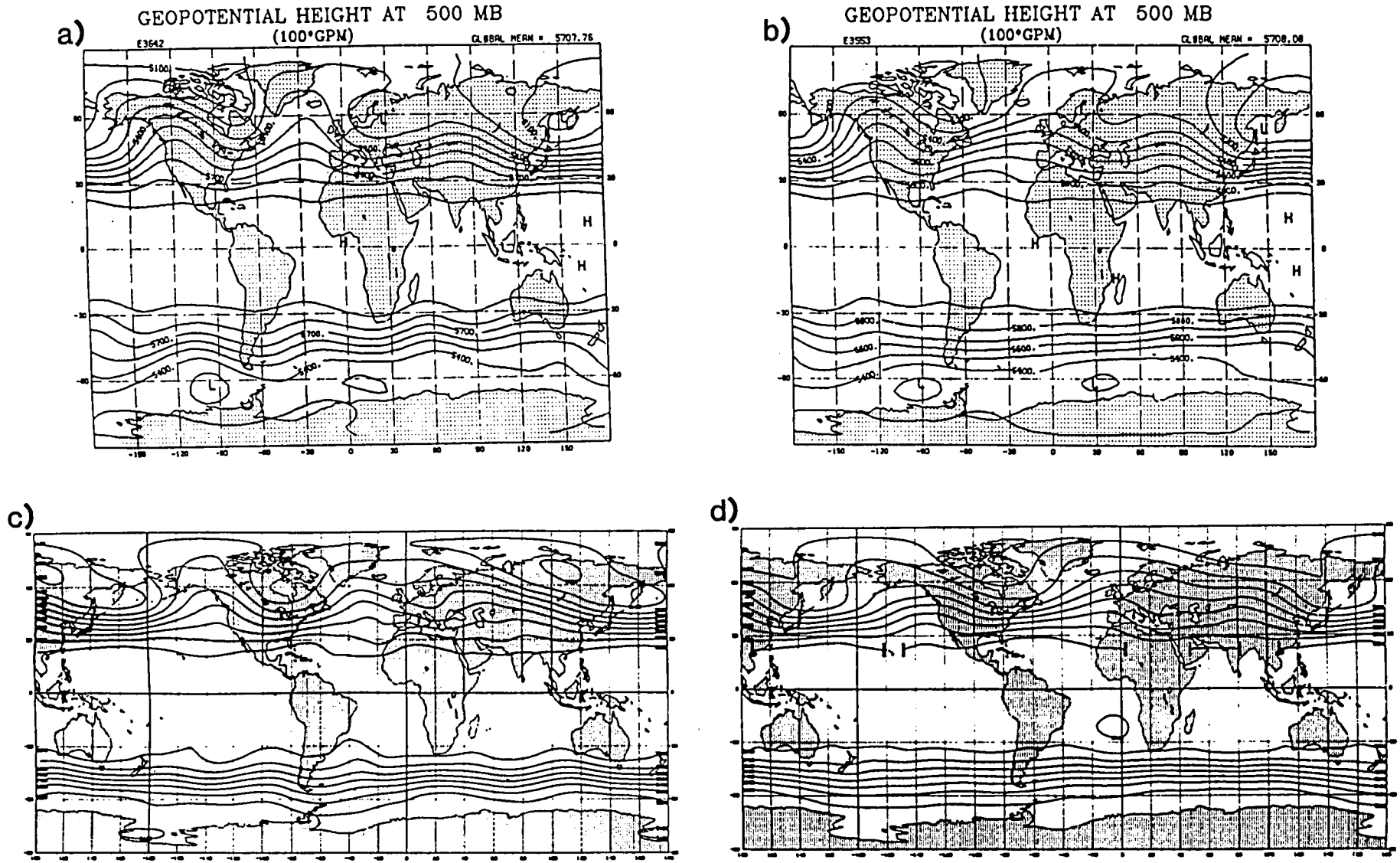

Fig. 1 - Mean geopotential height field for the period 1 January - 1 February for a) an integration with the VVR model begun at 0Z 15 December, 1978, b) a similar integration with the production model, c) observations for the month of January, 1979, and d) climatology for the month of January.

Parameterization of Surface Fluxes in the VVR Fourth Order GCM

H. M. Helfand

The Variable Vertical Resolution (VVR) option of the GLAS Fourth Order GCM (described elsewhere in this volume as well as in the 1980/81 Research Review) allows one to enhance the vertical resolution of the region of the atmosphere adjacent to the earth's surface. This, in turn, makes it possible to compute turbulent suface fluxes of heat, momentum and moisture directly from the prognosticated properties of the lowest model layer by use of the Monin-Obukhov surface layer similarity theory. However, one must be extremely cautious in doing so, for the similarity theory applies formally only to the "constant flux" surface layer which is but a few tens of meters deep. It is not practically feasible to work with a lowest GCM layer thin enough to satisfy these formal constraints.

It is fortuitous that, at least under conditions of neutral stratification, the similarity theory can be extended beyond its formal limits. Panofsky (1973) points out that, because of the cancellation of opposing effects (decreasing stress and less-than-linearly increasing mixing length), the theory still gives reasonable looking results, when the distance from the ground becomes as large as 150 m.

It is not infeasible to run the VVR model with a lowest layer thickness on the order of 300 m (the center of the layer would then be 150 m above the earth's surface), and so if one can prescribe similarity functions $\phi_m(\zeta)$ and $\phi_h(\zeta)$ to adequately describe the entire "extended surface layer", the problem of surface flux parameterization is solved.

For small values of $|\zeta|$, the similarity functions should approach the behavior of the similarity functions of conventional surface layers such as those of Businger et al. (1971):

$$\phi_m(\zeta) = \begin{cases} (1 - \gamma_m\zeta)^{-1/4} & \zeta \leq 0 \\ 1 + \alpha_m\zeta & \zeta \leq 0 \end{cases}$$

$$\phi_h(\zeta) = \begin{cases} (1 - \gamma_h\zeta)^{-1/2} & \zeta \leq 0 \\ 1 + \alpha_h\zeta & \zeta \leq 0 \end{cases} \qquad (1)$$

As $|\zeta|$ becomes large, ϕ_m and ϕ_h should exhibit the appropriate asymptotic behavior. For the unstable case $\zeta < 0$, this behavior is

$$\phi_{m,h}(\zeta) \sim \zeta^{-1/3} \quad . \qquad (2)$$

For the stable case $\zeta > 0$, Clarke's (1970) mean stable case for the Wangara Experiment suggests the asymptotic form

$$\phi_{m,h}(\zeta) \sim \zeta^{-1} \quad . \tag{3}$$

To interpolate between the limits (1) and (2), the similarity functions for the unstable case $\zeta < 0$ have been taken as the solutions to

$$\phi_m^4 - \gamma_m \zeta \phi_m^3 = 1$$

$$\phi_h^2 - \gamma_h \zeta \phi_h^3 = 1 \quad . \tag{4}$$

For the stable case $\zeta > 0$, the similarity fuctions are

$$\phi_{m,h}(\zeta) = \frac{1 + \alpha_{m,h}\, \zeta_1}{1 + \beta_{m,h}\zeta\, (1 + \alpha_{m,h}\zeta_1)} \tag{5}$$

where

$$\zeta_1 = \min\, (\zeta_1,\ \zeta^*_{m,h}) \quad .$$

Thus (5) interpolates between (1) and (3).

For the stable case, $\frac{\phi_{m,h}(\zeta)}{\zeta}$ can be integrated directly, while for the unstable case, the integrals can be integrated in terms of the solutions of (4) which can be solved, in turn, through mathematical iteration. The momentum and heat transfer coefficients so obtained are shown in Fig. 1. Note that they approach the solutions of Businger et al. (1971) for small $|Ri_b|$. For $Ri_b \to -\infty$ one has

$$C_H = C_U C_T \sim Ri_b^{1/2}$$

which gives the proper asymptotic limit

$$\overline{w\theta_s} = C_H\, U\, \Delta\Theta \sim \Delta\Theta^{3/2} \quad .$$

For $Ri_b \to \infty$ the surface fluxes remain positive which correctly reflects the facts that the Richardson number remains subcritical in an increasingly narrower neighborhood of the earth's surface.

References

Businger, J. A., J. C. Wyngaard, Y. Izumi, and E. F. Bradley, 1971: Flux profile relationships in the atmospheric surface layer. J. Atmos. Sci., 28, 181-189.

Clarke, R. H., 1970: Observational studies in the atmospheric boundary layer. Quart. J. Roy. Meteoro. Soc., 96, 91-114.

Panofsky, H. A., 1973: Tower micrometeorology. In Workshop on Micrometeorology, D. A. Haugen, ed., Boston, Amer. Meteoro. Soc., 392 pp.

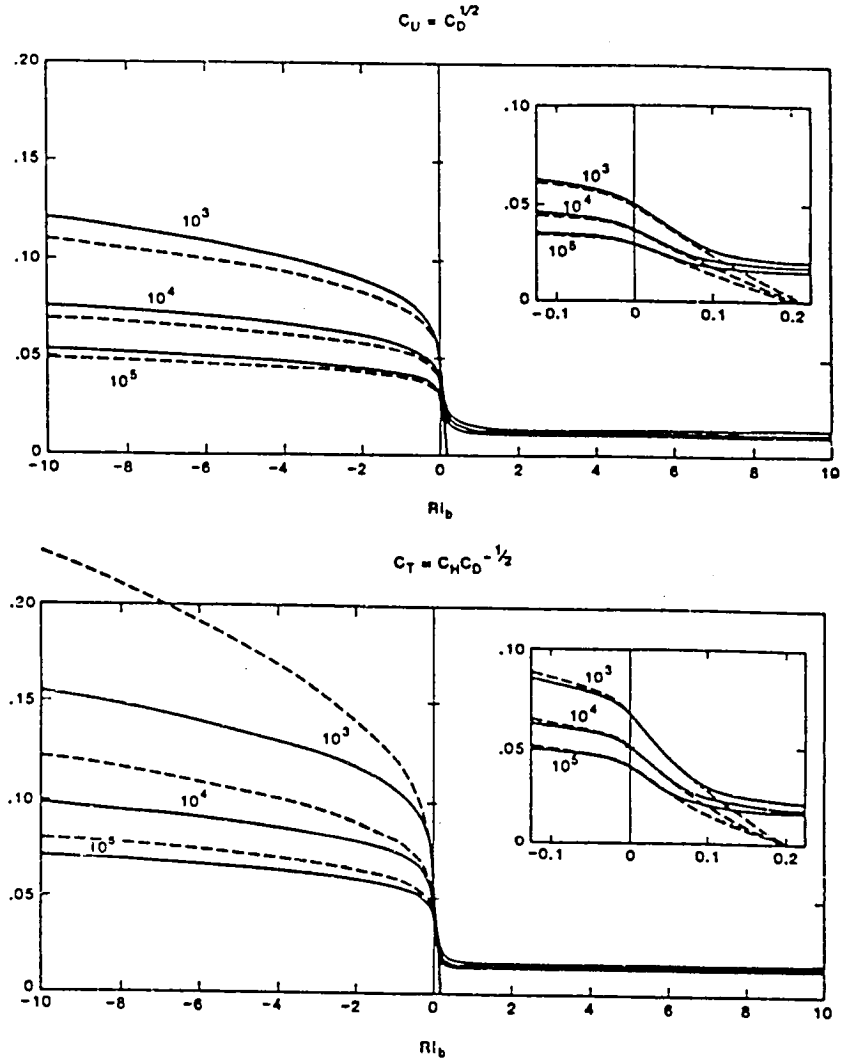

Fig. 1 Momentum and heat transport coefficients C_U and C_T versus bulk Richardson number Ri_b. Solid lines represent present model while dashed lines represent the model of Businger et al. (1971). Graphs are given for h/z_0 equal to 10^3, 10^4 and 10^5 where h is the depth of the surface layer and z_0 is the surface roughness height, described elsewhere in this volume. The inset shows the behavior of the curves on an expanded Richardson number scale about the neutral case $Ri_b = 0$.

Specification of Surface Roughness

Over Oceans in the GLAS Fourth Order GCM

H. M. Helfand

The surface roughness height z_0 is a parameter which measures the effect of surface irregularities on the mean profiles which occur in the atmospheric surface layer. Over land surfaces, z_0 is a function of soil composition, plant canopy type and distribution and other factors such as buildings and structures. Over open water, z_0 depends only on the distribution of waves, wavelets and other surface irregularities. These, in turn, are thought to be determined by the mean wind within the surface layer.

Large and Pond (1981) have derived an empirical relationship between the mean wind speed U_{10} at the ten meter level over open water and the neutral drag coefficient C_{DN} Their relationship covers the range $U_{10} \geq 2$ ms^{-1}.

Earlier, Kondo (1975) had computed a relationship between U_{10} and C_{DN} on the basis of laboratory observations which extended down to the range of infinitely small wind speeds. Fig. 1 is an interpretation between the relationships of Large and Pond for large wind speed and of Kondo for small wind speed.

One can convert the relationship of Fig. 1 to the relationship between the wind stress velocity

$$u_* = C_{DN}^{1/2} U_{10}$$

and the surface roughness length z_0. This has been done for the Monin - Obukhov surface flux scheme in the GLAS Model so that z_0 can be expressed as

$$z_0 = \frac{A_1}{u_*} + A_2 + A_3 u_* + A_4 u_*^2 + A_5 u_*^3,$$

Where the A_i are defined separately over three separate domains of u_*. The function (1) is shown in Fig. 2.

REFERENCES

Kondo J., 1975 : Air-sea bulk transfer coefficients in conditions. Bound. Layer Meteoro., 9, 91-112.

Large W.G. and S. Pond, 1981: Open ocean flux measurements in moderate to strong winds. J. Phys. Ocean , 11, 324-336.

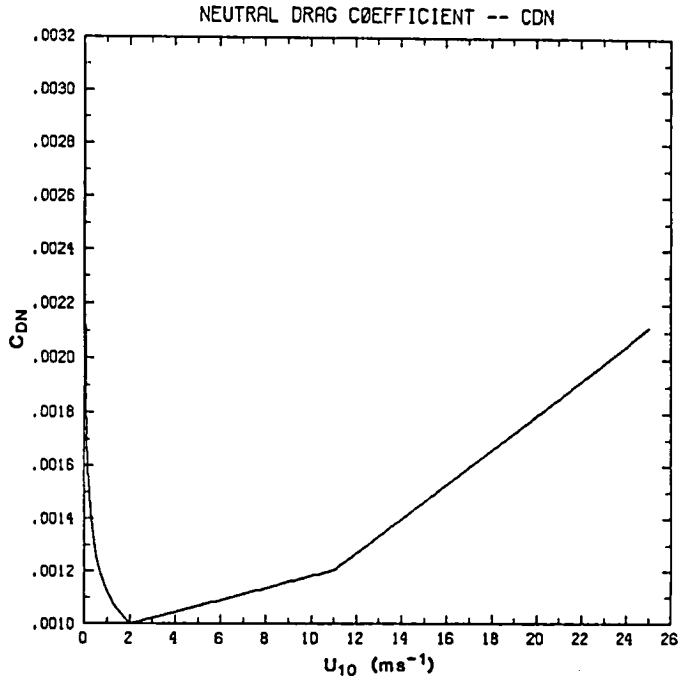

Fig. 1. Neutral drag coefficient C_{DN} expressed as a function of 10m wind speed U_{10} given in ms $^{-1}$. This function interpolates between that of Large and Pond (1981) for strong winds and that of Kondo (1975) for weak winds.

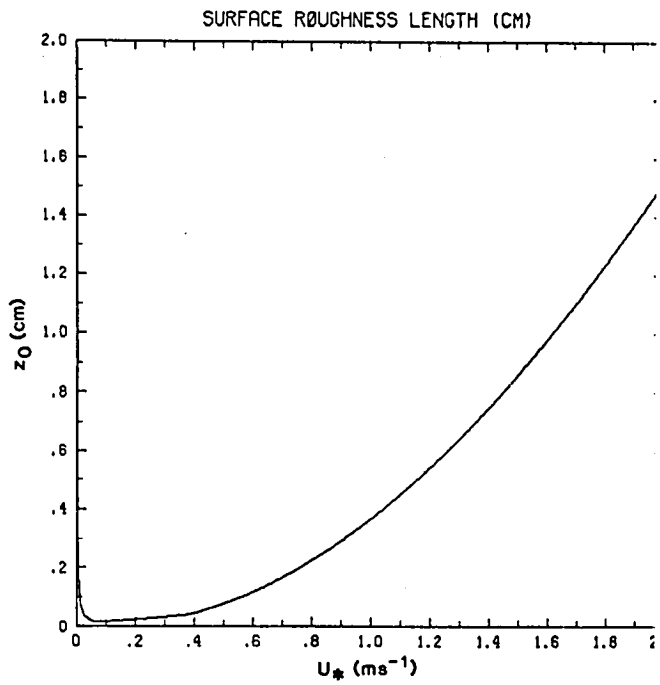

Fig. 2. Surface roughness height z_0 in cm expressed as a function of the surface stress velocity u_* given in ms^{-1}. This function is computed on the basis of the relationship shown in Fig. 1.

Development of an Optimum Interpolation Analysis Method for the CYBER 205

M. Nestler, J. Woollen, and Y. Brin

The GLA optimum interpolation (OI) analysis method is a state-of-the-art technique to assimilate the diverse observational database obtained during FGGE, and thus create initial conditions for numerical forecasts. The OI analyzes pressure, winds, and temperature at sea level, mixing ratio at six mandatory pressure levels up to 300 mb, and heights and winds at twelve levels up to 50 mb.

Conversion to the CYBER 205 required a major re-write of the Amdahl OI code to take advantage of the CYBER vector processing capabilities. Structured programming methods were used to write the programs and this has resulted in a modular, understandable code. We note here that the conversion effort is continuing at the time of this writing.

We have included some degree of flexibility in the vector code in anticipation of future experiments with the analysis. The options available include:

1) variable horizontal resolution (4° x 5°, 2° x 2.5°)

2) variable vertical resolution (12 or 18 levels)

3) a two-dimensional or three-dimensional analysis

4) a two-dimensional troposphere/stratosphere analysis to 0.4 mb on a 4° x 5° x 18 level grid

5) the use of significant level data

6) the use of up to 20 observations to influence the analysis of a grid point

7) the use of different forecast error correlation models

Table 1 compares the Amdahl and CYBER CPU time required for one three-dimensional analysis on a 4° x 5° x 12 level grid. A maximum of twenty observations influences any grid point. Among the contributors to the increased speed of the CYBER code are a vectorized covariance-calculation routine, an extremely fast matrix equation solver, and an innovative data search and sort technique. The solver stores up to 400 matrix equations for simultaneous solution. During matrix decomposition, time is saved by computing the expensive reciprocal of the square root operation on only selected diagonal terms. Vectorized routines move the matrix elements into and out of the format needed for solution. To locate data for use in the analysis, all grid points in the vicinity of a data point are listed. After each data point has an associated list of gridpoints, the lists are sorted so that each gridpoint now has an associated list of data points. This search and sort routine has also contributed to a marked decrease in wall clock time required for the analysis.

Table 1: CPU Time in Seconds for One Analysis

	Amdahl	Cyber	Amdahl/Cyber
Sea Level Temperature	66	9	7.3
Sea Level Pressure and Winds	120	18	6.7
Mixing Ratio	348	31	11.2
Upper Air Heights and Winds	6240	306	20.4

Model Development Highlight for 1984: The GLA 4th Order GCM

J. Pfaendtner

A number of improvements have been made to the GLA Fourth Order GCM and its associated run procedures during the past year. The purpose of this note is to document the major changes which have been made, and to indicate the current direction of our model development efforts.

- Model Resolution

Model versions using the 4 degree latitude by 5 degree longitude grid resolution and 9 sigma layers are now completely core contained in the 1 M word CYBER memory. They need 175 seconds of real time to complete a standard 1 day forecast (Matsuno time scheme, 7 1/2 minute timestep, physics every 30 minutes, longwave radiation every 3 hours, history records written at 6 hour intervals). Forecasts are also routinely being done with a 2 degree latitude by 2 1/2 degree longitude, 9-layer version of the model. At this resolution the hydrodynamics is also core contained, but paging occurs in the model physics. A one day forecast requires 26 minutes of real time and 14 minutes of CPU time. A 15-layer version, which can use non-equidistant sigma levels, is also running in core at the 4 by 5 horizontal resolution.

On April 1,1985 an additional 1 M words of memory are scheduled to be installed on the CYBER 205. With this additional space all model versions should run in core. It is projected that a planned 2 by 2 1/2 degree, 15-layer model will require 22 minutes of real time for one simulated day. The code management and run procedures have been modified so that any version of the model can be run at any desired resolution from a single set of resolution independent masters for that version.

- Boundary Fields and Topography

The model was modified to allow the boundary fields (sea surface temperature, albedo, ground wetness, sea ice extent) to be interpolated in time during a forecast or climate simulation. The fields can be taken either from climatology or from the actual observed anomalies during the period being simulated. This feature was used extensively for the recent study of the 1980 heat wave drought (Wolfson and Atlas). It is also being used for a study of the effect of local SST anomalies on the Ethiopian drought. A number of improved topography fields, including an envelope topography, have been prepared for both horizontal resolutions of the model (Balgovind). The effects of the altered topographic forcing on medium range forecasts and the model climatology were considerable (Helfand).

- Post-processing of model results on the CYBER

Changes were made to the model to enable it to output history fields on mandatory pressure levels as well as on sigma surfaces. This feature, which will appear in the next production version of the model, is important in two respects. First, it will provide an orderly sequence of pressure level history tapes for each experiment with data management handled automatically by the model merge job. Second, when running the forecast/analysis cycle, it will

enable the direct examination of the analysed fields. Until now, the GLAS analysis has been interpolated from the pressure levels on which it is done to the model sigma levels for inclusion in the sigma level history tapes. An interpolation from the sigma levels back to pressure was required when examining the analysis.

The generation of verification statistics using the pressure level history on the CYBER has been implemented. Plans are being made to extensively expand the options available for examination of model results on the CYBER. Model energetics and time averages will be the first options to be added.

- Improvements to model source code

The model code for parameterizations of physical processes, including that for the longwave radiative cooling, was rewritten and modularized. The new code will be considerably easier to maintain and modify.

Response of Winter Forecasts made with the GLA 4th Order GCM to Changes in the Horizontal Grid Resolution

J. Pfaendtner

The GLA Fourth Order General Circulation Model was modified in 1984 to allow it to be run at a finer horizontal grid resolution. Previously the standard model versions integrated the primitive equations on a 4 degree latitude by 5 degree longitude grid. In this paper forecasts made at this resolution are compared to others which were made using the finer 2 degree latitude by 2 1/2 degree longitude grid resolution.

Three winter cases are included with initial conditions from 15 December 1978, 5 January 1979 and 21 January 1979. The 21 January 1979 initial conditions were taken from a GLAS analysis (experiment 2728) which incorporated the GLAS temperature retrievals. The other two cases used European Center Analysis for initial conditions. The forecasts were all verified against European Center Analysis.

Table 1 presents a summary for the three winter cases over North American and Europe. In general, the forecasts done on the finer grid were better out to day six. The first four days show significant reductions in the RMS errors. After day six, the 2 by 2 1/2 degree forecasts are worse than those done at 4 by 5 degrees. A possible cause for this degredation is the stronger smoothing (8th order Shapiro filter rather than 16th order) used in the finer resolution model. The RMS errors for the individual forecasts are shown in tables 2 through 5. A summer case (European Center initial condition from 15 June 1979) is also included in these tables.

Table 1: Percent Change in RMS Forecast Errors (2 x 2 1/2) vs. (4 x 5) Average of Three Winter Cases

verification day

	1	2	3	4	5	6	7	8	9	10
North Amer. pres.	-6	-16	-9	-6	+2	-12	+8	-14	+13	-1
Europe pres.	-3	-23	-38	-29	+4	-13	+1	+36	+20	+28
North Amer. 500 mb height	-13	-21	-26	-10	-10	-18	+5	-15	+15	+38
Europe 500 mb height	-15	-29	-27	-25	-20	-4	+3	+1	-5	-4

Table 2: RMS Sea Level Pressure Errors for North America (mb)

		verification day									
		1	2	3	4	5	6	7	8	9	10
4 x 5 cases	3553 15 Dec 78	3.2	5.5	5.8	10.1	13.7	14.5	11.0	11.5	12.1	15.9
	3509 05 Jan 79	3.1	4.1	5.8	6.1	8.0	8.1	9.8	14.3	16.3	14.8
	3533 21 Jan 79	4.1	7.1	9.4	10.1	6.7	7.7	8.0	9.1	7.6	10.7
	Ave. of 3 winter cases	3.5	5.6	7.0	8.8	9.5	10.1	9.6	11.6	12.0	13.8
	3577 15 June 79	2.8	3.1	4.6	5.5	5.0	5.8	8.1	7.2	4.1	4.6
2 x 2 1/2 cases	3643 15 Dec 78	3.6	4.5	5.5	10.4	15.3	13.0	11.0	9.0	13.5	13.7
	3511 05 Jan 79	2.7	3.5	5.7	6.4	7.1	7.0	9.7	10.9	13.5	-
	3531 21 Jan 79	3.5	6.0	8.1	8.2	6.7	6.8	-	-	-	-
	Ave. of 3 winter cases	3.5	4.7	6.4	8.3	9.7	8.9	10.4	10.0	13.5	13.7
	3727 15 June 79	2.7	3.8	4.8	5.7	7.0	9.0	8.4	9.1	9.3	12.8

Table 3: RMS Sea Level Pressure Errors for Europe (mb)

		verification day									
		1	2	3	4	5	6	7	8	9	10
4 x 5 cases	3553 15 Dec 78	3.2	4.5	7.5	10.1	11.7	15.7	18.3	17.1	19.1	16.6
	3509 05 Jan 79	2.5	5.2	12.7	11.5	9.3	7.9	11.4	13.8	15.1	17.4
	3533 21 Jan 79	3.0	4.8	6.5	10.0	9.3	10.5	14.0	10.6	12.8	15.7
	Ave. of 3 winter cases	2.9	4.8	8.9	10.5	10.1	11.4	14.6	13.8	15.7	16.6
	3577 15 June 79	2.5	4.2	5.0	5.2	4.6	5.9	9.0	9.1	9.0	8.9
2 x 2 1/2 cases	3643 15 Dec 78	3.4	3.5	5.3	5.8	10.8	12.5	17.4	20.5	21.4	21.5
	3511 05 Jan 79	2.3	2.8	5.5	8.5	12.1	9.0	11.9	17.1	16.2	-
	3531 21 Jan 79	2.7	4.8	5.8	7.9	8.6	8.2	-	-	-	-
	Ave. of 3 winter cases	2.8	3.7	5.5	7.4	10.5	9.9	14.7	18.8	18.8	21.5
	3727 15 June 79	2.4	4.0	4.2	5.5	4.7	5.8	7.9	8.5	11.9	11.8

Table 4: RMS 500 mb Geopotential Height Errors for North America (m)

		verification day									
		1	2	3	4	5	6	7	8	9	10
4 x 5 cases	3553 15 Dec 78	41.7	68.7	91.0	124.0	154.0	158.0	126.0	113.0	125.0	135.0
	3509 05 Jan 79	24.2	50.0	60.0	66.7	82.6	81.9	98.9	146.0	145.0	132.0
	3533 21 Jan 79	41.1	78.0	110.0	134.0	134.0	130.0	107.0	125.0	124.0	121.0
	Ave. of 3 winter cases	35.7	65.6	87.1	108.0	124.0	123.0	111.0	128.0	131.0	129.0
	3577 15 June 79	25.2	32.4	46.8	52.7	54.8	50.6	62.4	58.2	50.9	52.5
2 x 2 1/2 cases	3643 15 Dec 78	36.0	54.3	71.8	125.0	180.0	168.0	155.0	122.0	152.0	178.0
	3511 05 Jan 79	22.6	38.2	44.1	62.7	62.6	60.9	76.8	96.4	150.0	-
	3531 21 Jan 79	34.2	63.7	78.3	104.0	91.4	74.3	-	-	-	-
	Ave. of 3 winter cases	30.9	52.1	64.7	97.2	111.0	101.0	116.0	109.0	151.0	178.0
	3727 15 June 79	21.5	27.5	48.3	58.5	66.9	82.0	82.1	61.9	64.4	81.4

Table 5: RMS 500 mb Geopotential Height Errors for Europe (m)

		verification day									
		1	2	3	4	5	6	7	8	9	10
4 x 5 cases	3553 15 Dec 78	23.3	45.9	93.6	124.0	144.0	148.0	179.0	210.0	203.0	174.0
	3509 05 Jan 79	25.2	67.2	133.0	146.0	119.0	90.2	119.0	180.0	232.0	258.0
	3533 21 Jan 79	35.0	44.5	65.4	91.8	120.0	111.0	161.0	182.0	179.0	196.0
	Ave. of 3 winter cases	27.8	52.5	97.3	121.0	128.0	116.0	153.0	191.0	205.0	209.0
	3577 15 June 79	23.4	43.3	65.3	63.6	63.5	69.5	81.3	77.8	84.3	101.0
2 x 2 1/2 cases	3643 15 Dec 78	20.7	41.8	79.5	92.4	107.0	143.0	188.0	211.0	217.0	201.0
	3511 05 Jan 79	20.1	31.8	71.4	89.7	115.0	105.0	128.0	174.0	171.0	-
	3531 21 Jan 79	30.4	38.0	61.3	88.5	86.2	85.2	-	-	-	-
	Ave. of 3 winter cases	23.7	37.2	70.7	90.2	103.0	111.0	158.0	193.0	194.0	201.0
	3727 15 June 79	23.9	39.8	61.8	64.5	64.6	57.4	80.0	103.0	151.0	168.0

D. ATMOSPHERIC DYNAMICS AND DIAGNOSTIC STUDIES

Comparison of Forecast and Observed Energetics

W. E. Baker and Y. Brin

The objective of this investigation is to perform diagnostic studies aimed at furthering the understanding of the atmospheric general circulation and providing useful insight into the NASA/Goddard analysis/forecast system as it continues to evolve.

An energetics analysis scheme has been developed for this purpose to compare the observed kinetic energy balance over North America with that derived from forecast fields of the GLAS fourth order model for the 13-15 January 1979 cyclone case. The major findings of that investigation are:

1) The observed and predicted kinetic energy and eddy conversion are in good qualitative agreement, although the model eddy conversion tends to be 2 to 3 times stronger than the observed values (see Figs. 1 and 2). The eddy conversion being stronger in the 12 h forecast than in observations may be due to a number of factors (e.g. an imbalance from the initial data, overestimation of the release of available potential energy from the physical parameterizations, etc.) which we plan to investigate.

2) In agreement with previous studies of cyclonic disturbances (see Fig. 3) vertical profiles of kinetic energy generation and dissipation exhibit lower and upper tropospheric maxima in both the forecast and observations.

3) An interesting time lag is noted in the observational analysis with the maximum in the observed kinetic energy occurring at 0000 GMT 14 January over the same region as the maximum eddy conversion 12 h earlier (compare Fig. 1a with Fig. 2a).

Future work includes the examination of the forecast error over North America in terms of the energetics utilizing the limited-area, analysis scheme previously developed. The observed energetics will be compared with those from model forecasts in which the resolution, physics, or initial data have been modified.

Reference

Baker, W. E., and Y. Brin, 1985: A comparison of observed and forecast energetics over North America. Quart. J. R. Meteor. Soc., in press.

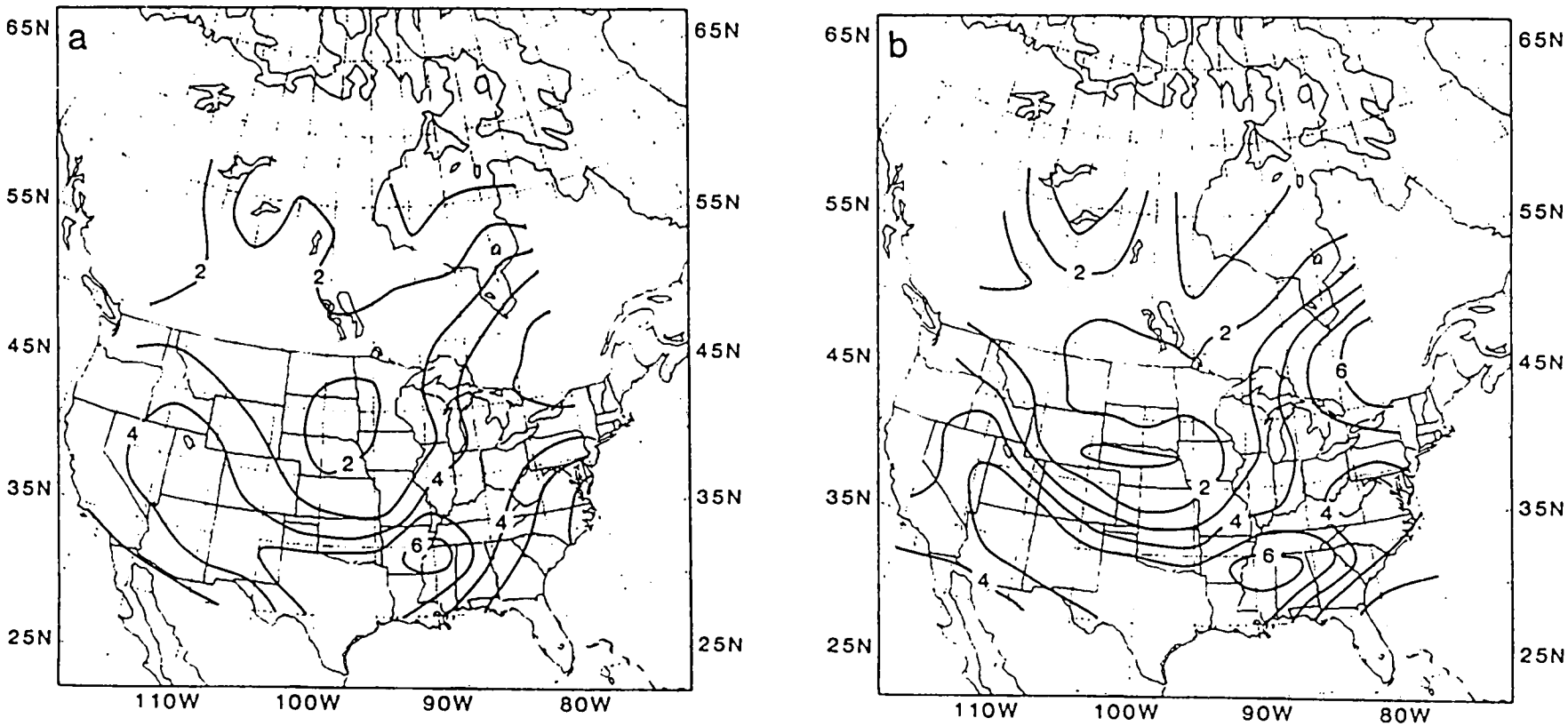

Fig. 1. Vertically integrated (surface to 100 mb) kinetic energy in $10^6 Jm^{-2}$ for 0000 GMT 14 January 1979.
a. Observations (station analysis).
b. 24h forecast.

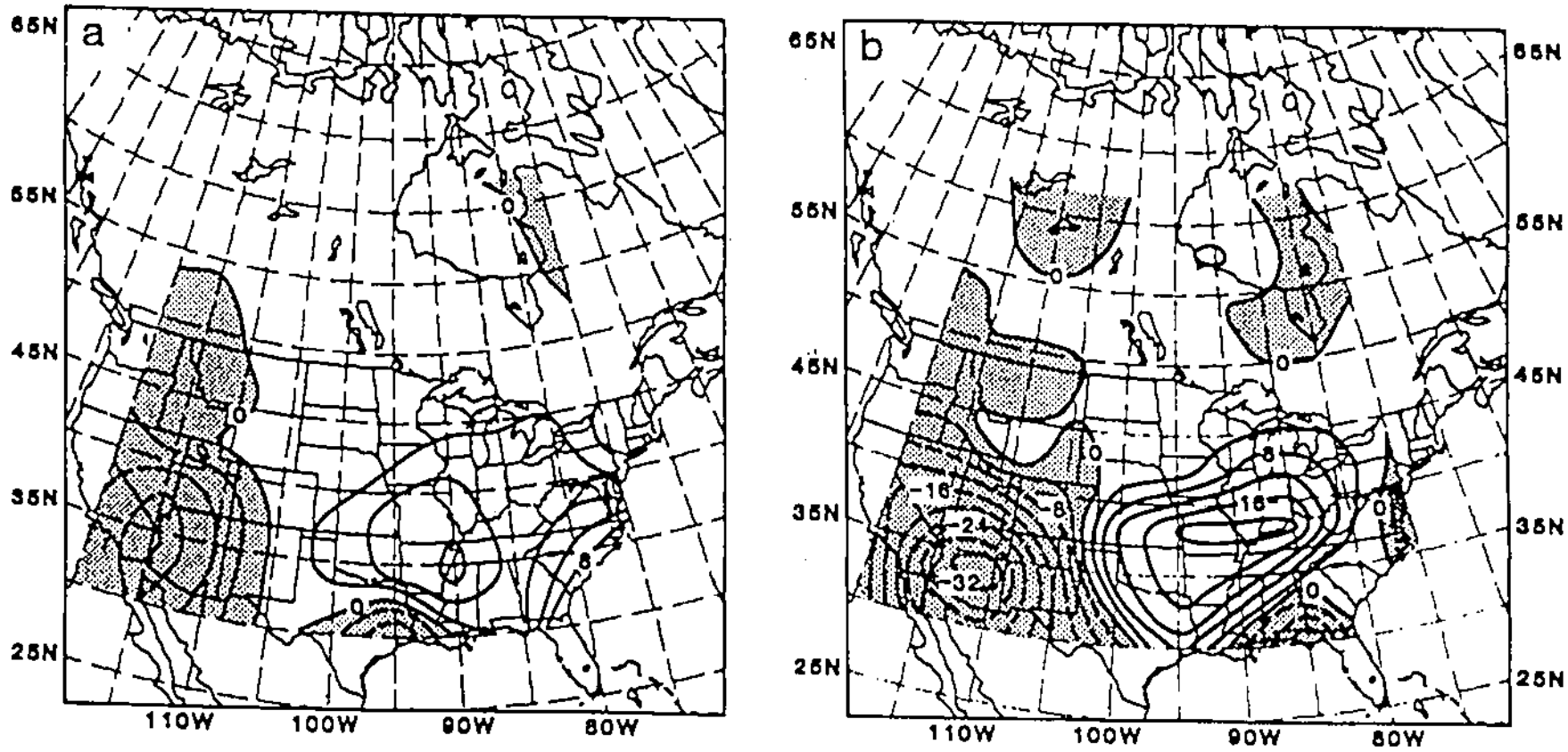

Fig. 2. Vertically integrated (surface to 100 mb) eddy conversion in 10 wm^{-2} for 1200 GMT 13 January 1979. Stippling indicates areas of negative conversion.
a. Observations (station analysis).
b. 12h forecast.

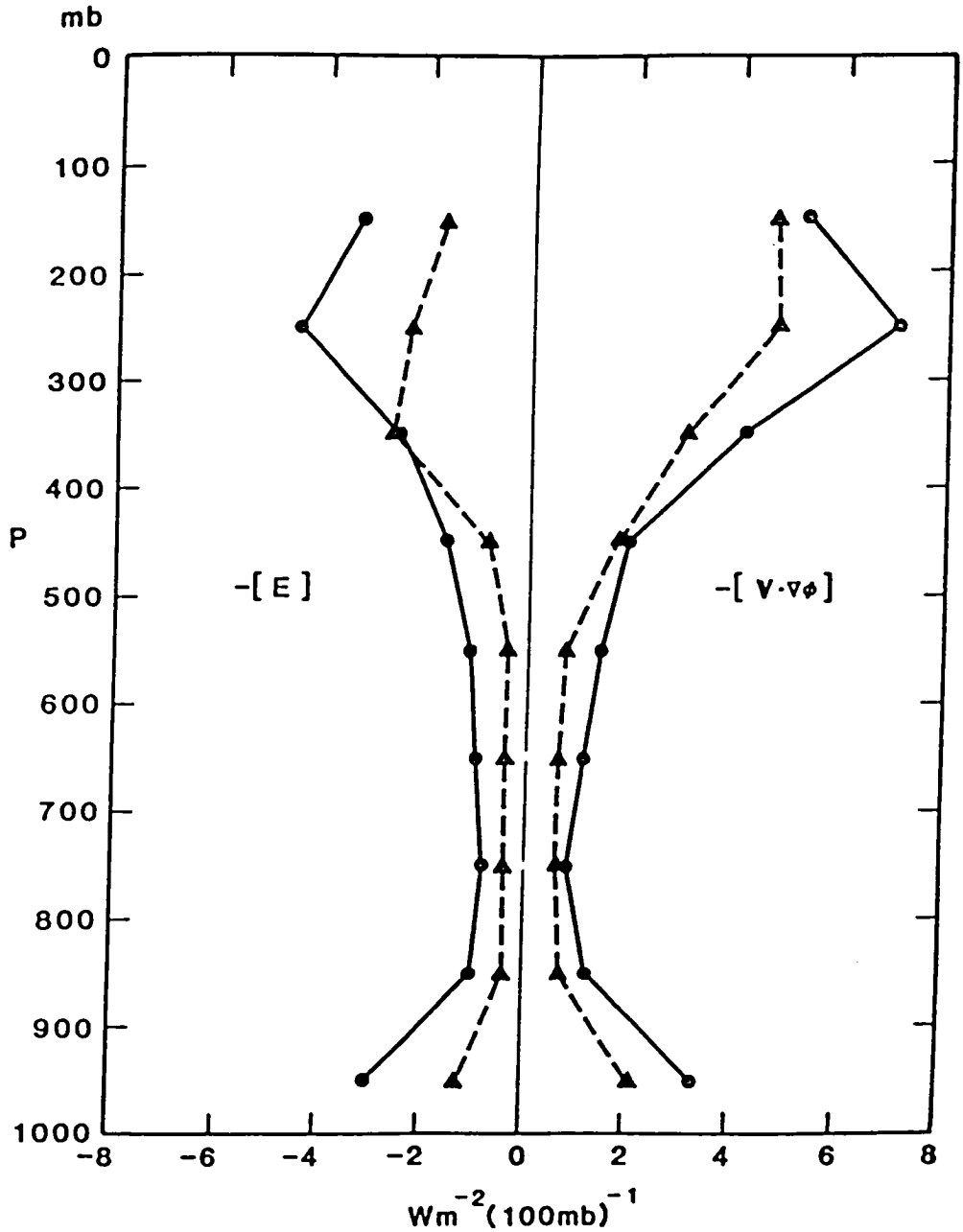

Fig. 3. Vertical profiles of area-averaged kinetic energy generation and dissipation for 1200 GMT 13 January 1979. The station values are denoted by a solid line and the 12h forecast by a dashed line.

Error Growth in Operational 10-day Forecasts

E. Kalnay and A. Dalcher*

Laboratory for Atmospheres
NASA/Goddard Space Flight Center
Greenbelt, Maryland, U.S.A.

Lorenz (1981) estimated the rate of growth of forecast errors using as data base 100 consecutive 10-day operational forecasts from the European Centre for Medium Range Forecasting (ECMWF). He parameterized the growth of the difference between two model forecasts verifying the same day. We extended Lorenz' parameterization of error growth by including the effect of model deficiencies as well as their scale dependence . In this way we are able to fit real forecast error growth and determine the scale dependence of the derived parameters (rate of error growth, external error source due to model errors, and saturation levels). This work is a necessary step in the application of the Lagged Average Forecasting (LAF) technique (Hoffman and Kalnay, 1983, 1984) to the ECMWF 10-day forecasts (Dalcher et al., 1985). Like Boer (1984) and Savijarvi (1984), we found that for both the analyses and the forecasts, there is an approximate equipartition of energy between all the zonal wavenumbers m corresponding to the same total wavenumber n.

In this work, we parameterize the growth of the error variance V by including both an external source of error and the saturation effects:

$$\frac{dV}{dt} = \alpha\ (V + S)\ (V_\infty - V) \qquad (1)$$

This equation has the solution

$$V(t) = V_\infty \frac{\mu}{1+\mu} - S \frac{1}{1+\mu} \qquad (2)$$

where $\mu = ce^{\alpha}\ (V_\infty + S)t$, and the constant $c = \frac{V(o) + S}{V_\infty - V(o)}$ is related to the initial error variance V(o).

The solution (2) can also be expressed as

$$V(t) = 1/2\ (V_\infty + S)(1 + \tanh\ (\ln c + \alpha\ (V_\infty + S)t)/2) - S \qquad (3)$$

This parameterization work works remarkably well when all scales are combined together. Furthermore, the shape of the individual error growths for each total wavenumber suggests that the same parameterization can be applied to each total wavenumber. In Fig. 1 we apply the same function to three individual wavenumbers n, also showing an excellent fit, and indicating that the saturation error is attained at different times for different scales.

*M/A COM Sigma Data Corp. at NASA/Laboratory for Atmospheres

Equation 1 is scaled for each wavenumber by dividing the error variance by the maximum observed value, which generally occurs at day 10. Some resulting parameters are presented in Fig. 2. In Fig. 2a we see that the scaled error growth rate α increases rapidly with wavenumber and is larger for the external errors (comparing forecasts with analyses) than for the internal errors (comparing two forecasts).

The last result, Fig. 2b corresponds to the predictability time as a function of wavenumber, defined as the time needed to reach 95% of the error saturation value. The external error curve shows that for low wavenumbers ($n < 9$), there is still predictability in the ECMWF model after 10 days, whereas larger wavenumbers become saturated at increasingly shorter times. The curve corresponding to internal errors suggests that with a perfect model, predictability would be significantly larger, reaching over 3 weeks for $n < 5$.

References

Boer, G. J., 1984: A spectral analysis. Mon. Wea. Rev., 112, 1183-1197.

Dalcher, A., E. Kalnay and R. N. Hoffman, 1985: Application of the lagged average forecast method of ECMWF 10 day forecasts. Proceedings of AMS 7th Conf. on NWP, Montreal, June 1985.

Hoffman, R. N., and E. Kalnay, 1983: Lagged averge forecasting an alternative to Monte Carlo forcasting, Tellus, 35A, 100-118.

Hoffman, R. N. and E. Kalnay, 1984: Lagged average forecasting, some operational considerations. Predictability of fluid motions, American Inst. of Phys. Conf. Proc., G. Holloway and B. J. West, Editors, 106, 141-147.

Lorenz, E. N., 1982: Atmospheric predictability experiments with a large numerical model. Tellus, 34, 505-513.

Savijarvi, H., 1984: Spectral properties of analyzed and forecast global 500 mb fields. J. Atmos. Sci., 41, 1745-1754.

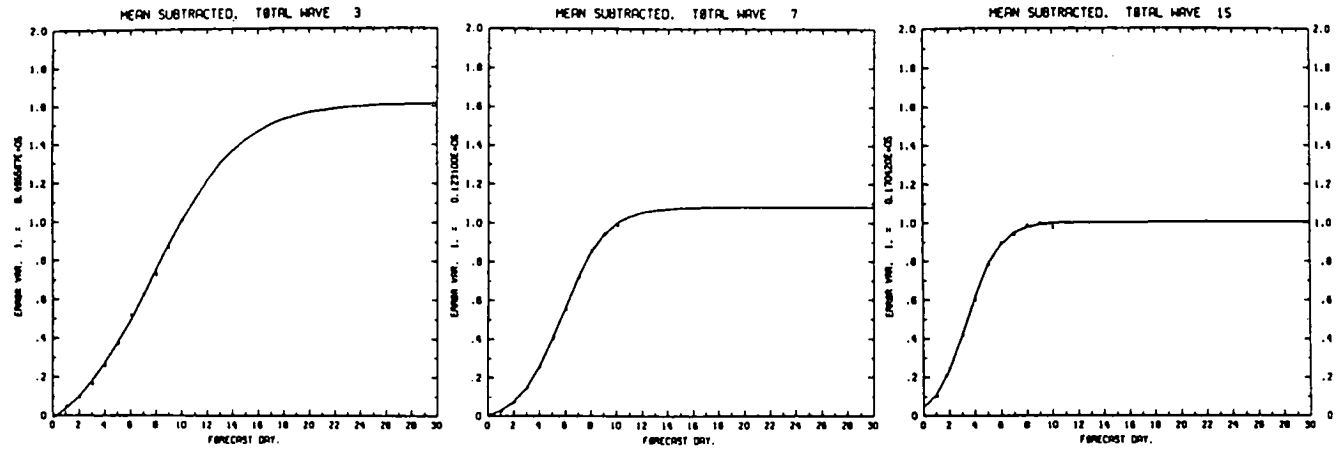

Fig. 1. Fit of the error variance growth for waves with total wave number n = 3, 7 and 15. The data values are marked by dots. The curve is the fitted solution and is extrapolated up to 30 days.

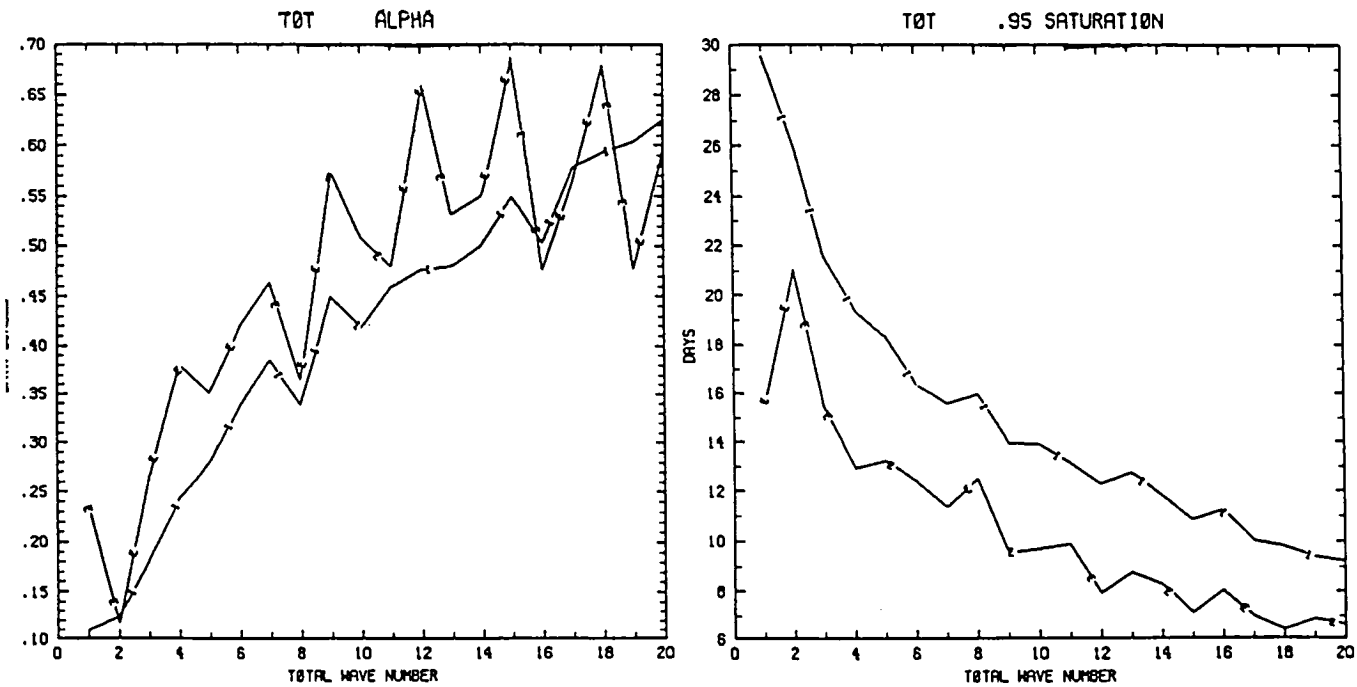

Fig. 2. Fitted parameters (6 parameters model) as a function of total wave number. a) Scaled error growth rate. b) Predictability time (E-external growth, I-internal growth).

Mechanistic Experiments to Determine the Origin of Southern Hemisphere Stationary Waves

Eugenia Kalnay and Kingtse C. Mo
Laboratory for Atmospheres
NASA/Goddard Space Flight Center
Greenbelt, MD 20771

Kalnay and Paegle (1983) reported the existence and structure of large amplitude stationary Rossby waves with zonal wavenumber ~ 7 between 20°S and 40°S over and in the lee of South America. (Fig.1) These waves, present during January 1979, disappeared in February 1979. Kalnay and Paegle (1983) discussed their possible origin, and concluded that the waves were not orographically forced because they corresponded to a ridge in the lee of the Andes, and were not forced by observed sea surface temperature anomalies because of their space and time phase relationship. They suggested that the waves were probably forced by tropical heating.

In this paper we perform two 15 day forecast experiments with the GLAS Fourth Order General Circulation Model, and initial conditions corresponding to 5 January and 4 February 1979. These forecasts reproduce reasonably well the presence of the January wave. (Fig.2) and their absence in February. Several mechanistic experiments to determine the origin of the waves are then performed. A "No Andes" forecast shows that the waves do indeed exist independently of orographic forcing. (Fig.3) Several experiments modifying the coefficient of latent heat lead to the conclusion that tropical heating is important in the maintenance of the waves (Fig.4). Furthermore, the convection in the subtropical waves themselves is important in sustaining their amplitude and phase, and the Walker type of circulation associated with the SPCZ is also a contributor to the maintenance of the South American waves. These results confirm the existence of a relationship between the occurrence of a strong South Pacific Convergence Zone (SPCZ), (Fig.5) somewhat eastward from its climatological position, and the strong "South Atlantic Convergence Zone" (Fig. 6) observed in outgoing long wave radiation maps.

Reference

Kalnay, E., and J. Paegle 1983: Large amplitude stationary wind in the Southern Hemisphere observations and theory. Proceedings of the first International Conference on Southern Hemisphere Meteorology.

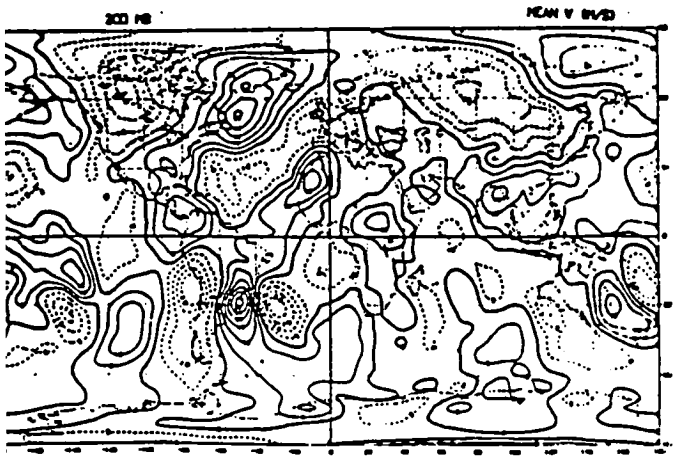

Fig.1 15 day averaged meridional velocity at 200 mb from the GLAS analysis, from 5 to Jan 20, contour interval 5 m/s.

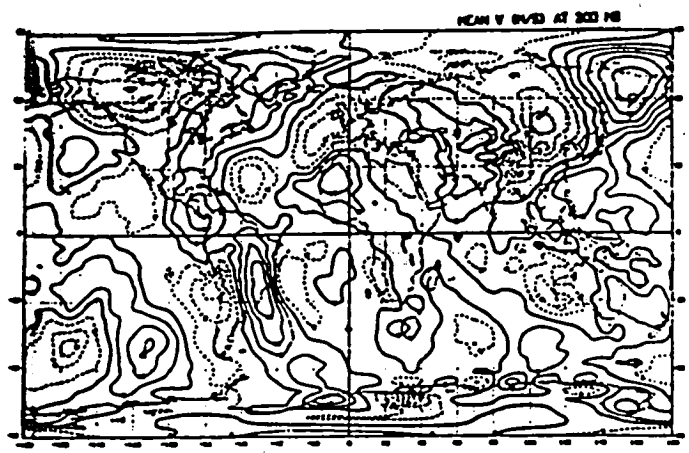

Fig.2 Same as Fig.1 but for the January control forecast.

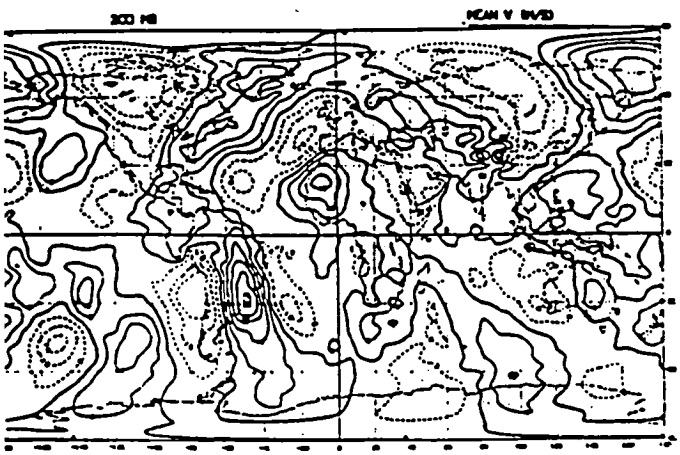

Fig.3 Same as Fig.2 but for the "no Andes" experiment.

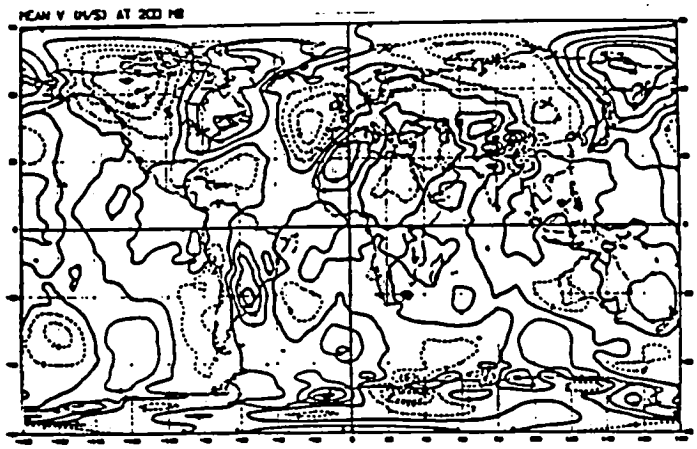

Fig.4 Same as Fig.2 but for the reduced tropical heating experiment.

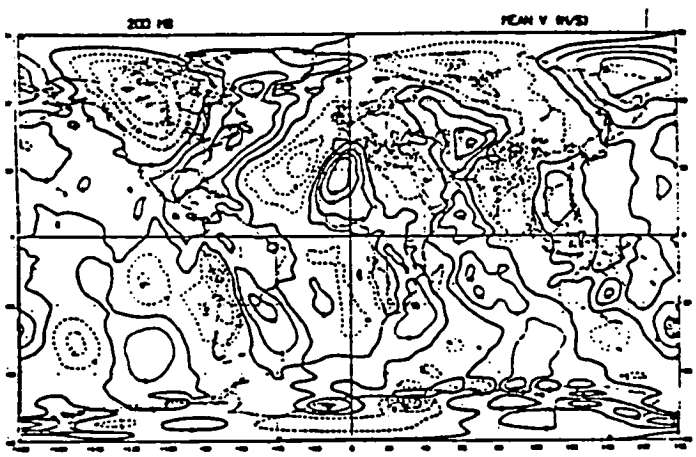

Fig.5 Same as Fig.2 but for the "Suppressed Pacific heating experiment.

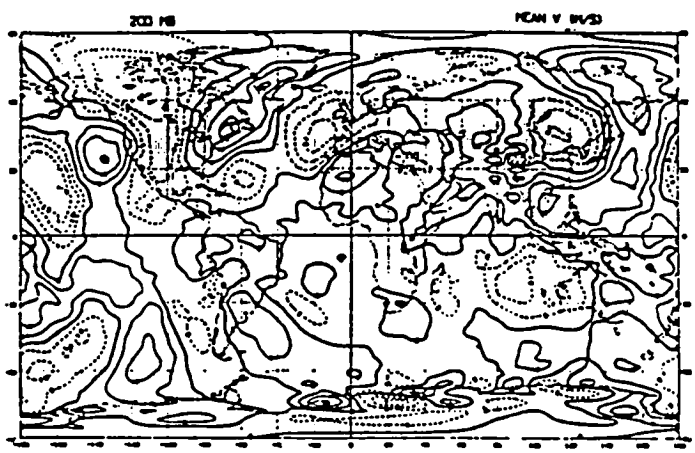

Fig.6 Same as Fig.2 but for the "Suppressed Atlantic heating" experiment.

Energy Sources of the Dominant Frequency Dependent 3-Dimensional Atmospheric Modes

Siegfried Schubert

As part of an on-going study of atmospheric variability we present here the energy sources and sinks associated with the zonally asymmetric winter mean flow. The observational work of Blackmon et al., (1984) showed distinctly different horizontal structures for the long, intermediate and short time scale atmospheric variations. In this study we look into the 3-dimensional structure of the fluctuations and examine the relative roles of barotropic and baroclinic terms.

In the context of a two-level quasi-geostrophic model the energy tendency terms are

$$\langle \dot{K}_\tau + \dot{K}_\psi + \dot{P} \rangle = 1/4\pi \int \{\nabla^2\psi\,(kx\,\nabla\psi \cdot \nabla\psi^s) + \nabla^2\tau\,(k \times \nabla\psi \cdot \nabla\tau^s)$$

$$+ \nabla^2\psi\,(k \times \nabla\tau \cdot \nabla\tau^s) + \nabla^2\tau\,(k \times \nabla\tau \cdot \nabla\psi^s) + r^2\tau^s\,(k \times \nabla\psi \cdot \nabla\tau)\}\, d< \quad (1)$$

where K_τ and K_ψ are the vertical mean flow and shear flow kinetic energy (KE) associated with the anomalies, respectively and the superscript (s) denotes the winter mean flow. The available potential energy (APE) associated with the anomalies is $P = r^2\tau^2/2$ where r is the non-dimensional inverse Rossby deformation radius. The anomalies are defined as deviations from the winter mean flow where τ and Ψ are one-half the vertical sum and difference of the 200 mb and 700 mb stream function fields, respectively. The data consists of 10 years of Northern Hemisphere winter stream function fields where, in practice, Ψ is approximately by the 500 mb field. The first four terms on the RHS of (1) combine to give the total barotropic conversion, while the fifth term represents the conversion of the time mean flow APE to the anomaly APE.

In order to isolate the relative roles of these terms for the wide range of frequencies which exist in the atmosphere, five different filters were applied to the anomalies. Filters A-E were designed to retain fluctuations longer than 45 days, 20-45 days, 10-20 days, 6-10 days, and 2.5-6 days, respectively. For each of the five frequency bands the data was expanded in empirical orthogonal functions and only the first five EOFs were retained.

Figure 1 compares the time averaged total KE conversion term and the APE conversion term for the first five EOFs in each frequency band for a deformation radius typical of middle latitudes (1000 km). Positive values indicate a source (sink) for the anomalies (mean flow). These results show a dramatic shift in the nature of the source terms from a predominantly barotropic source for the lowest frequency modes to a predominantly baroclinic source for the synoptic time scales. Further details of these conversion terms including their spatial distributions may be found in Schubert, 1985.

References

Blackmon, M. L., and Y.-H. Lee, and J. M. Wallace, 1984: Horizontal structure of 500 mb height fluctuations with long, intermediate and short time scales. J. Atmos. Sci., 41, 961-979.

Schubert, S., 1985: The structure and energetics of the dominant frequency-dependent three-dimensional atmospheric modes. In preparation.

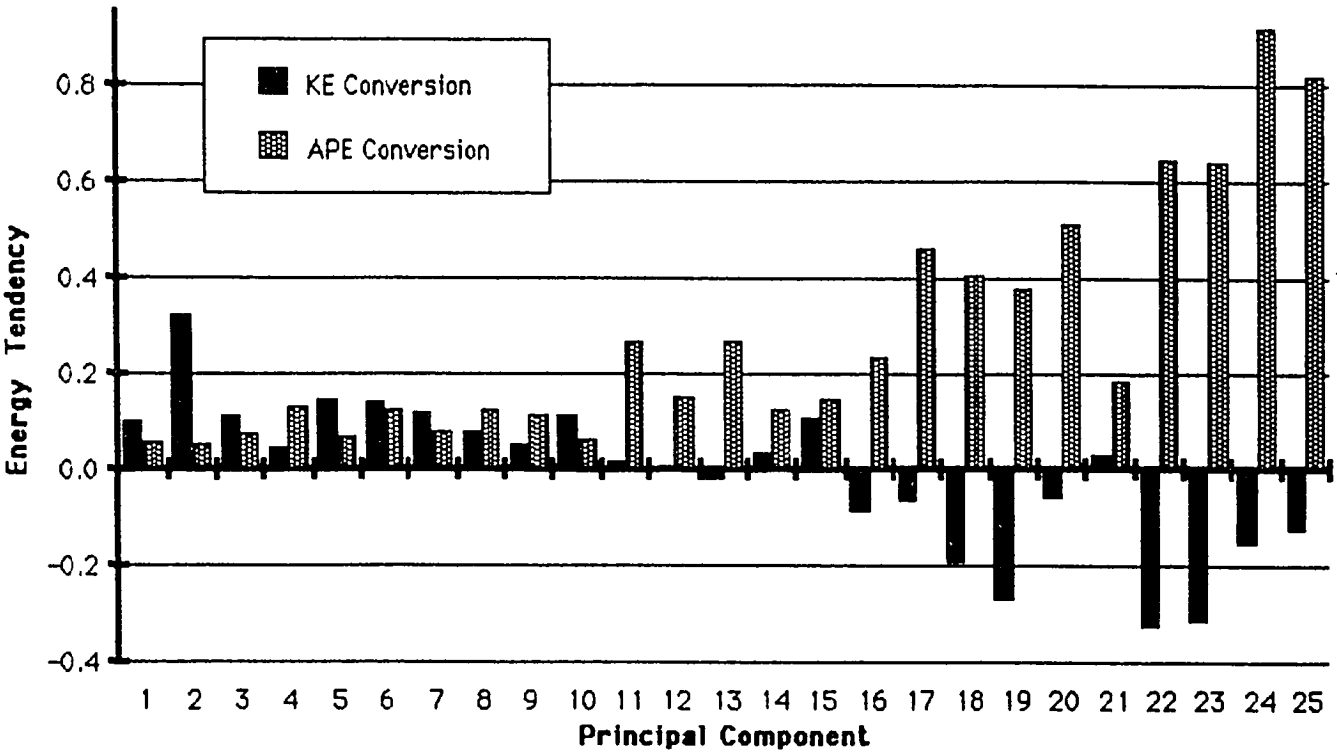

Figure 1. The time-average energy sources associated with the winter mean flow for the first five PCs for filters A through E. PCs 1-5 correspond to filter A (lowest frequencies), PCs 6-10 correspond to filter B, etc. See text for filter characteristics. The ordinate is the energy tendency divided by the variance of the associated PC.

A Comparison of the Bounded Derivative and the Normal Mode Initialization Methods Using Real Data

F. H. M. Semazzi and I. M. Navon

Browning et al. (1980) proposed an initialization method called the bounded derivative method (BDI). They used analytical data to test the new method. Kasahara (1982) theoretically demonstrated the equivalence between BDI and the well known nonlinear normal mode intialization method (NMI). The purposes of this study are the extension of the application of BDI to real data and comparison with NMI. The unbalanced initial state (UBD) is data of January 1979 00Z which were interpolated from the adjacent sigma levels of the GLAS GCM to the 300 mb surface. We use the global barotropic model described by Takacs and Balgovind (1983). Orographic forcing is explicitly included in the model.

Many comparisons are performed between various quantities. However, we only present a comparison of the time evolution at two grid points A(50° S, 90° E) and B(10° S, 20° E) which represent low and middle latitude locations. To facilitate a more complete comparison an initialization experiment based on the classical balance equation (CBE) was also included. Figs. 1a, 1b and 1c show the time evolution of the height corresponding to UBD, CBE, BDI, and NMI at coordinate A. The forecast starting from UBD suffers from contamination by high frequency oscillations with a dominant period of about 6 hours. Regarding CBE, BDI and NMI the time evolution is smooth. The classical balance equation performs well since the influence of orography is small at A. The plots for the time evolution for coordinate B are presented in Figs. 2a, 2b and 2c. Notice the balance equation performs relatively worse than the NMI and BDI. This is mainly because the balance equation is not capable of handling the gravity waves produced by orography In this case these waves are excited by the high elevation over equatorial Africa. It is also instructive to note that at low latitudes the amplitude of gravity waves can be larger than that of synoptic motions. However, over higher latitudes the relative importance of gravitational motions is smaller. This indicates the importance of performing suitable initialization over the low latitude regions of the earth, particularly for purposes of short range numerical weather prediction.

References

Browning, G., A. Kasahara and H. O. Kreiss, 1980: Initialization of the primitive equations by the bounded derivative method. J. Atmos. Sci., 37, 1424-1436.

Kasahara, K., 1982: Nonlinear normal mode initialization and the bounded derivative method. Rev. Geophys. Space Phy., 20, 385-397.

Takacs, L. L., and R. C. Balgovind, 1983: High latitude filtering in grid point models. Mon. Wea. Rev., 111, 2005-2015.

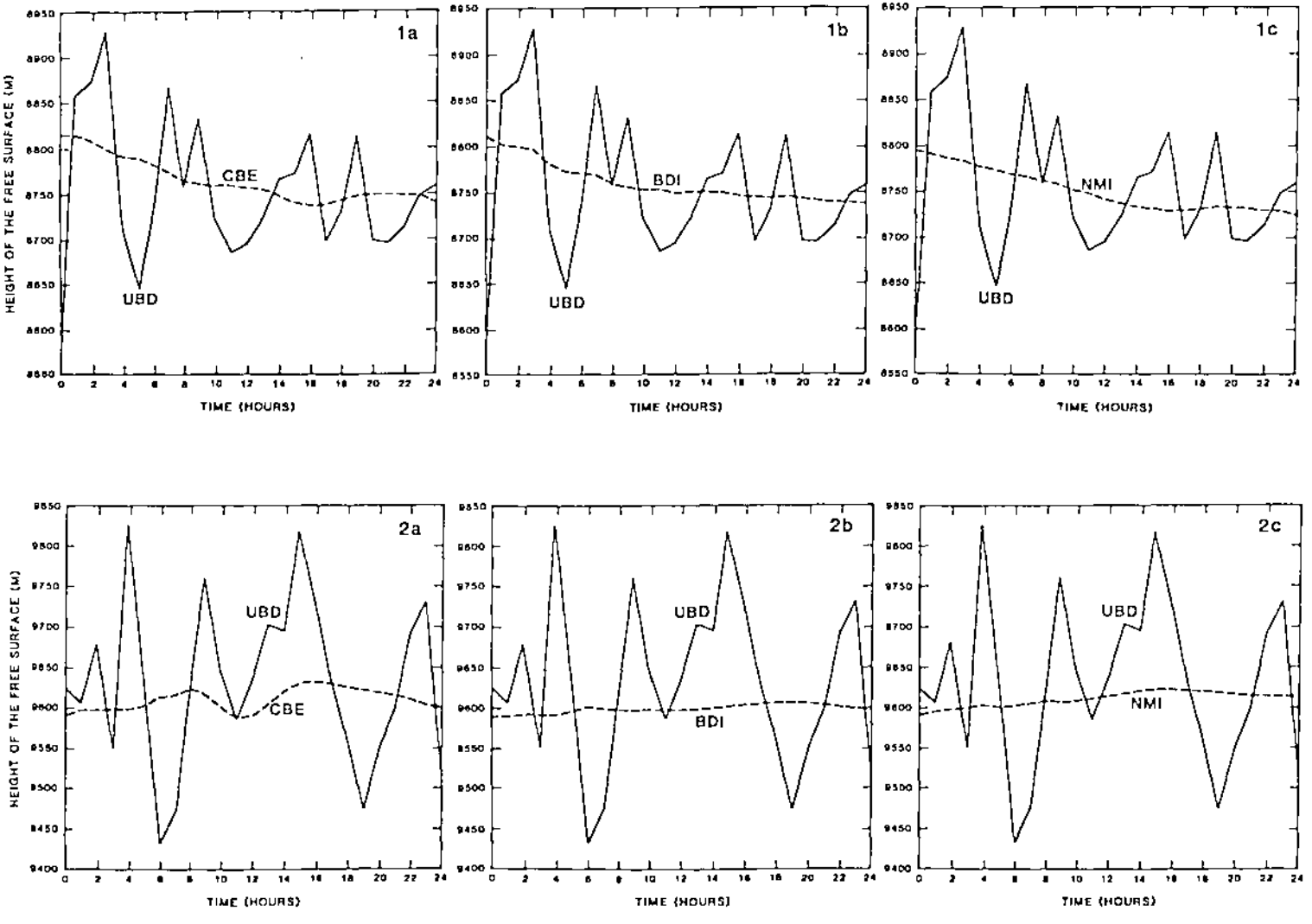
1a
1b
1c
2a
2b
2c
UBD
CBE
BDI
NMI
HEIGHT OF THE FREE SURFACE (M)
TIME (HOURS)

The Vertical Structure of Global Rotational Normal Modes

David M. Straus

The relevance of global rotational normal modes to the behavior of the atmosphere has been a concern of meteorologists for nearly half a century. Although the mathematical properties of these fundamental linear solutions have been explored at various levels of approximations over the years, it is only recently that the availability of reliable global data has made meaningful global observational studies possible.

In one such recent study, Lindzen et al. (1984) examined the amplitude and phase evolution of Hough mode projections at 500 mb. The Hough modes represent the simplest normal mode approximation available, and correspond to the neutral eigenfunctions of a shallow water fluid with no mean zonal flow. In this study, it was found that when the observed amplitude of a rotational Hough mode was large, it tended to propagate at the phase speed of a normal mode in the presence of mean 500 mb winds, giving a strong indication that normal modes are of relevance to the atmosphere.

Continuing along these lines, we have explored the vertical structure of the approximately defined rotational normal modes by projecting observed data (from the ECMWF's FGGE analyses) onto Hough functions at levels other than 500 mb. As in Lindzen et al. (1984), the stationary and eastward propagating components were filtered out at each level. The evolution of the amplitude in time throughout the troposphere is shown for several modes during summer and winter in Figures 1-4. The episodic nature of the normal modes at 500 mb found by Lindzen et al. is evident at other levels, and it continues to be true that large amplitude is associated with phase propagation at the theoretical phase speed (corrected for the presence of mean zonal winds).

What is suprising about the vertical structure depicted in these figures is that the level of maximum amplitude is 300 mb, so that the amplitude decreases with altitude in the upper troposphere. This is contrary to the predictions of both the simple theory and more complete theoretical-numerical determinations of normal mode vertical structure that the amplitude increases throughout the troposphere and even, in some cases, the stratosphere.

This anomalous distribution of amplitude is potentially of great interest, for it may indicate either that some vital ingredient has been left out of standard normal mode calculations, or that the observed modes' phase progression at the normal mode speed is fortuitous and the identification as normal modes incorrect. (These two possibilities are not necessarily distinct.) A third, and perhaps more likely alternative, is that the vertical structure observed in the figures is the result of using Hough functions, rather than eigenfunctions which take into account the presence of the mean zonal wind, which itself tends to be a maximum above 300 mb.

Current research centers on projecting data from each level onto shallow water eigenfunctions which take into account the mean zonal wind at that level in order to clarify the question of vertical structure. This is of importance for future work on the role of these modes in numerical forecasts.

Reference

Lindzen, R. S., D. M. Straus and B. Katz, 1984: An observational study of large-scale atmospheric Rossby waves during FGGE. J. Atmos. Sci., 41, 1320-1335.

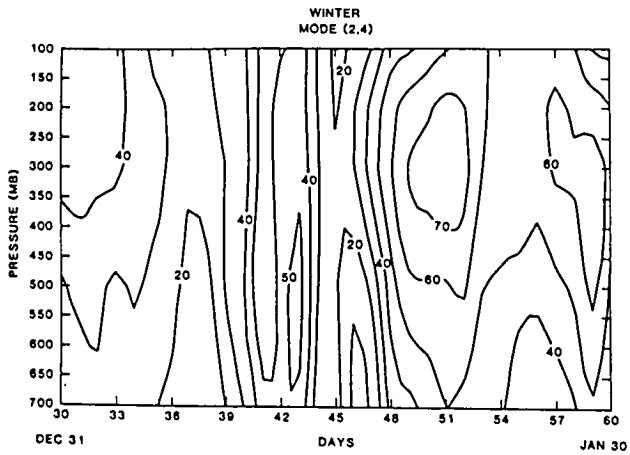

Fig. 1 Evolution of amplitude for the (2, 4) (wavenumber 2, first antisymmetric) mode as a function of level for the period of Dec. 31, 1978 to Jan. 28, 1979. The amplitude represents the value of the geopotential height in meters. The Hough mode projections were carried out at 700, 500, 300 and 100 mb.

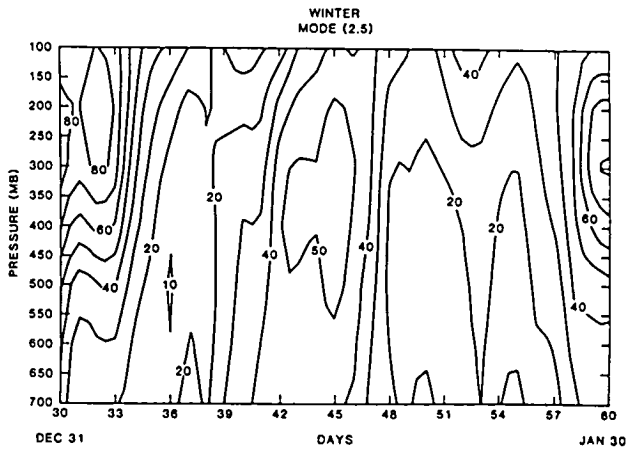

Fig. 2 Evolution of amplitude for the (2, 5) (wavenumber 2, second symmetric) mode for the period of Dec. 31, 1978 to Jan. 28, 1979).

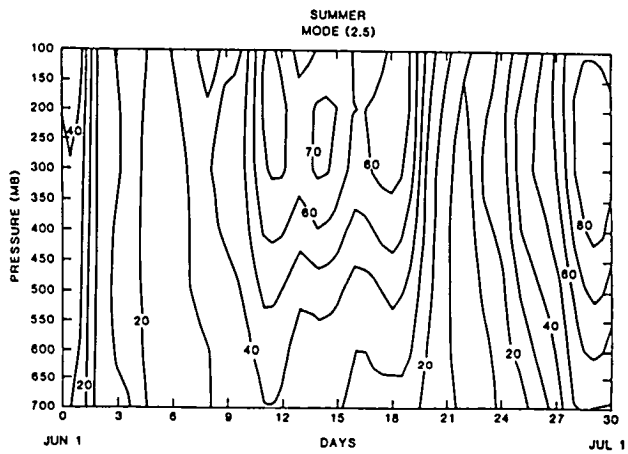

Fig. 3 Evolution of amplitude for the (2, 5) mode for the period of June 1 to June 30, 1979.

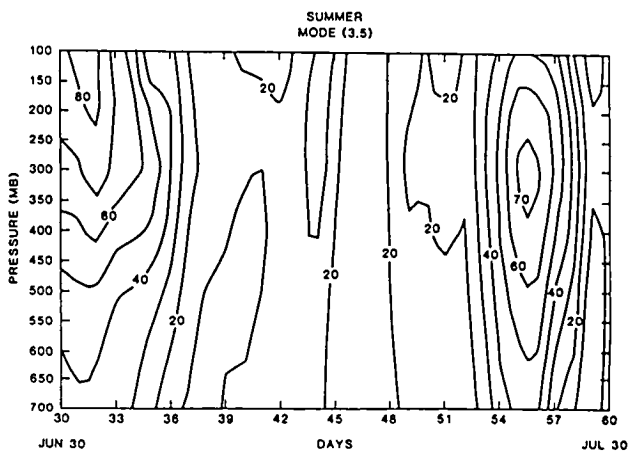

Fig. 4 Evolution of amplitude for the (3, 5) (wavenumber 3, first antisymmetric) mode for the period of June 30 to July 30, 1979.

II. CLIMATE/OCEAN-AIR INTERACTIONS

A. DATA ANALYSIS

Quasi stationary states in the Southern Hemisphere

Kingtse C. Mo

Pattern correlations between daily anomalies (Horel 1984) have been used to study the persistency of the Southern Hemisphere circulations. The data set consists of the daily Australian analyses of 500 mb heights and sea level pressure for the period from 1972 and 1983. Compared to the Northern Hemisphere, the pattern correlations are much smaller and more variable in the Southern Hemisphere. The mean one day lag is only 0.57, (0.82 for the NH). The correlations increase significantly for the filtered anomalies which consist of the long planetary waves from 0 to 4.

Subjective criteria based on the pattern correlations are used to select the quasi stationary events. A series of 5 or more daily maps is quasi stationary if the pattern correlations between all consecutive pairs of maps in this time series are larger or equal to 0.5.

In winter, events can be classified in terms of wave numbers. Wave 3 and 4 are by far the most dominant waves. There are total 24 events in winter. There are 14 events which have large 3 amplitude. 8 out of these 14 events have fixed phase locations. The composite (Fig. 1) of the total anomalies for these 8 events shows lows at 50S, 115E, 60S, 0W and 55S, 140W. The same wave 3 signal has been found in the winter teleconnection pattern using monthly mean data. (Mo and White, 1984).

There are 3 events which also have a large wave 3 amplitude but opposite phase locations. The composite of the total anomalies of these 3 events is given in Fig. 2. The reversal of positions of highs and lows may suggest the superresonant and subresonant states described by the multiple equilibria theory. (Charney and Straus 1980).

In summer, these are only 12 events. All of them fall in months where the Southern Oscillation reaches extremes.

References

Charney J. G. and D. M. Straus, 1980: Form drag instability, multiple equilibria and propagating planetary waves in baroclinic orographically forced planetary wave systems. J. Atmos. Sci., 37, 1157-1166.

Horel, J. D., 1984: Persistence of the 500 mb height field during Northern Hemisphere winter. Mon. Wea. Rev., in press.

Mo, K. C. and G. H. White, 1985: Teleconnections in the Southern Hemisphere. Mon. Wea. Rev., 113, 22-37.

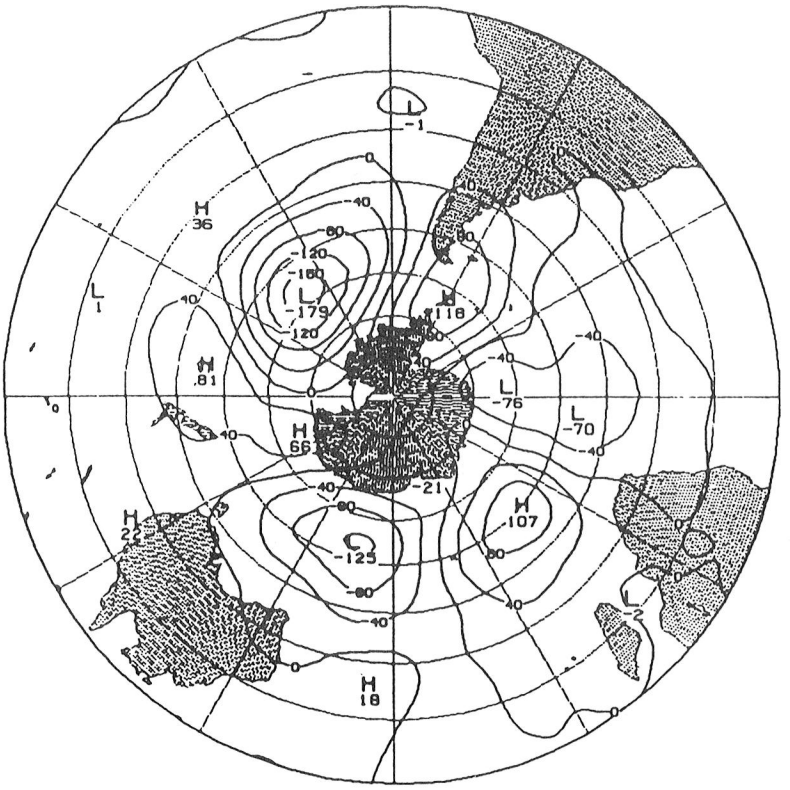

Fig. 1 Composite of anomalies for 8 quasi stationary states with large wave 3 amplitude.

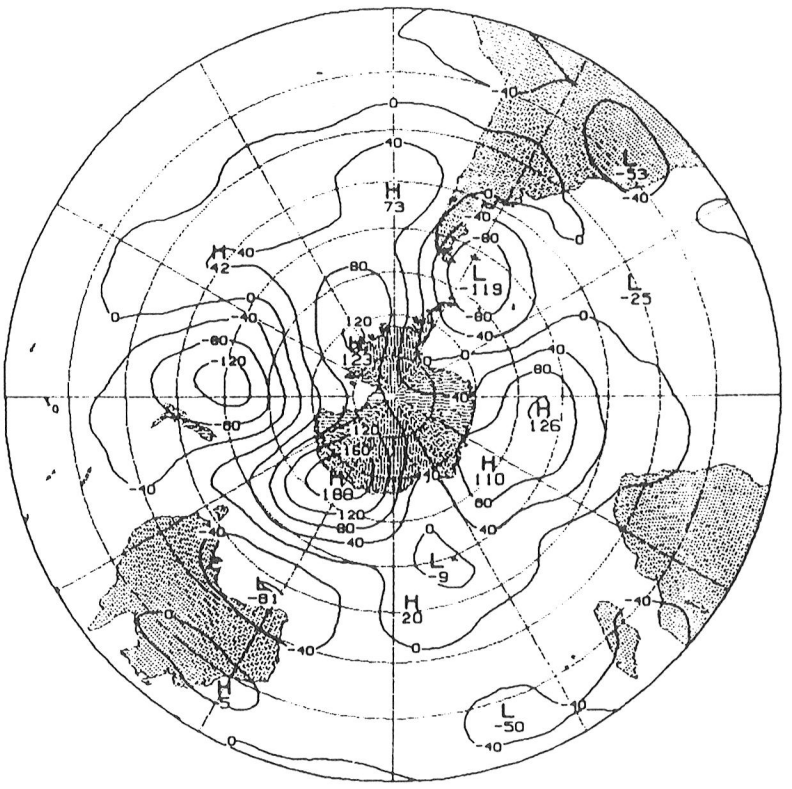

Fig. 2 Composite of anomalies for 3 quasi stationary states with large wave 3 amplitude but different phase relation from Fig. 1.

Trends in the Southern Hemisphere

Kingtse Mo

and

Harry van Loon

I. Introduction

The station data of monthly mean sea level pressure, surface air temperature as well as monthly mean upper air rawinsonde observations were used to study the trends in the southern winter (June, July and August) and summer (December, January and February). This study covers the period 1951 to 1981. Most of the surface data have continuous 31 year records, however, for some high latitude stations, both surface and upper air records started in 1957 or even later.

The normalized anomaly for a given variable Z is defined as the departure from the 1951-1981 grand mean divided by the standard deviation during the same period. To eliminate the large fluctuations in the data, the 1-3-1 smoothing has been applied to the time series of normalized anomalies.

II. The Sea level pressure

Figure 1 plots the smoothed normalized anomalies of sea level pressure for 31 stations during the winter season. The thick line gives the parabola fit for unsmoothed anomalies. The trends are highly regionally dependent. Except for stations at high latitudes, the mean sea level pressure fell at stations on the Indian and Atlantic side of the hemisphere from the 1950's to the 1960's but it rose over the other half of the hemisphere. These trends in general reversed from the 1960's to the 1970's.

At higher latitudes, e.g. Campbell and Macquarie on the Pacific side, sea level pressure increased during these 30 years. On the opposite side, e.g. Ushuaia and Stanley, the pressure fell. At Halley Bay and S.A.N.A.E. the sea level pressure was higher during the 1960's than the 1970's.

These trends affected the amplitude of the half yearly wave in the midlatitudes (Mo and van Loon, 1984, Swanson and Trenberth, 1981). They also influenced on amplitude of the planetary waves.

III. Other Points

In this study, we document the trends of monthly mean temperatures and heights from the surface to 200 mb level. Other conclusions are: 1. Trends of all these elements are highly regionally dependent. The mean temperature of the earth and its changes can not be adequately described if the selected stations are not evenly distributed over the globe. 2. The trends of the height fields are equivalent barotropic. 3. There are no major differences in trend between stations on land or sea (Chen 1982). 4. A linear trend indicates a large increase in heights throughout Antarctica from 1957 to 1981

at all levels. This shows an increase of the total mass in the atmosphere over that region (Kraus 1977). 5. There was a notable warming over Antarctica from the 1960's to the 1970's except in a small area from 90W to 120W at all upper levels. (Hanson et al., 1981).

References

Chen, R. S., 1982: Combined land/sea surface air temperature trends 1949-1972. Report No. 6, Department of Meteorology and Physical Oceanography, M.I.T., Cambridge, Mass. 02139.

Hansen, J., D. Johnson, A. Lacis, S. Lebedeff, P. Lee, D. Rind and G. Russell, 1981: Climate impact of increasing atmospheric Carbon dioxide. Science, 213, 957-966.

Kraus, Z. E. B., 1977: Subtropic droughts and cross equatorial energy transports. Mon. Wea. Rev., 105, 1009-1018.

Mo, K. and H. van Loon, 1984: Some aspects of the interannual variation of mean monthly sea level pressure on the Southern Hemisphere. J. Geophy. Res., 89, 9541-9546.

Swanson, G. S. and K. Trenberth, 1981: Trends in the Southern Hemisphere troposphere circulation. Mon. Wea. Rev., 109, 1879-1889.

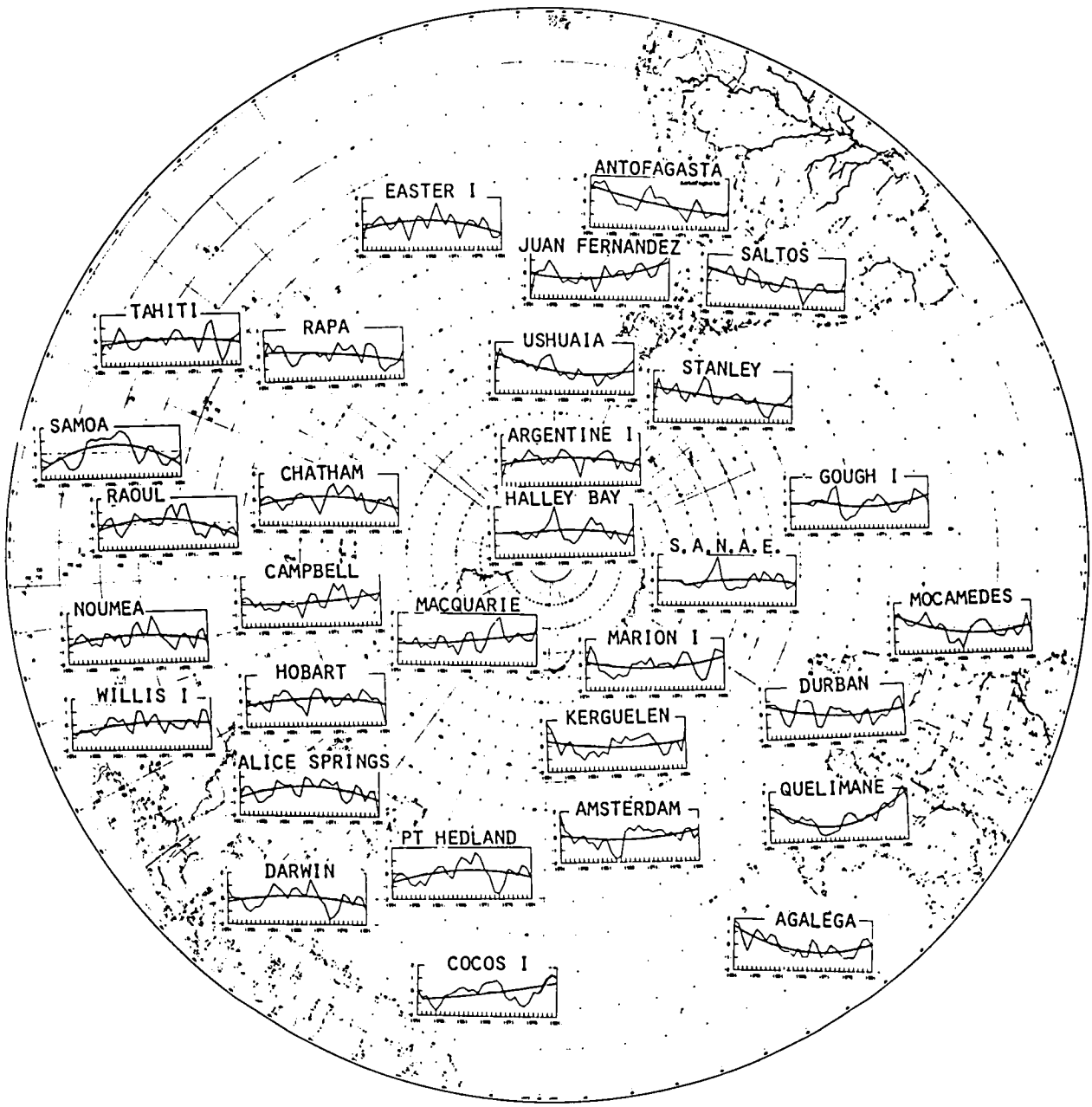

Fig. 1 The smoothed normalized anomalies (thin line) of sea level pressure in winter, the thick line gives the parabala fit for unsmoothed anomalies.

The Seasonal Cycle of Storminess as Measured by Band-Pass Fluctuations

David M. Straus

An important prerequisite to the successful modeling of climate variations is the ability to simulate the observed seasonal cycle in both the time and space averaged fields and in the fluctuations of these fields. With the advent of high speed vector computers, a number of multi-year simulations with differen GCMs has been carried out with the seasonal cycle in boundary conditions (solar insolation, sea surface temperature, etc.) imposed. The comparison of the seasonal cycles produced by the GCMs with the observations should be a priority item on the agenda of modeling groups.

This endeavor will require the compiling of appropriate observational statistics. The seasonal variation of the mean fields is well documented and several climatologies of local time variances during winter and summer are available. However, good statistics for the transition seasons of spring and fall are harder to obtain. We are undertaking the compiling of climatologies of local time variances and covariances for all four seasons from a 15 year dataset consisting of NMC operational (Northern Hemisphere) analyses from May 1963 through December 1977. The emphasis is to be on the clear depiction of the seasonal change of the (co)variances.

In this note we present a sample of such statistics, namely the seasonal cycle of baroclinic storms, as represented by band-pass filtered geopotential height variances at 850 mb. The particular filter used is that suggested by Blackmon and White (1982), and retains periods of approximately 2.5 to 10 days. The time series of height (at each grid point) were filtered by removing the annual and semiannual cycles for that point, and by removing zonal wavenumbe higher than 20. The band-pass filter was then applied. The height variances of the filtered fields were then computed for each winter season (December-February), each spring season (March-May), each summer season (June-August) and each fall season (September-November). These variances were then averaged by season. Figures 1(a)-(d) show maps of the standard deviation. These figures show clearly the seasonal cycle of bandpass fluctuations. The strong maxima over the Atlantic and Pacific Oceans are present in all seasons, with a signific weakening (and slight northward shift) only in the summer. The major seasonal variation is thus seen to consist mostly of a summertime weakening and shift; spring and fall appear nearly identical to winter. The corresponding results at 500 mb (not shown) are similar, but with the stormtrack variance being slightly larger in spring and fall compared to winter.

Reference

Blackmon, M. L., and G. H. White, 1982: Zonal wavenumber characteristics of Northern Hemisphere Transient Eddies. J. Atmos. Sci., 39, 1985-1998.

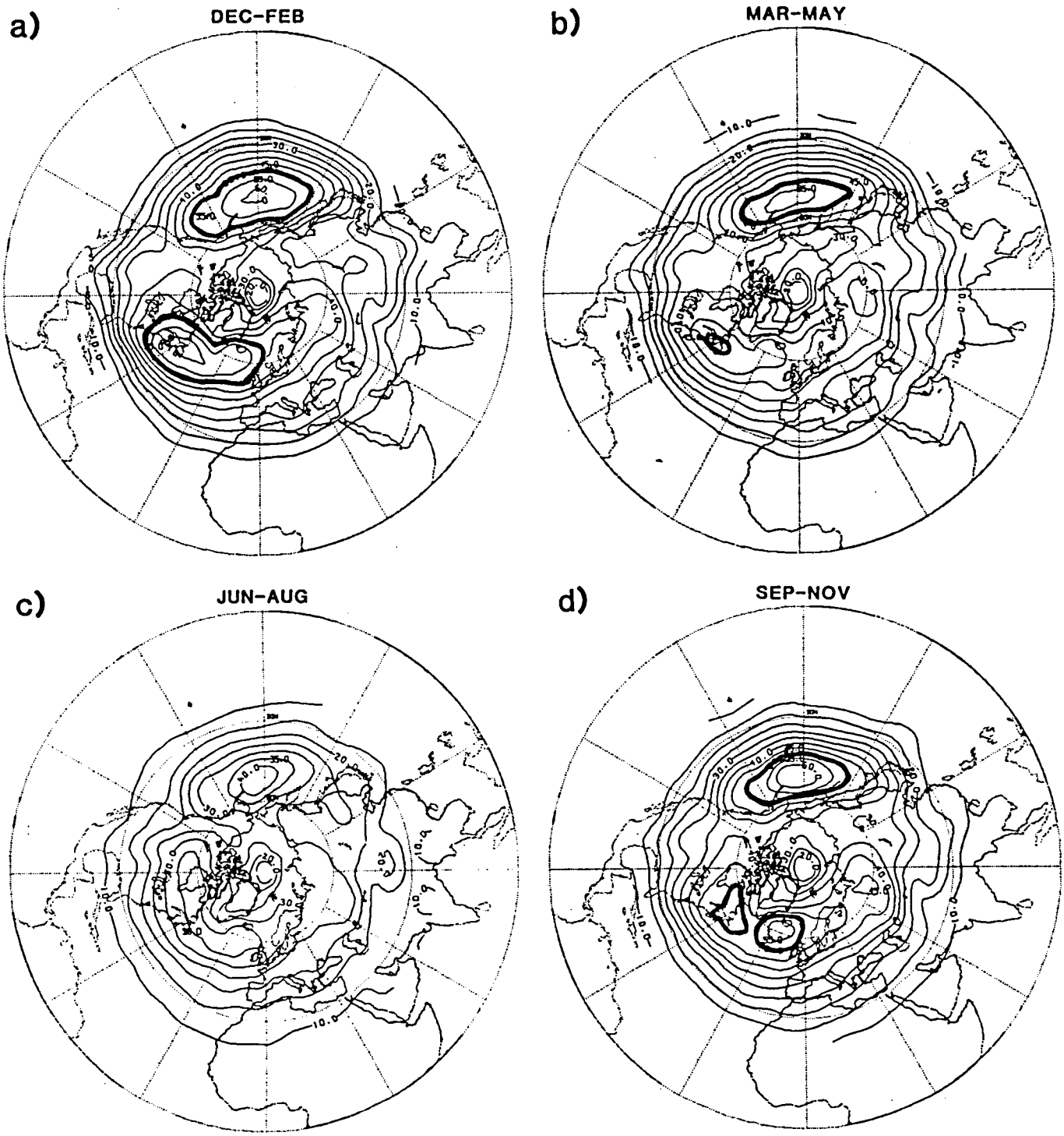

Fig. 1 Polar stereographic plots of Northern Hemisphere 850 mb standard deviation of band-pass filtered height fields, (a) Winter (Dec.-Feb.), (b) Spring (Mar.- May), (c) Summer (June-Aug.,), (d) Fall (Sept.-Nov.). The 50 m contour is drawn more heavily.

The Contrasting Northern Hemisphere Winters of 1980-81 and 1981-82

Glenn H. White

Seasonally averaged statistics calculated from daily operational analyses by the European Centre for Medium Range Weather Forecasts (ECMWF) for December 1980-February 1981 (winter 1) and December 1981-February 1982 (winter 2) are used to contrast the two seasonal mean circulation patterns present in the Northern Hemisphere and to investigate possible causes for the differences. The differences between winter 1 and winter 2 resemble patterns associated with the Southern Oscillation (White, 1984) and may be forced by a weak warm El Nino-Southern Oscillation (ENSO) event in 1980.

Low-level diabatic heating is much stronger over the North Atlantic in winter 2 (Fig. 1), where changes in sea surface temperatures imply a much greater loss of heat by the ocean to the atmosphere in winter 2. Changes in the flow pattern over the United States and the North Atlantic from winter 1 to winter 2 resemble the response to warm sea surface temperature anomalies found by Phillips (1982) in a nonlinear model of a baroclinically unstable atmosphere. A large change of opposite sign in diabatic heating, strongest at 500 mb, is observed over Japan.

Zonally averaged and three-dimensional Eliassen-Palm fluxes (Plumb, 1984) for the two winters (Fig. 2) suggest that stationary waves are mainly forced near the surface in midlatitudes. The forcing appears to be significantly less in winter 2, particularly near the south coast of Alaska where the low-level seasonal mean flow over orography was much weaker in winter 2. Since changes in the low-level flow over the Pacific appear related to changes in equatorial sea surface temperatures and precipitation in the Pacific (Fritz (1984)), a weak ENSO event in 1980 may have produced a delayed response in the circulation over the Pacific in winter 1 that resulted in unusually strong orographic forcing over Alaska and western Canada.

References

Fritz, S., 1984: The winter Aleutian low and its relation to tropical Pacific Ocean temperature. Proc. 8th Climate Diagnostics Workshop, Downsview, Ontario, Canada, 17-21 Oct. 1983, 177-184. [Available from NOAA Library, Washington, D.C.]

Phillips, T. J., 1982: On the interaction of surface heating anomalies with zonally symmetric and asymmetric atmospheric flow. J. Atmos. Sci., 39, 1953-1971.

Plumb, R. A., 1984: On the three-dimensional propagation of stationary waves. Submitted to J. Atmos. Sci.

White, G. H., 1984: Two contrasting Northern Hemisphere winters: 1980-81 and 1981-82. Research Review-1983, GMSB, GLAS, NASA/GSFC, NASA Technical Memo. 86053, 209-212.

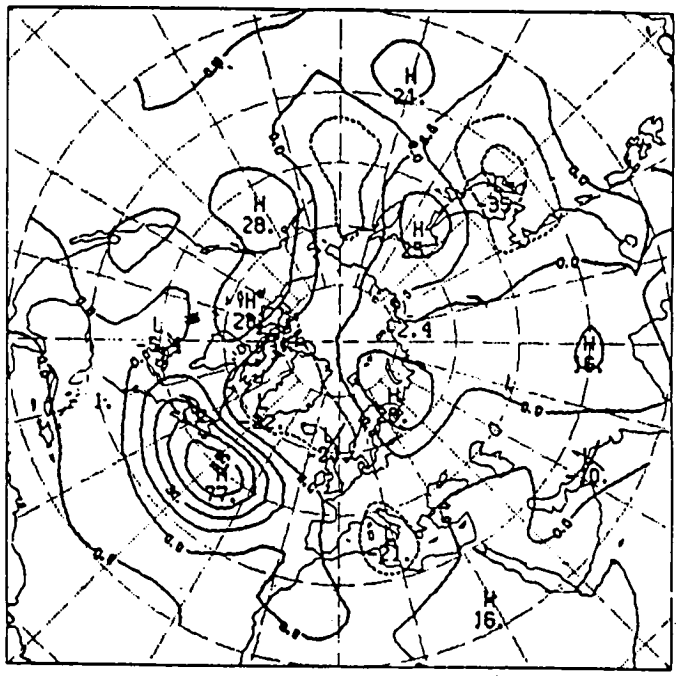

Fig. 1 Change in diabatic heating in the 1000-775 mb layer from winter 1 to winter 2. Contour interval 15 watts/m^2, dashed contours represent cooling.

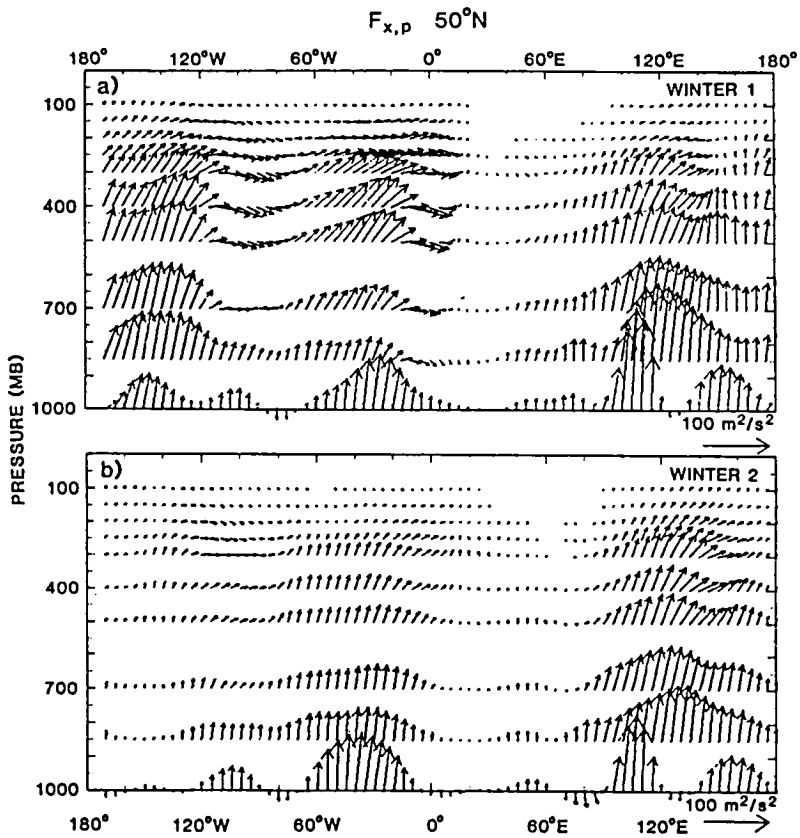

Fig. 2 Longitude-height cross-section of 3-D Eliassen-Palm fluxes for stationary waves (Plumb, 1984) at 50°N for winter 1 (Fig. 2a) and winter 2 (Fig. 2b)

On the Global Distribution of Three-dimensional Eliassen-Palm Fluxes by Stationary Waves

Glenn H. White

New insights into the propagation of atmospheric waves have recently been gained from the use of zonally averaged Eliassen-Palm (EP) fluxes (Edmon et al., 1980). If wave dynamics can be described by linear planetary-wave theory and if the poleward gradient of quasi-geostrophic potential vorticity is positive, EP fluxes measure the net propagation of waves and can be used to infer the forcing of waves. A three-dimensional EP flux for stationary waves has recently been derived by Plumb (1984):

$$\underset{\sim}{F} = \left(\frac{p}{p_o}\right) \cos\phi \left[\left(\overline{v}^{*2} - \frac{1}{2f}\frac{\partial(\overline{v}^{*}\overline{\phi}^{*})}{\partial x}\right)\hat{i} + \left(-\overline{u}^{*}\overline{v}^{*} + \frac{1}{2f}\frac{\partial(\overline{u}^{*}\overline{\phi}^{*})}{\partial x}\right)\hat{j}\right.$$

$$\left. + \frac{f}{S}\left(\overline{v}^{*}\overline{T}^{*} - \frac{1}{2f}\frac{\partial(\overline{\phi}^{*}\overline{T}^{*})}{\partial x}\right)\hat{k}\right]$$

where $\overline{(\ )}$ represents a time-mean, $(\ )^*$ the departure from the zonal mean, u and v the zonal and meridional winds, T temperature, Φ geopotential, ϕ latitude, f the Coriolis parameter, S static stability (allowed to vary only with pressure p), and p_o = 1000 mb. Plumb (1984) presented observational results for the extratropical Northern Hemisphere wintertime climatological circulation based on statistics calculated from NMC operational analyses for 1965-1976.

This study investigated the global distribution of three-dimensional EP fluxes (Fig. 1) by using statistics for Dec. 1980-Feb. 1981 (Figs. 1a, b) and June-August 1981 (Figs. 1c,d) calculated from operational analyses by the European Centre for Medium-range Weather Forecasts. Results at 1000 (Figs. 1a,c) and 150 mb (Figs. 1b,d) are shown. During the Northern Hemisphere (NH) winter strong upward fluxes can be seen at 1000 mb (Fig. 1a) in the lee of the Himalayas and Rockies, windward of the Canadian Rockies in the east Pacific, to the north of the Atlantic stormtrack and over the west Pacific in a region of strong land-sea thermal contrast. Upward fluxes also appear near the west coasts of the Southern Hemisphere (SH) subtropical continents regions of strong land-sea thermal contrast. At 150 mb (Fig. 1b) the strongest upward flux now occurs south of Alaska. The horizontal fluxes imply poleward propagation from the convection over Indonesia to 20°N, a region where the assumptions underlying EP fluxes are not well-met. Equatorward propagation dominates the NH midlatitudes except over the Pacific.

During June-August 1981 at 1000 mb (Fig. 1c) upward fluxes appear off the western coasts of the subtropical continents in both hemispheres but are particularly strong in the NH where strong land-sea thermal contrast is found. At 150 mb (Fig. 1d) strong fluxes from the Indian monsoon into the SH can be seen where easterly winds prevail, which theory and numerical models predict would prevent propagation (Webster and Holton, 1982). Strong fluxes also occur at 30°N over the eastern Mediterranean, a region of strong sinking, and over the Pacific and the southeastern U.S., regions of rising motion (White, 1983).

The fluxes shown in Fig. 1 offer tantalizing hints of the sources of stationary waves, but also show several puzzling features and a rather cavalier

disregard of regions of easterly wind. The physical meaning and interpretation of three-dimensional EP-fluxes is not yet clear.

References

Edmon, H. J., Jr., B. J. Hoskins, and M. E. McIntyre, 1980: Eliassen-Palm cross-sections for the troposphere. J. Atmos. Sci., 37, 2600-2616.

Plumb, R. A., 1984: On the three-dimensional propagation of stationary waves. Submitted to J. Atmos. Sci.

Webster, P. J., and J. R. Holton, 1982: Cross-equatorial response to middle-latitude forcing in a zonally varying basic state. J. Atmos Sci., 39, 722-733.

White, G. H., 1983: Estimates of the seasonal mean vertical velocity fields of the extratropical Northern Hemisphere. Mon. Wea. Rev., 111, 1418-1433.

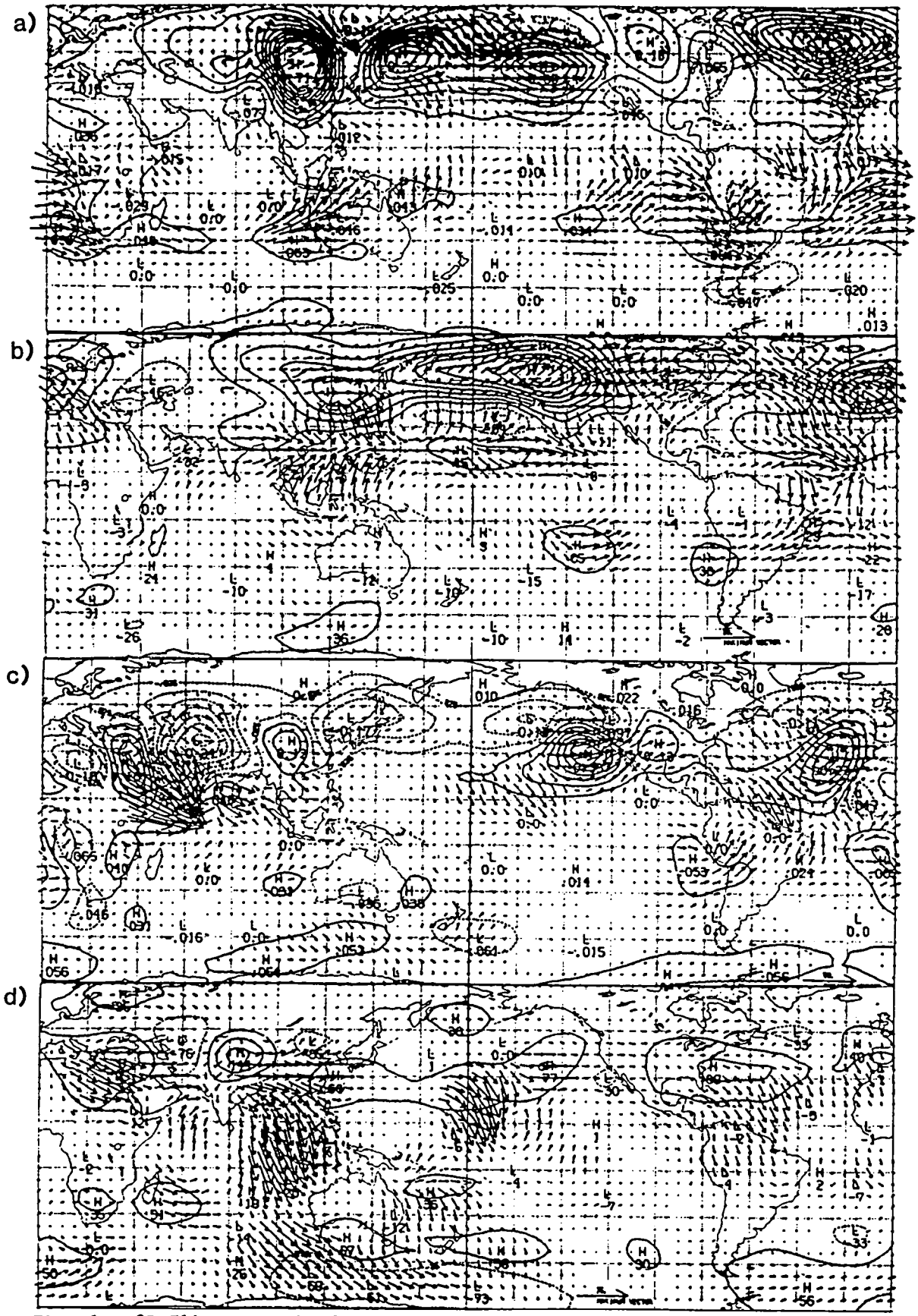

Fig. 1. 3D Eliassen-Palm fluxes during Dec. 1980-Feb. 1981 at a) 1000 and b) 150 mb and during June-August 1981 at c) 1000 and d) 150 mb. Solid contours denote upward fluxes and dashed contours downward fluxes; contour interval at 1000 mb is ten times that at 150 mb.

Transient eddies in the UCLA GCM

Glenn H. White

The simulation of transient eddies in the nine-level UCLA general circulation model (GCM) has been examined and compared to observations, with emphasis on the Northern Hemisphere winter. Qualitatively, the UCLA GCM reproduces many features of the observed circulation and the relationship between the time-mean flow and transient eddies; however, the magnitudes of transient eddies in the UCLA GCM, particularly at frequencies lower than those associated with baroclinic instability, appear to be much less than those observed.

Fig. 1a shows the wintertime mean 500 mb height field for one simulated winter. The Asian trough appears broader than in the observed climatology (Lau et al., 1981) while the ridge over western Canada is well to the east of its climatological position. The North American trough is much weaker than observed, while an unusually strong ridge occupies the east Atlantic. Such anomalous features can be observed in seasonal mean fields for individual winters (Lau et al., 1981); however, the other two winters in the simulation examined show very similar anomalous features, implying a departure of the climatology of the UCLA GCM from observations.

The patterns of low-level transient eddy heat fluxes were similar to observations and acted to dissipate the low-level seasonal-mean temperature field, as observed (Lau et al., 1981). The simulated shape of transient disturbances also appeared similar to observations, with eddies of baroclinic time scales displaying a north-south elongation and disturbances of longer time scales an east-west elongation (Hoskins et al., 1983). Baroclinic eddies in the simulation dissipated when they encountered a longer-lived ridge, a pattern also observed (Hoskins et al., 1983).

The simulated transient eddy kinetic energy at 300 mb is displayed in Fig. 1b for eddies of all time scales shorter than a season, in Fig. 1c for time scales associated with baroclinic instability, and in Fig. 1d for time scales longer than in Fig. 1c. (The actual filters used were the "Lorenz" filters discussed on pg. 7 of Lau et al., 1981.) The pattern in Fig. 1b is somewhat similar to that observed at 250 mb by White (1983, pg. 10); however the maximum values in Fig. 1b are only a third of the maximum values found by White (1983) and are located 10° further north. The maximum values for eddies of baroclinic timescales (Fig. 1c) are three-fourths of those observed (White, 1983), suggesting, as Fig. 1d shows, that the UCLA GCM is deficient in low-frequency variability, a shortcoming found in other GCM's (Straus and Shukla, 1981). The poleward shift of the simulated storm tracks relative to observations may reflect a similar shift in the region where the seasonal mean flow is baroclinically unstable, particularly in the Pacific.

References

Hoskins, B. J., I. N James, and G. H. White, 1983: The shape, propagation and mean-flow interaction of large-scale weather systems. J. Atmos. Sci., 40, 1595-1612.

Lau, N.-C., G. H. White, R. L. Jenne, 1981: Circulation Statistics for the Extratropical Northern Hemisphere based on NMC Analyses. National Center for Atmospheric Research, Tech. Note NCAR/TN-171+STR, 138 pp.

Straus, D. M., and J. Shukla, 1981: Space-time spectral structure of a GLAS general circulation model and a comparison with observations. J. Atmos Sci., 38, 902-917.

White, G. H., 1983: The Global Circulation of the Atmosphere Dec. 1981-Nov. 1982 Based on ECMWF Analyses . Technical Report, Dept. Meteor., Univ. of Reading, U. K., 209 pp.

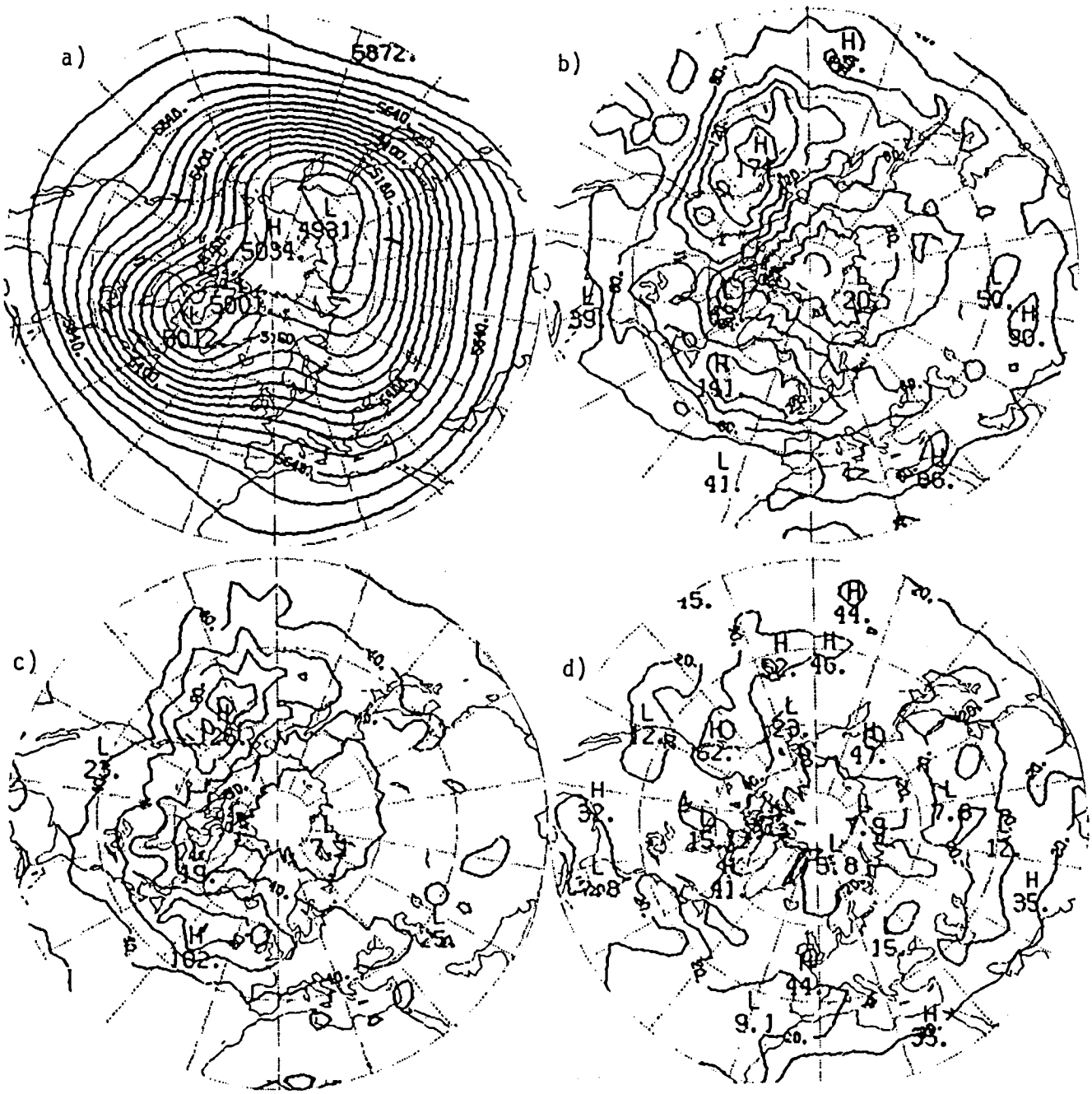

Fig. 1 UCLA GCM simulations of wintertime mean a) 500 mb geopotential height and 300 mb transient eddy kinetic energy, b) unfiltered, c) high-pass filtered, and d) low-pass filtered.

B. CLIMATE AND OCEAN MODELING

On Fofonoff's Mode

Lee - Or Merkine

Department of Mathematics Technion Israel Institute of Technology

Kingtse Mo and Eugenia Kalnay

The classical barotropic ocean model of Veronis (1966) is re-examined to verify the possible existence of Fofonoff's (1954) steady free inertial mode by considering the balance

$$J (\eta, R\nabla^2\eta + y) = 0 \qquad (1)$$

where J is the Jacobian, η is the streamfunction of the horizontal velocity, and R is a parameter of nonlinearity. A linear functional relationship between the potential vorticity and the streamfunction and inertial boundary layers along the ocean basin was suggested by Fofonoff.

$$R\,\nabla^2\eta + y = G(\eta)$$

where $G(\eta)$ is an unknown function

As in Veronis' work, we assume a square basin with the consequent boundary conditions.

$$\eta = 0 \text{ on } x = 0,\ \pi \text{ and } y = 0,\ \pi$$

and a wind stress given by

$$k \cdot \nabla \times \vec{\tau} = -\sin x \sin y$$

We consider a very strong beta effect such that $R = 10^{-6}$ and $\varepsilon = 10^{-4}$ where ε measures the strength of the dissipation. This set of parameters puts the system in the range where the Fofonoff's hypothesis holds.

However the numerical integration shows that the system is barotropically unstable. The typical instantaneous field is shown in Fig. 1. The statistical equilibrium state $\bar{\eta}$ is depicted in Fig. 2. Although it resembles Fofonoff's solution, it is maintained by the Reynolds stress field induced by the eddies in addition to the wind stress and dissipation. The plot of η versus $R\,\nabla^2\eta + y$ is given in Fig. 3. It shows that the Fofonoff's linear relation between the potential vorticity and the streamfunction does not hold uniformly over the entire basin. The above results show that the Fofonoff's solution can not be realized physically.

References:

Fofonoff, N. P., 1985: "Steady flow in a frictionless homogeneous ocean" J. Mar. Rev. 13, 254 - 262.

Veronis G., 1966: "Wind driven ocean circulation part 2 - numerical solutions of the nonlinear problem" Deep Sea Rev., 13 31-55.

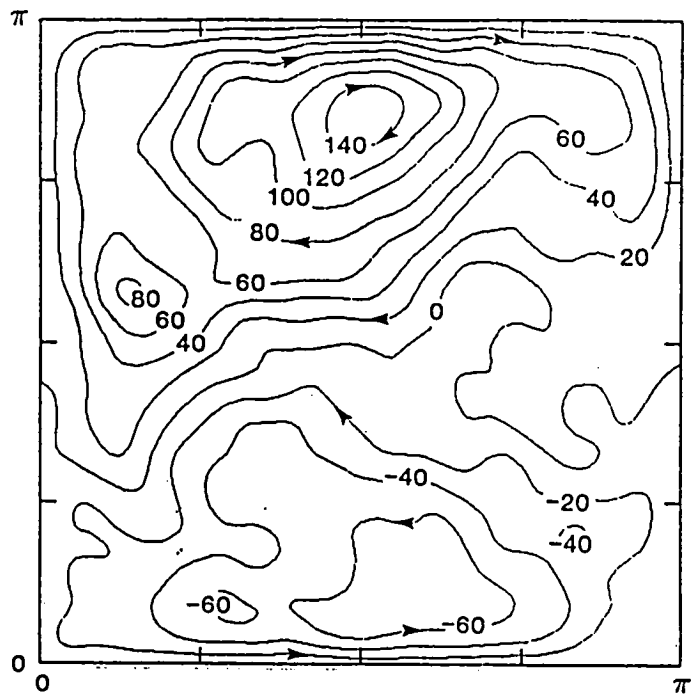

1. An instantaneous streamfunction field. The contour intervals are in percentage of n/η max.

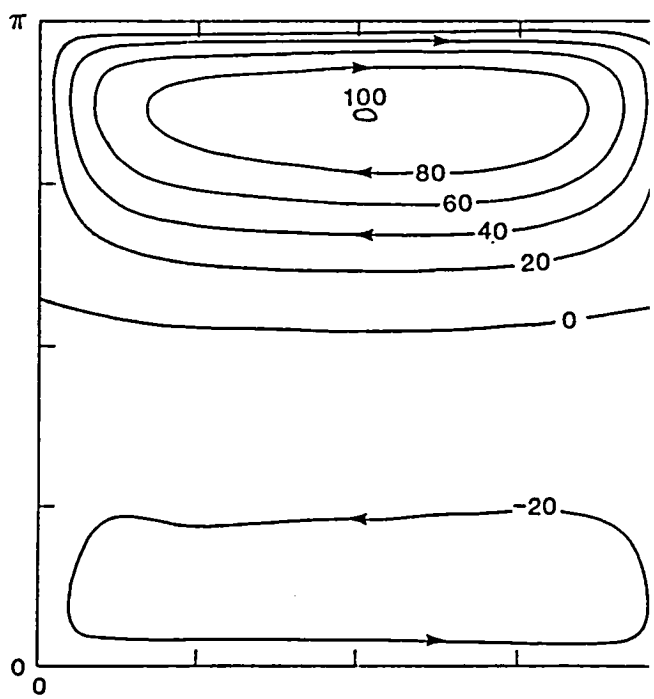

2. Averaged streamfunction field.

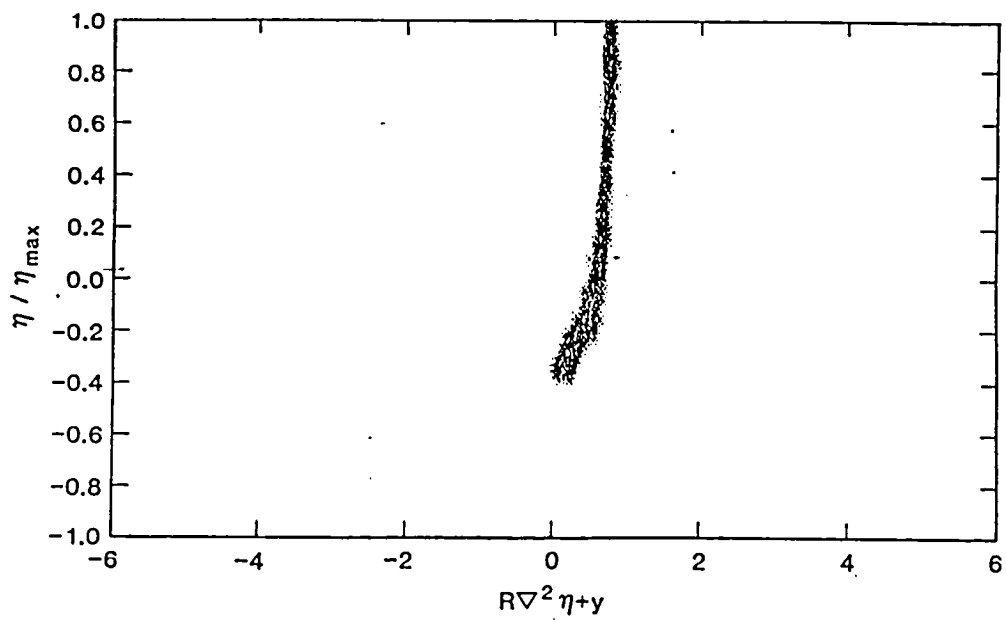

3. Scatter diagram of the R ∇^2 + y against $\bar{\eta}/\eta$ max. Where $\bar{\eta}$ max = 51500.

Analysis of a Simulated Cloud Climatology

D. Randall, Harshvardhan, D. Short, and T. Corsetti

Cloudiness simulations with the UCLA/Goddard GCM have been analyzed by comparison of simulated cloud and radiation statistics with corresponding observations. A description of the model formulation is given by Suarez et al. (1983), and some results are discussed by Randall et al. (1985).

The global mean cloudiness is near 50%, in agreement with observations. However, comparison with the satellite observations of Susskind et al. (1983) shows that the model produces too many low-level clouds at high latitudes and too few high clouds in the tropics. The Intertropical Convergence Zone is hardly visible in the simulated cloudiness maps, although it is quite apparent in the simulated precipitation field. In the subtropics, the marine subtropical stratocumulus regimes are correctly positioned, but the cloud amounts are seriously underpredicted. The Arctic summer stratus is not well simulated. Over the Northern Hemisphere continents in winter the model produces an overabundance of low clouds, although these are geometrically and optically very thin, and might well be missed in the observations.

The simulated outgoing longwave radiation at the top of the atmosphere is too low in middle and high latitudes, and much too high in regions of deep convection (Fig. 1). The standard deviation of daily mean outgoing longwave radiation is overpredicted in regions of deep convection. These results suggest that cirrus clouds are too infrequent and too variable in the model results.

Seasonal variations of outgoing longwave radiation in the tropics and subtropics, as measured by the phase of the first annual harmonic, are fairly realistic in regions of observed low-level cloudiness, and quite unrealistic in regions of observed high-altitude cloudiness.

In summary, the most serious deficiency of the current model's cloudiness simulation is its gross underprediction of the cirrus cloudiness associated with deep convection. We are currently working to remedy this problem by incorporating a prognostic variable for cirrus cloud water.

References

Randall, D. A., J. A. Abeles, and T. G. Corsetti, 1985: Seasonal simulations of the planetary boundary layer and boundary-layer stratocumulus clouds with a general circulation model. J. Atmos. Sci. (to appear).

Suarez, M. J., A. Arakawa, and D. A. Randall, 1983: The parameterization of the planetary boundary layer in the UCLA general circulation model: Formulation and results. Monthly Weather Review, 111, 2224-2243.

Susskind, J., J. Rosenfield, D. Reuter, and M. T. Chahine, 1984: Remote sensing of weather and climate parameters from HIRS2/MSU on TIROS-N. J. Geophys. Res., 89D, 4677-4698.

TERRESTRIAL RADIATION AT THE TOP OF THE ATMOSPHERE (W m^{-2})

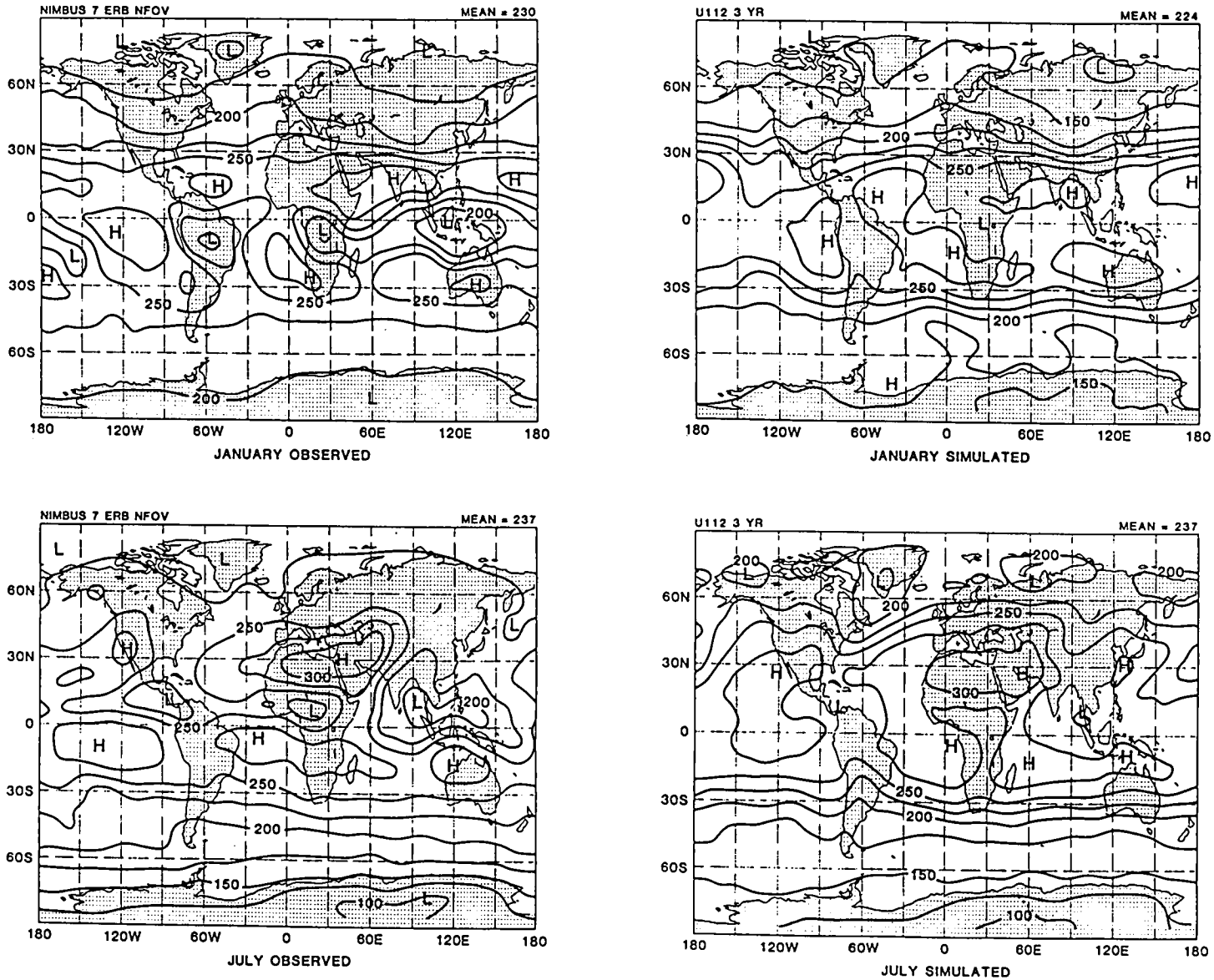

Figure 1: Model-simulated (right) and NIMBUS 7 - observed (left) terrestrial radiation at the top of the atmosphere for January (top) and July (bottom). The contour interval is 25 W m^{-2}.

The Moist Available Energy of a Conditionally Unstable Atmosphere

D. Randall and T. Corsetti

Lorenz (1978, 1979) defined the moist available energy (MAE) of a given state of the global atmosphere as the difference between the moist enthalpy of the given state and that of a hypothetical "reference" state for which the moist enthalpy is minimized by reversible adiabatic rearrangement of the air parcels. Within the reference state, the pressure and density are horizontally stratified, hydrostatic equilibrium holds, and the stratification is statically stable. However, a given horizontal surface in the reference state may contain both a saturated cloudy region and an unsaturated clear region.

For an atmosphere containing no moisture, the MAE is identical to the "available potential energy" or "dry available energy" discussed by Lorenz (1955). In general, however, the MAE of a humid atmosphere is greater than its dry available energy. For a realistic atmosphere which is everywhere statically stable (or neutral) in the dry sense, but contains regions of conditional instability, the moist available energy arises in part from horizontal temperature gradients and in part from the conditional instability.

Consider a hypothetical horizontally homogeneous atmosphere for which the temperature and moisture soundings are typical of conditionally unstable regions in the tropics. For such an atmosphere the MAE is entirely due to the presence of conditional instability, and is a measure of the degree of conditional instability. How is the MAE of this atmosphere related to the cloud work function of Arakawa and Schubert (1974), or to other conventional measures of conditional instability? The cloud work function is a measure of the energy available to a particular type of circulation, represented by a very simple model of a cumulus cloud. The simple cloud model is actually used in the computation of the cloud work function. The MAE, on the other hand, is the maximum energy available to <u>any</u> circulation, and its definition does not involve a particular cloud model. It is therefore more general than the cloud work function, and must exceed the cloud work function in most cases.

Lorenz (1978, 1979) suggested graphical and numerical algorithms for computing the MAE for a given state of the atmosphere. Both algorithms encounter some difficulty when the given state is conditionally unstable. We have devised two simple methods for computing the MAE for cases in which the total number of parcels is fairly small. The first is a "swapping" routine that finds the reference state by exchanging parcels whenever the swap reduces the total enthalpy. However, we can prove by contrived example that the swapping algorithm does not always find the true reference state. A second "brute force" routine actually examines all possible arrangements of the parcels and chooses the one with the smallest moist enthalpy. At present, both routines allow only horizontally homogeneous reference states.

In an exploratory study, we have used the swapping routine to find MAE and reference state for a time-sequence of GATE soundings, all of which are conditionally unstable. In spot checks, the brute-force routine always agreed with the swapper. Results show that in passing from the given state to the reference state the lowest three hundred mb of the atmosphere typically exchanges places

with the 300 mb above it. The reference state then contains a dry warm layer near the surface, and a supersaturated but cool layer in the middle troposphere. The upper portion of the sounding is not modified in passing from the given state to the reference state.

We are continuing this work by comparing the MAE with the cloud work function, by investigating the rates at which MAE is generated by surface fluxes and large-scale vertical motion, and by investigating the possibility of horizontally inhomogeneous reference states.

References

Arakawa, A., and W. H. Schubert, 1974: The interaction of a cumulus cloud ensemble with the large-scale environment, Part I. J. Atmos. Sci., 31, 674-701.

Lorenz, E. N., 1955: Available potential energy and the maintenance of the general circulation. Tellus, 7, 157-167.

Lorenz, E. N., 1978: Available energy and the maintenance of a moist circulation. Tellus, 30, 15-31.

Lorenz, E. N., 1979: Numerical evaluation of moist available energy. Tellus, 31, 230-235.

Preliminary GCM Results with a New Radiation Parameterization

D. Randall, Harshvardhan, R. Davies, and T. Corsetti

We have developed new parameterizations of solar and terrestrial radiation and they have been tested UCLA/Goddard GCM. The solar radiation parameterization is based on that of Lacis and Hansen (1974), but with zenith-angle-dependent surface albedoes, and revised treatments of cloudiness. The terrestrial radiation parameterization is based on the work of Chou 1984) for water vapor, Chou and Peng (1983) for carbon dioxide, and Rogers (1968) for ozone, with a new parameterization of the effects of clouds. Some details are given by Harshvardhan and Corsetti (1984).

The codes have been designed for efficient execution on a vector processor, and we find that, for all gridpoints in a 4 x 5 degree 9-level GCM, one pass consumes about 2 cpu seconds on Goddard's two-pipe CDC Cyber 205. This excellent computational speed allows us to do a full radiation calculation once each simulated hour.

We have compared results obtained with the new parameterizations to those obtained with the earlier parameterization described by Schlessinger (1976). Several dramatic improvements have come to light. For the most part these are related to the fact that the new terrestrial radiation paramerization includes the effects of the water vapor continuum, while the earlier parameterization does not. In the moist tropical planetary boundary layer, continuum emission leads to much stronger cooling of the PBL over the oceans. Over land, however, the cooling of the PBL is significantly reduced. The latter, somewhat paradoxical result is due to the strong diurnal cycle of the continental PBL. At night the shallow continental PBL is overlain by a moist layer created by mixing during the previous afternoon. The moist upper layer acts as a radiative blanket, reducing the time-averaged radiative cooling of the continental PBL.

The stronger cooling of the marine tropical PBL leads to an increase in the surface sensible heat flux, and an increase in the relative humidity at the PBL top. These are both improvements in the realism of the model results.

We have corrected an error which caused cumulus anvils to be ignored, with radiation calculation. As shown in Fig. 1, this has resulted in a simulated diurnal cycle of precipitation over the oceans, in agreement with the observation of Gray and Jacobsen (1977).

In summary, changes to the model's radiation parameterization have led to significant improvements in the simulated climate.

References

Chou, M.-D., and L. Peng, 1983: A parameterization of the absorption in the 15 μm Co_2 spectral region with application to climate sensitivity studies. J. Atmos. Sci., 40, 2183-2192.

Chou, M.-D., 1984: Broadband water vapor transmission functions for atmospheric IR flux computation. J. Atmos. Sci., 41, 1775-1778.

Gray, W. M., and R. W. Jacobsen, Jr., 1977: Diurnal variation of oceanic deep cumulus convection. Mon. Wea. Rev., 105, 1171-1188.

Harshvardhan, and T. G. Corsetti, 1984: Longwave radiation paramterization for the UCLA/GLAS GCM. NASA Tech. Memo. 86072, 51 pp.

Lacis, A. A., and J. E. Hansen, 1974: A parameterization for the absorption of solar radiation in the earth's atmosphere. J. Atmos. Sci., 31, 118-135.

Rodgers, C. D., 1968: Some extensions and applications of the new random model for molecular band transmission. Quart. J. Roy. Met. Soc., 94, 99-102.

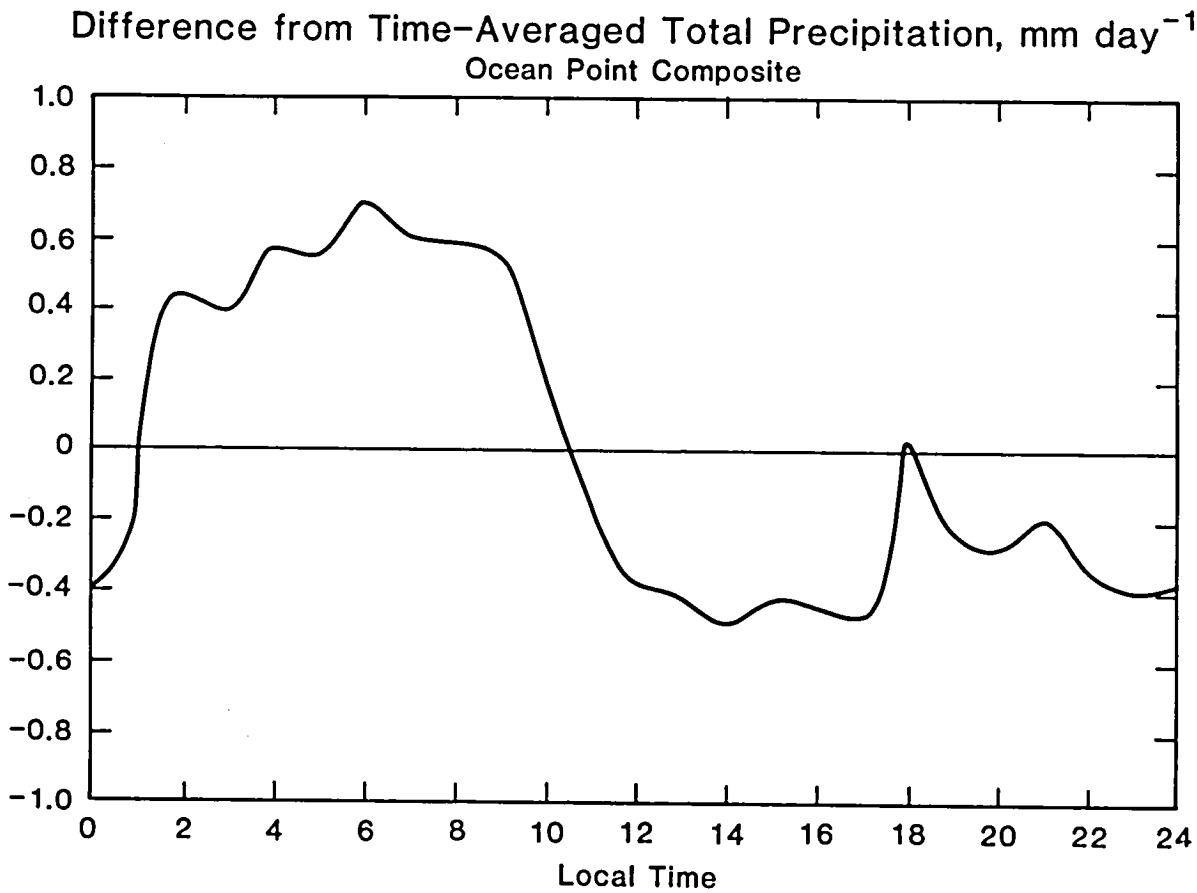

Figure 1. Simulated departure of the total precipitation rate from the time mean, as a function local time of day, composited for 24 ocean grid points.

Multiple Equilibria of the Barotropic Vorticity Equation on a Sphere

M. J. Suarez

In their landmark paper on multiple-equilibria, Charney and Devore (1979) (CD) argued that in the presence of topography a forced zonal flow can satisfy the zonal momentum balance in more than one way. For a strong zonal flow the stationary wave is small and results in little form drag on the zonal flow so that it can be at equilibrium near its forced value. A second state can occur provided the mountain is sufficiently high, the wave damping sufficiently small, and the forced wave is contained in a resonant cavity. In this state the wave amplitude is large, and the form drag on the zonal flow can balance a large departure from the forcing. Such a state is possible only if the zonal flow is being forced to a value well above that at which one of the waves excited by the topography is resonant.

For a two-dimensional non-divergent flow between rigid boundaries the zonal momentum balance is

$$\frac{\partial [u]}{\partial t} = [v^* \zeta^*] + \frac{f}{H_o} [v^* h^*] - \kappa ([u] - [u]_e) \quad . \tag{1}$$

Here brackets indicate zonal means and asterisks deviations from the zonal mean. The height of the topography is h and the mean depth of the fluid H_o. The zonal flow is forced to a value $[u]_e$ in time κ^{-1}. f is the coriolis parameter and ζ the relative vorticity. In CD's argument a relative maximum of the second term on the r.h.s as a function of [u], which is associated with a strong wave response near resonance, results in the second and third terms balancing each other in the ways just described. The first term on the r.h.s. plays no role. Although the argument is based on the linear wave response for a given zonal flow, CD goes on to show through numerical solutions that the full equations on a beta-plane channel also possess multiple stable states.

The purpose of this paper is to present multiple states of the barotropic vorticity equation in which the balance is between the first and third terms on the r.h.s. of (1). Solutions of this type were also considered by CD in their discussion of thermally, rather than topographically, forces waves. Whereas in the case of topographic forcing the multiplicity arises from what they called "form-drag instability" in the wave-zonal flow interaction, in the "thermal forcing" case the associated instability appears to be the Rossby-wave instability discussed by Lorenz (1972), and the multiple states of the highly truncated model proved to be unstable when more degrees of freedom were added.

The multiple statistically steady solutions described below are thus novel in that they do not involve form-drag instability, they have stable statistics in calculations with a large number of degrees of freedoms, and they occur on the sphere, with no artificial confinement in a resonant cavity. Further the solutions are obtained with no external forcing of the zonal flow.

We will use the full non-linear equations for two-dimensional non-divergent motion between smooth, rigid boundaries on a sphere. The zonally asymmetric part of the flow is governed by

$$\frac{\partial \zeta^*}{\partial t} = -\frac{1}{a\cos\phi}\left\{\frac{\partial}{\partial\lambda}(uq - [uq]) + \frac{\partial}{\partial\phi}\cos\phi\,(vq - [vq])\right\} + F^*, \qquad (2)$$

where $q \equiv \zeta + f$ is the absolute vorticity. We will consider only simple forcings of the form

$$F^* = \kappa\,(\zeta_e - \zeta^*) \quad , \qquad (3)$$

where κ is constant and ζ_e a prescribed function of latitude and longitude, with

$$[\zeta_e] = 0 \ .$$

With no topography ($h^* = 0$), and no external forcing of the zonal flow ($[u]_e = 0$) (1) becomes

$$\frac{\partial [u]}{\partial t} = [v^*\zeta^*] - \kappa\,[u] \quad , \qquad (4)$$

a simple balance between frictional and eddy stresses. Eqs. (1) and (4) are solved numerically using finite differences on latitude-longitude coordinates. A resolution of 2° latitude by 2.5° longitude is used. Integrations are carried forward until a meaningful statistical steady state can be obtained, usually 400 days. The forcing used is of the form

$$\zeta_e = \zeta_o \exp -\left\{\frac{\phi + \phi_o}{\Delta\phi}\right\}^2 \sin(m\lambda) \quad . \qquad (6)$$

In all cases $\Delta\phi = 15°$, $\phi_o = 40°$, and $k = 1/15\ d^{-1}$.

Experiments with m = 3.

Experiments were performed with various wavenumbers and frequencies of forcing. Here we show results only for a stationary forcing in wavenumber 3, which illustrate the multiple states we found. Similar multiplicities occur for shorter waves with eastward propagating forcing.

Figure 1 shows the zonal flows obtained for four values of ζ_o when the calculations were started from rest. The interpretation of these is straight forward: westerlies appear at the latitudes where the waves are forced and friction on the zonal wind balances eddy convergence of westerly momentum. Away from the forcing the forced wave is damped, depositing easterly momentum. This produces a zonal flow with critical latitudes for the forced stationary wave just north and south of the region of forcing. Note that easterlies are stronger on the poleward than on the equatorward side, as one would expect if the waves tend to transport equal angular momentum in both directions.

As the forcing is increased this zonal flow pattern is amplified. However, since the zonal mean absolute vorticity gradient is being modified as the zonal flow changes, this amplification cannot continue indefinitely with increased forcing without a substantial change in the flow. Figure 2 shows the quantity β_m, as defined by Hoskins and Karoly (1981),

$$\beta_m \equiv \frac{2\Omega}{a}\cos^2\phi - \frac{\cos\phi}{a}\frac{\partial}{\partial\phi}\frac{1}{\cos\phi}\frac{\partial}{\partial\phi}(\cos\phi\,[u]$$

which is $\cos\phi$ turns the absolute vorticity gradient. In the westerly jet, it is increased above its planetary value, and in the easterly jets it is depressed. For the largest forcing it is already slightly negative in the polar easterly jet, so that the inviscid stability condition is not satisfied. This is in fact the strongest forcing for which solutions like those in figure 1 were obtained. Above this value the solution is dramatically different, with no polar easterlies, a broad, strong westerly jet over the forcing, and balancing easterlies in the subtropics of forced hemisphere and mid-latitudes of the unforced hemisphere. This very sharp transition in the response suggested a bifurcation of the solution for which two stable branches may exist for some range of parameters. To explore this possibility the four experiments were repeated using initial conditions with a westerly jet of ~ 80 m/s at 40° in both hemispheres and easterlies in the tropics. The first three cases quickly evolved to the solutions shown in figure 1. For the strongest forcing, however, a stable upper branch solution was obtained. Figure 3 shows the time evolution for this case when started from rest and when started from the strong westerly jet. The characteristics of the upper branch steady state just described are evident.

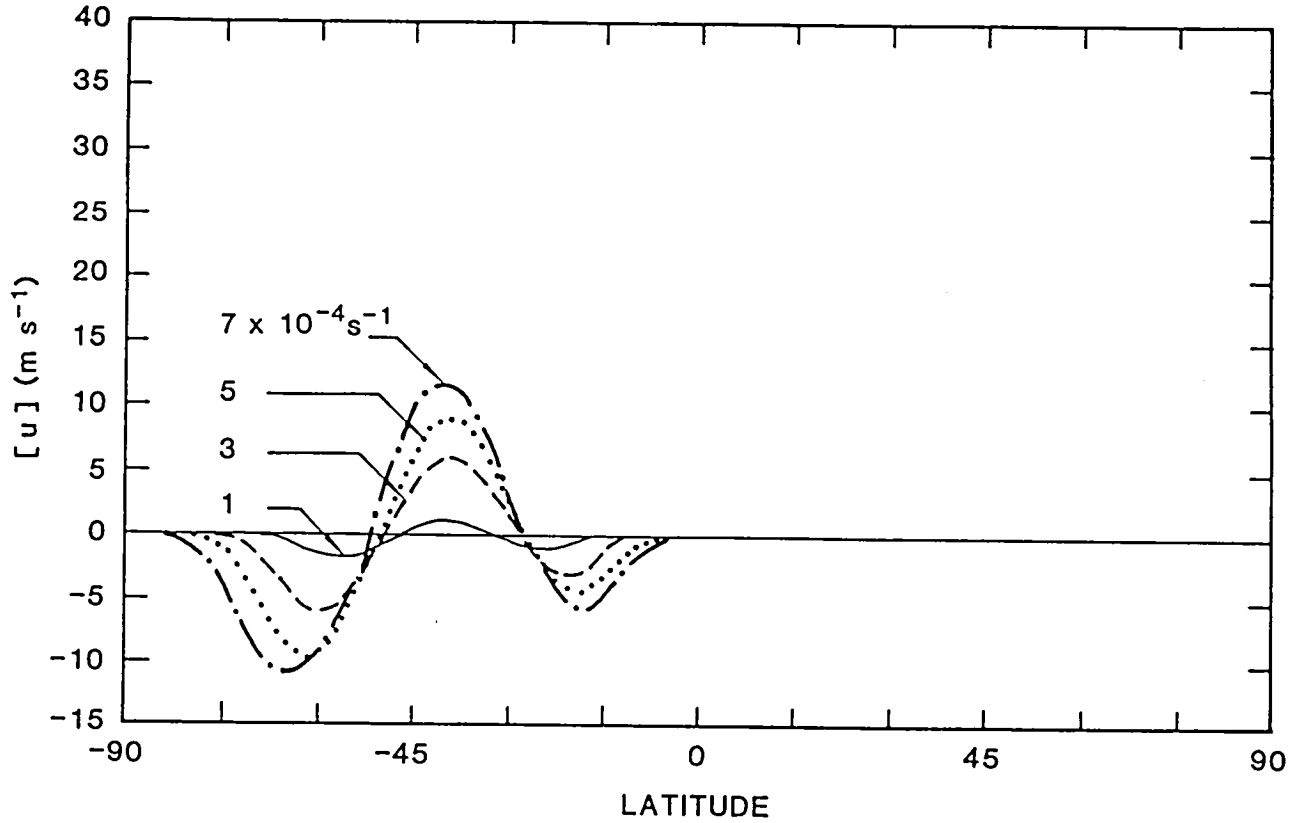

Figure 1

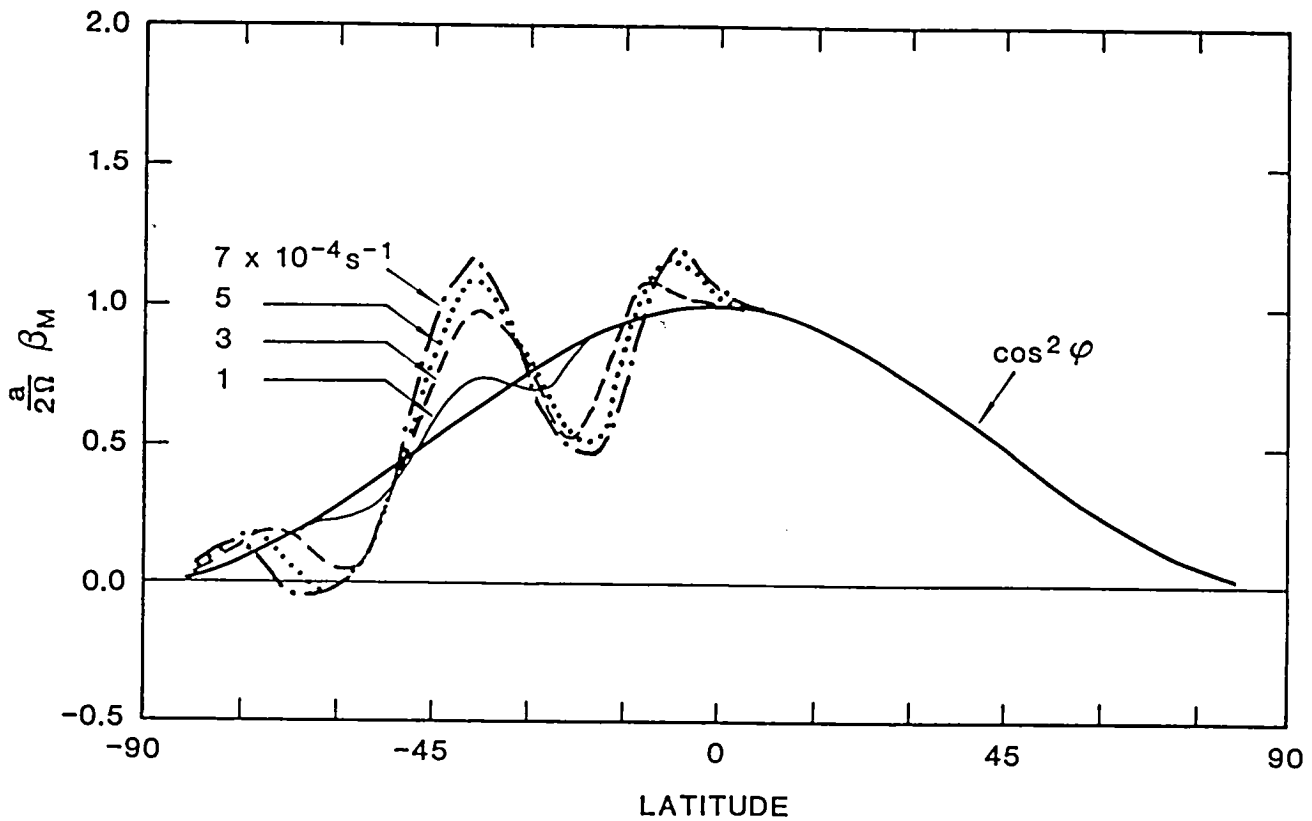

Figure 2

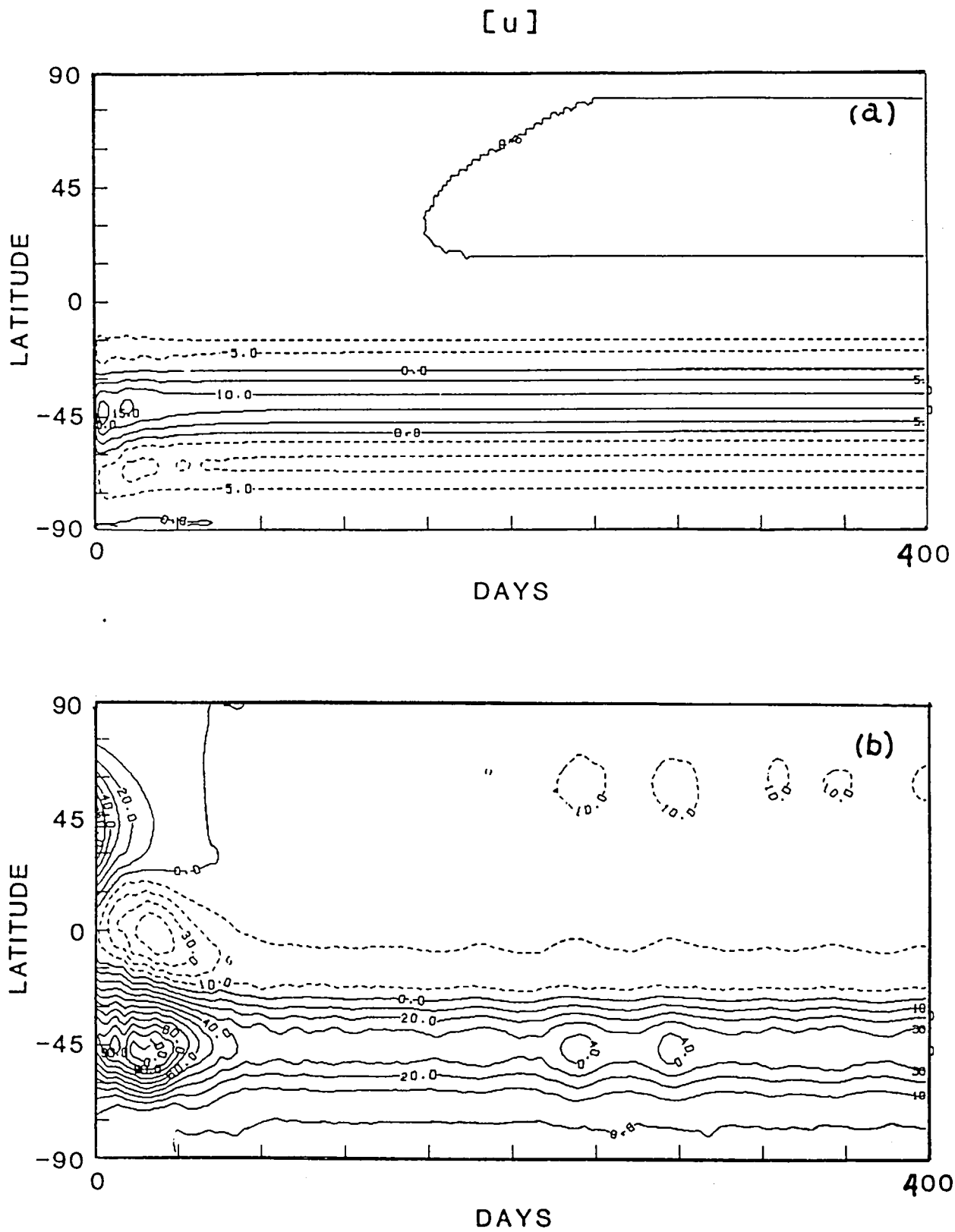
[u]
(a)
90
45
0
-45
-90
LATITUDE
0
400
DAYS
(b)
90
45
0
-45
-90
LATITUDE
0
400
DAYS

Figure 3

A New CO_2 Transmittance Parametization and its Impact on the GLA GCM

R. L. Wobus, M.-L. C. Wu, and J. Susskind

As reported last year (Wobus et al., 1984), we are improving the Wu-Kaplan radiation parameterization (Krishnamurthy, 1982) used in the GLA GCM by replacing its fixed tables of CO_2 transmittance in the 15 μm band with models developed by regression on line-by-line transmittances.

The transmittances ($\tau_{i,j}$) between layers are modeled ($\tilde{\tau}_{i,j}$) as products of effective sublayer transmittances ($\tilde{\tau}^{i}_{k,k+1}$):

$$\tilde{\tau}_{i,j} = \prod_{k=i}^{j-1} \tilde{\tau}^{i}_{k,k+1}$$

Of the models tested offline, we select for the first sublayer (k=i) the 4-term model bilinearly dependent on layer temperature and surface pressure and for the remaining sublayers (k≠i) the 2-term model linearly dependent on layer temperature.

We have integrated the GLA GCM for 20 days starting at 0Z, January 21, 1979, using the transmittance model described above. In the control run the fixed table of 15 μm CO_2 transmittances is used. The effect of the change of initial cooling rate is illustrated by (Fig.1) a map of the difference of 50 mb temperature after 6 hours. The cooling is reduced over high topography, where the fixed table underestimates the transmittance, and is reduced slightly throughout the tropics and the north polar area where the stratosphere is relatively cold. Over elevated topography the surface cooling (not shown) increases, also as expected. The final 10-day cross-section of temperature is shown in Fig. 2. The stratospheric temperature increases over a degree in the arctic and smaller amounts over Antarctica and elsewhere. Tropospheric equilibrium temperature response is obscured by time dependent differences in synoptic disturbances.

The introduction of more accurate CO_2 transmittances allows us to evaluate two effects which are neglected in the present model. The increase of transmittance between levels as the layers grow thinner over elevated terrain affects both surface and stratospheric cooling rates. The change of CO_2 transmittance in the stratosphere with temperature, due to the inactivity of the hot bands at low temperatures, leads to warming over the winter pole. If this result is confirmed when the test runs are extended we plan to implement the new parameterization in the GLA GCM.

References

Krishnamurthy, V., 1982. Documentation of the Wu-Kaplan longwave radiative routine. NASA Tech. Memo. 83926, 93 pp.

Wobus, R. L., J. Susskind, and M.-L. C. Wu, 1984: A new parameterization of 15 micron radiative transfer for a GCM. NASA Tech. Memo. 86053, pp. 292-297.

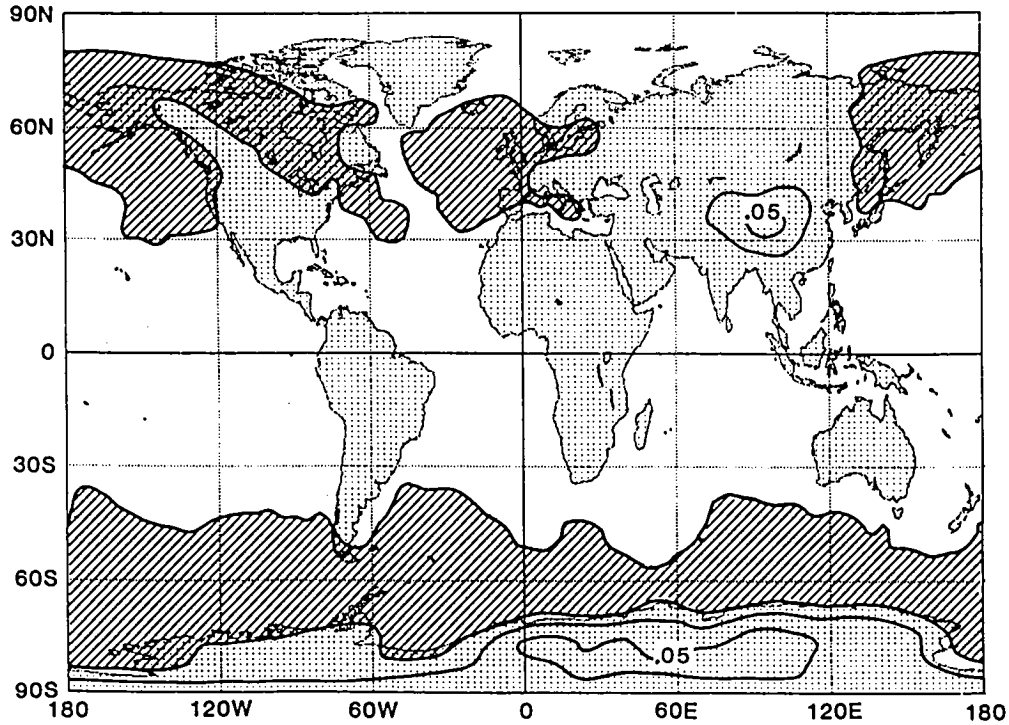

Fig. 1 50 mb temperature difference (new method-control) after 6 hours (6Z 21 January 1979), negative areas shaded, contours correspond to .1°K/day.

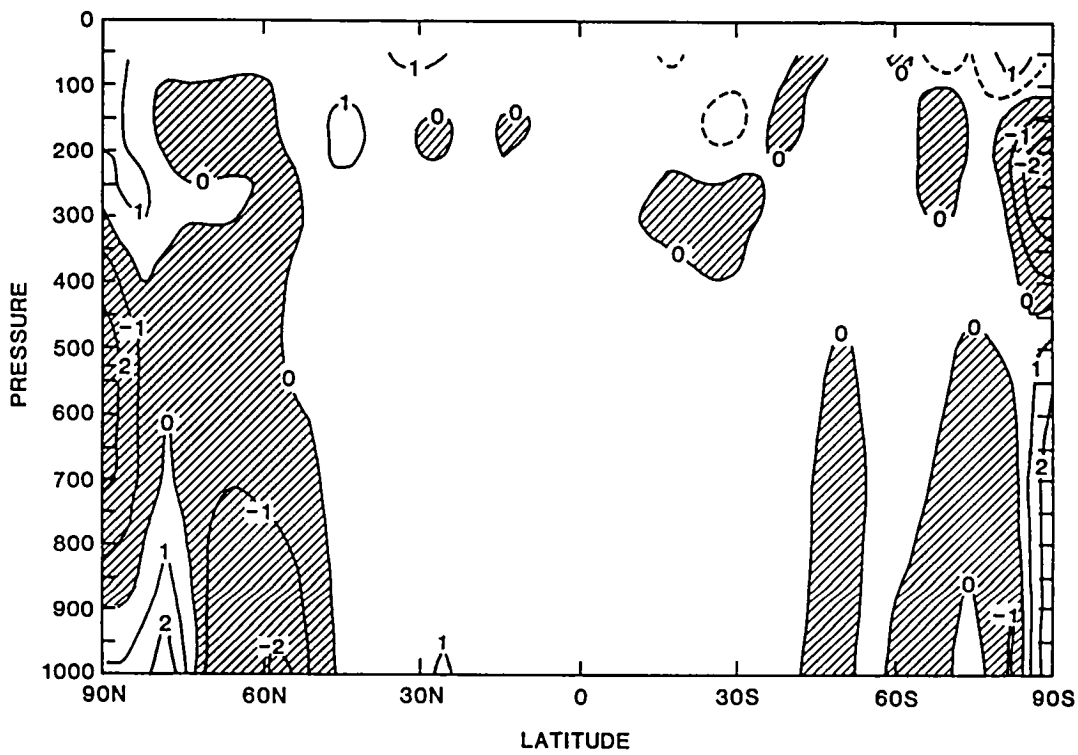

Fig. 2 50 mb temperature difference (new method-control), 10-day average after 10 days (6Z 31 January 1979 - 0Z 10 February 1979), negative areas shaded.

C. CLIMATE SENSITIVITY EXPERIMENTS

A GCM STUDY OF THE ATMOSPHERIC RESPONSE TO TROPICAL SST ANOMALIES

Max. J. Suarez

The response of the atmosphere to anomalies in equatorial sea surface emperatures (SSTs) has received a great deal of attention in recent years. oth statistical studies using observational data and general circulation odel experiments have clearly established that the ocean temperature perturbaions occurring during warm El Niño episodes cause a discernible climate ignal over much of the globe. A body of theory has also been developed that ttempts to explain the mid-latitude portion of the response in terms of global eleconnection patterns and propagating Rossby waves forced by the anomalous tmospheric heating. The most recent (1982/83) warm episode is of particular nterest because of the exceptional strength and highly unusual sequence of he SST anomalies.

The purpose of the work presented here is to understand the evolution of he atmospheric anomalies associated with the most recent warm episode by the se of simulation studies with the UCLA general circulation model (GCM). Our pproach is to integrate the model using the observed sequence of SST anomalies uring 1982/1983, and compare it with a control run in which all boundary onditions vary from month to month as in the climatology.

The control for the experiment was a three year simulation using seasonally arying climatological SSTs. The anomaly calculation was initialized from 15 une of the first year of the control. From 15 June to 1 July, the SST was radually modified by the anomalies observed during June - July of 1982. rom 1 July on, the run was continued using the control's SST plus the 1982-83 nomalies. SSTs were varied daily, interpolating between monthly means. This econd integration was carried to the end of February of the second year ('83 n the anomaly). Only anomalies over the tropical Pacific were used.

Figures 1 and 2 summarize the model's response. Seasonally averaged ST anomalies are shown together with the resulting precipitation and surface ind anomalies. During September - October - November (SON) maximum precipitaion anomalies occur over the equator between the dateline and 120°W with the reatest anomalies just east of the dateline. The precipitation anomaly is hus well west of the SST anomaly. By December-January-February (DJF) the esponse has shifted east some 30° and anomalies of ~ 6mm/day extend to the outh American coast. The total rainfall averaged over the tropical Pacific hanges little. Positive anomalies over the equator are compensated by negaive anomalies over a large horseshoe-shaped region poleward and westward of he increased rainfall. The major effect of the SST anomaly is thus a redisribution of the precipitation over the tropical Pacific. The anomaly in the urface wind, which must be doing the bulk of the anomalous transport of water apor, is also shown on the figure. Over the western half of the region of aximum forcing - (180W-150W during SON and 150W-120W during DJF), - the result s qualitatively as one would expect from the simplest linear theory. Cyclonic urface flow north and south of the equator just west of the maximum forcing, nd strong westerly anomalies over the equator. East of the maximum rainfall nomaly, however, the response is very different from what one would expect rom linear theory. The model produces a strong meridional convergence with

particularly strong northerly flow just north of the equator. The linear response about a state of rest would lead to either flow away from the equator or, far east of the forcing, no meridional component.

(SON)

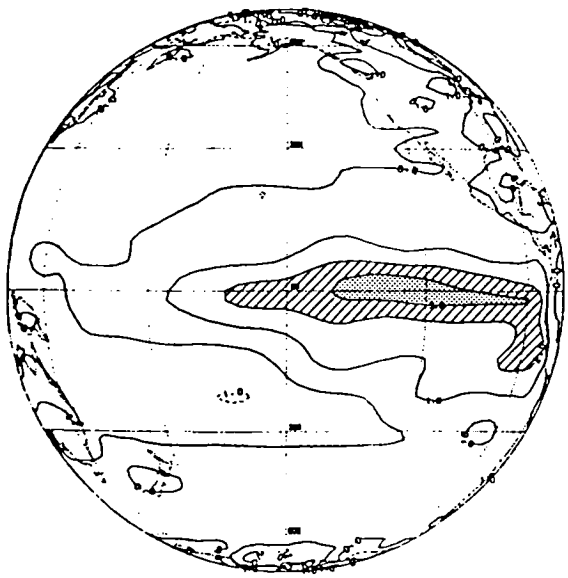

Surface Temperature Anomaly

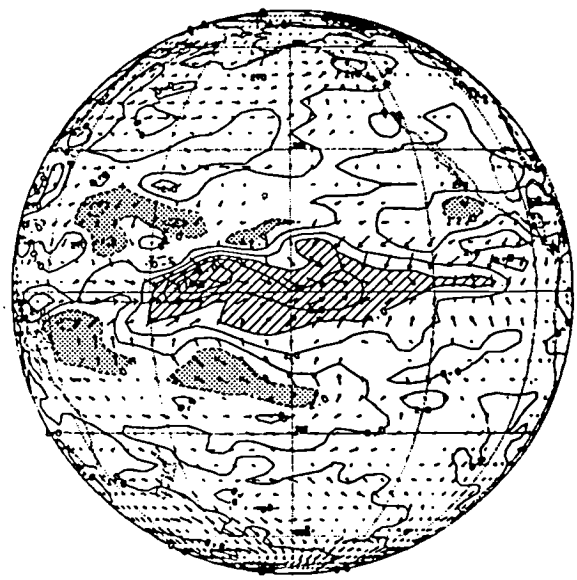

Precipitation and
Surface Wind Anomalies

Figure 1

(DJF)

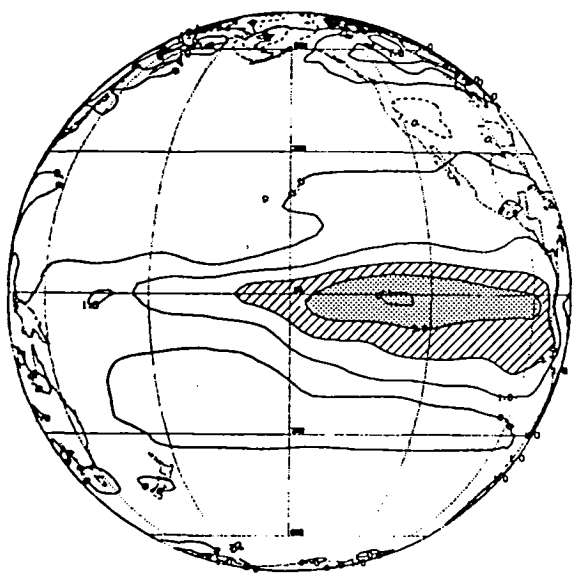

Surface Temperature Anomaly

Precipitation and
Surface Wind Anomalies

Figure 2

INFLUENCE OF LAND SURFACE PROCESSES ON THE INDIAN MONSOON

- A NUMERICAL STUDY -

Y. C. Sud and W. E. Smith*

Laboratory for Atmospheres, Goddard Space Flight Center, Greenbelt, Md 20771

Twelve July integrations are made with the GLAS GCM (Sud and Smith, 1984) to investigate the influence of local changes in the land surface fluxes, that may be produced by changes in the land surface vegetation, on the monsoon circulation and rainfall over the Indian subcontinent. The study consists of an ensemble mean of three integrations each for four separate cases: (a) Control integrations with normaly prescribed boundary conditions, called C; (b) three other integrations with the surface albedo increased (from 0.14 to 0.20) on the Indian subcontinent, called E_1; (c) another set of three integrations with the surface albedo increased as above together with a decrease of surface roughness (from 45 cm to 0.02 cm), called E_2; and (d) a last set of three integrations with higher surface albedo and low surface roughness as above, but with no evapotranspiration, called E_3. Except for these changes in the anomaly region (delimited by solid line, Fig. 1a) all other boundary conditions were prescribed, (Kalnay et al., 1983); consequently, their time evaluation is unaffected by the earth-atmosphere interactions.

Table 1 gives the regional summary of important physical and diagnostic fields as well as the intrinsic model variability. Except for 500 mb heights, all other differences are statistically significant. The most important fields are those of heat and moisture balance. Large differences were expected in these fields for E_1 and E_3; nevertheless, the surface roughness anomaly experiment E_2 has also shown significant differences in the surface radiation balance and the PBL fluxes. The rainfall differences for the three experiments are shown in Figs. 1a, b and c respectively. The surface albedo and surface roughness anomalies have produced comparable changes. For experiment E_2, the most significant reductions in rainfall are found over north-northwest India (Fig. 2). The overall influence of the increased surface albedo is to reduce the rainfall over India; the rainfall differences E_1 minus C show an average decrease of about 1.6 mm/day with a maximum decrease of about 3 mm/day. This occurs due to relative subsidence (reduced rising motion) and diabatic cooling precisely in conformity with Charney's (1975) albedo hypothesis. For experiment E_2 the reduction in rainfall was even larger (2.7 mm/day) with a maximum decrease of about 5mm/day; it was caused by eastward shift of rainfall maxima.

*M/A-Com Sigma Data under contract No. NAS5-28074

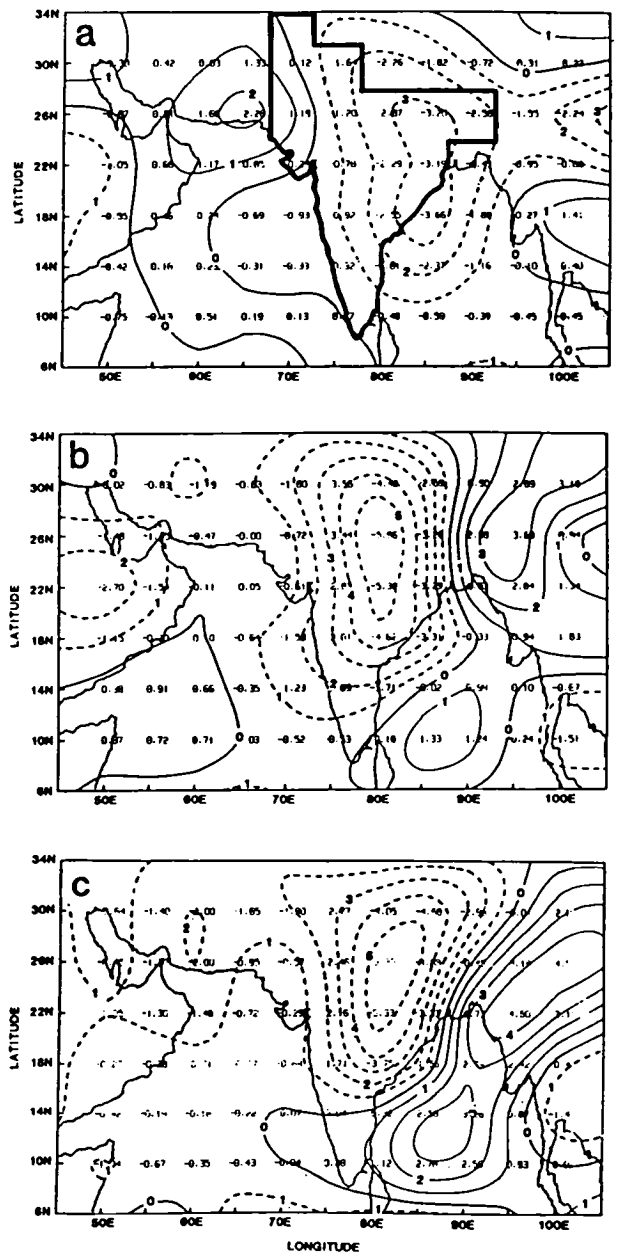

Fig. 1. Rainfall anomalies (Experiment-Control) mm/day for E_1, E_2 and E_3 designated by a, b and c, negative contours are dashed.

The current findings could be easily understood by examining the moisture convergence fields for experiments E_1 and E_2. In nature, the July rainfall anomalies over India are caused by changes in moisture convergence in the lower troposphere. Often, small changes in the moisture flux ($\overline{Vq}$) can produce a large change in the moisture convergence ($\nabla \cdot \overline{Vq}$). This is indeed true for our simulations. We found that for smoother land the PBL wind vectors turned eastward which consequently produced the rainfall anomalies.

TABLE 1. EXPT. MINUS CONTROL AND STD. DEVIATION

Fields	Expt. - Control			St. Dev.
	$E_1 - C$	$E_2 - C$	$E_3 - C$	
Surf. Short Wave (ΔSW; W m^{-2})	-17.9	-18.9	-12.3	4.10
Surf. Net Radn. (ΔNR; W m^{-2})	-19.5	-35.8	-65.9	7.92
Surf. Sen. Flux (ΔSH; W m^{-2})	-12.7	-44.5	45.5	2.72
Evapotranspiration (ΔE; mm/day)	-0.24	0.34	-3.85	0.10
Percepitation (ΔP; mm/day)	-1.62	-2.7	-2.8	0.68
Surface Stress ($\Delta\tau$; N m^{-2})	-0.04	-0.18	-0.16	0.03
Vert Vel. 500 mb ($\Delta\omega$; mb s^{-1})	2.2	3.0	0.15	1.14
Diabatic heating (ΔQ; W m^{-2})	-57.2	-111.6	12.1	19.50
Surface Temp. (ΔT_S; °C)	-0.5	-0.8	2.8	0.17
Ground Temp. (ΔT_G; °C)	-0.6	2.1	10.5	0.11
Geopotential 500 mb ($\Delta\phi$; GMP)	-4.72	-5.56	5.72	4.26

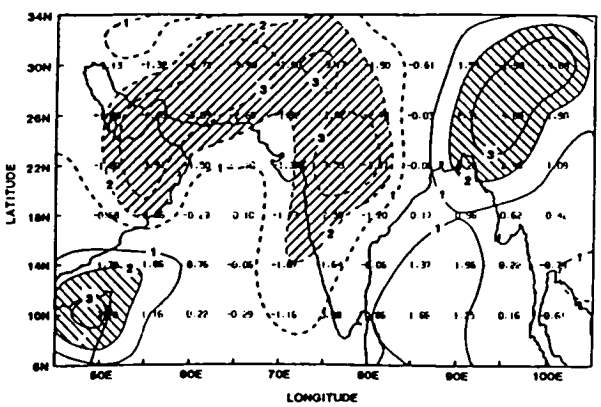

Fig. 2. Rainfall anomaly/model's Variability plots; negative contours are dashed; significant regions are hatched.

The evapotranspiration is set to zero in experiment E_3; however, there is little change in the rainfall between experiments E_2 and E_3 because the enhanced moisture convergence in the PBL, produced as a consequence of the increased sensible heating over dry land, compensated for the lack of evapotranspiration. This is an example of the typical 'heat island' effect, e.g. Malkus (1963). In July, the moisture for precipitation is advected from the nearby Indian Ocean; the increased sensible heating from non-evaporating land enhances this process. This is consistant with previous results (Shukla and Mintz, 1982; and Sud and Fennessy, 1984).

These studies demonstrate that any modification of the biosphere in the Indian subcontinent may be expected to influence the monsoon circulation by altering the surface energy balance, orientation of motion fields and moisture convergence, and the hydrological cycle. The results further suggest that excessive land use via destruction of vegetation would weaken the monsoon; conversely, increased surface roughness and more vegetation would strengthen the monsoon. One can also infer that even substantial changes in the biosphere may not install a permanent desert over India, but a 3-5 mm/day reduction in the monsoon rainfall would be enough to seriously impact the agriculture.

Despite various limitations of numerical models, we have confidence in the present results because they can be explained by a sequence of well understood physical mechanisms independent of the behavior of the GCM. We hypothesize that feedback effect of land surface processes may be partial contributors to the well documented progression of the Thar desert into neighboring arable regions. The non-critical role of evapotransporation for the monsoon rainfall is another important result.

References

Charney, J. G., 1975: Dynamics of Deserts and Drought in the Sahel. Quart. J. Roy. Meteoro. Soc., 101, 193-202.

Kalnay et al., 1983: Documentation of the GLAS Fourth-Order General Circulation Model. NASA Tech. Memo 86064, Vol.1 NTIS, Washington D.C.

Malkus, J. S., 1963: Tropical Rain Induced by a Small Natural Heat Source. J. Appl. Meteor., Vol. 2, No. 5, 547.

Shukla, J. and Y. Mintz, 1982: The influence of Land Surface Evapotranspiration on Earth's Climate. Science, 215, 1498-1501.

Sud, Y. C. and M. J. Fennessy, 1984: A Numerical Study of the Influence of Evaporation in Semi-arid regions on the July Circulation. J. of Climatology, 4, 383-398.

Sud, Y. C. and W. E. Smith, 1984: Ensemble Formulation of Surface Fluxes and Improvement in Evapotranspiration and Cloud Parameterization in a GCM. Bound. Layer Meteor., 29, 185-210.

INFLUENCE OF LAND-SURFACE ROUGHNESS ON ATMOSPHERIC CIRCULATION AND RAINFALL: A SENSITIVITY STUDY WITH A GCM

Y. C. Sud, J. Shukla* and Y. Mintz*

Laboratory for Atmospheres, Goddard Space Flight Center, Greenbelt, MD 20771

1. INTRODUCTION

The dependence of atmospheric circulation on various aspects of land surface boundary conditions has been discussed for many years. However, it is only recently that numerical model simulation studies have been made to investigate influences of surface albedo and soil moisture on the circulation. Mintz (1984) has reviewed eleven recent studies on the subject. Subsequently, a dozen more studies have appeared in the literature. All of them, without exception, have shown a strong influence of these parameters on the circulation and rainfall. In this study, we have chosen to investigate the sensitivity of atmospheric circulation to surface roughness of land. This work follows the recent study of Sud and Smith (1984b) on the influence of surface-roughness of deserts.

2. EXPERIMENTAL DESIGN

An ensemble of three pairs (Control and Experiment) of runs were made with a GCM (general circulation model). The GCM employed for this study has been described by Randall (1982). It has been used for several studies in the past.

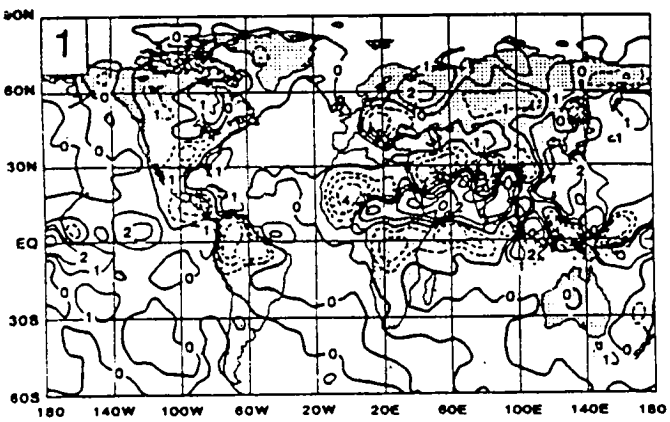

Fig. 1 Ensemble mean July rainfall differences: Experiment minus Control in mm d^{-1}. Negative contours are dashed.

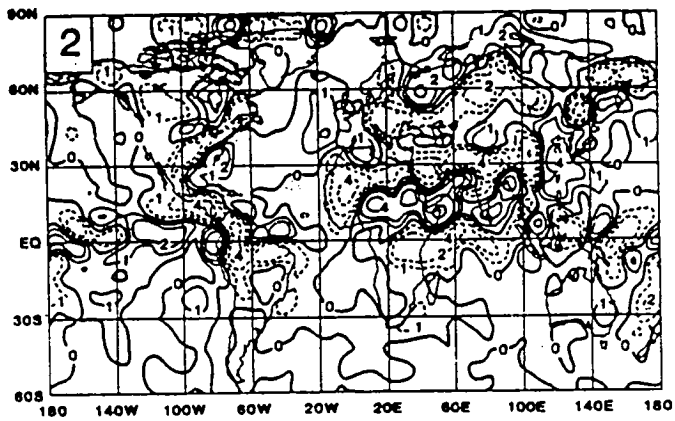

Fig. 2 Ensemble mean July moisture convergence differences: Experiment minus Control in mm d^{-1}. Negative contours are dashed.

However, the version of the GCM used in the present investigation includes an ensemble PBL formulation by Sud and Smith (1984a) which in turn was derived from the Deardorff (1972) PBL parameterization.

In the Control runs, the surface roughness values were: 45 cm for land, 0.02 cm for Ocean, and 0.01 cm for sea-ice. In the Experiment runs, the surface roughness over land was reduced to 0.02 cm which is a typical value for sandy deserts. For 1 km deep PBL this reduction in land surface roughness produces approximately a four fold reduction in the bulk aerodynamic drag coefficient. Such a range is typical of variations in the biosphere. Apart from this one change all other initial and boundary conditions were the same in each pair of runs.

The two cases consist of integrations thru the month of July starting from two initial states from the NMC analysis of observations for June 15, 1979, and June 15, 1980. The third initial state was for June 20, 1980; it was derived by averaging NMC analysis of observations from June 7 thru July 6, 1980. The differences in the July ensemble mean of the Controls and Experiments were analyzed.

*Professor Department of Meteorology University of Maryland, College Park, Maryland 20742

Although there was little difference in the sea-level pressure and 500 mb geopotential height, large differences were found in the low level winds, moisture convergence and rainfall. Large rainfall reductions are seen over the eastern U.S., Central America, and Amazons in South America, Fig. 1. The rainfall increases over the ITCZ region in the monsoonal North Africa and South India and China. Nevertheless, this increase is balanced by a corresponding reduction in rainfall to the north and south of the ITCZ. Whereas there was virtually no change in evapotranspiration, but the PBL moisture convergence ($\nabla \cdot \overline{Vq}$) differences, Fig. 2, show some very remarkable correspondence with rainfall differences. This one-to-one correspondence in the PBL moisture convergence and rainfall is not surprising because convective rain in July obtains most of the moisture from the PBL. This result suggests that it is the variation in deep cumulus convection which essentially responds to moisture convergence in the PBL.

The vector plot of moisture flux ($\overline{Vq}$) identify the physical mechanism responsible for the change. It is found that reduced surface drag over smoother land suppresses the cross-isobaric moisture convergence into the low pressure regions at high latitudes, Fig. 3. On the other hand, low surface roughness increases the intensity of winds and moisture convergence into the ITCZ. This produces sinking and moisture divergence at the neighboring latitudes. Some large difference over south China Sea and western Pacific merely reflect a slight shift in the strong monsoonal circulation.

The statistical significance of our results, represented by rainfall differences normalized with the natural variability of the model, is shown in Fig. 4. All the Americas are significantly affected. The rainfall in the monsoonal regions is also significantly affected. Over Europe and Asia too, there are several regions of significant rainfall changes.

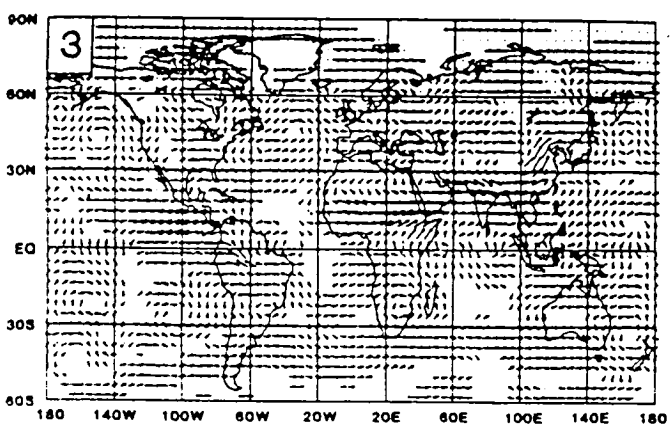

Fig. 3 Ensemble mean July moisture flux vector differences: Experiment minus Control in (mm d^{-1})m. Arrow lengths are discretised
Small arrows: 0.5 x 10^6 to 5.0 x 10^6
Medium arrows: 5.0 x 10^6 to 10.0 x 10^6
Long arrows: greater than 10.0 x 10^6

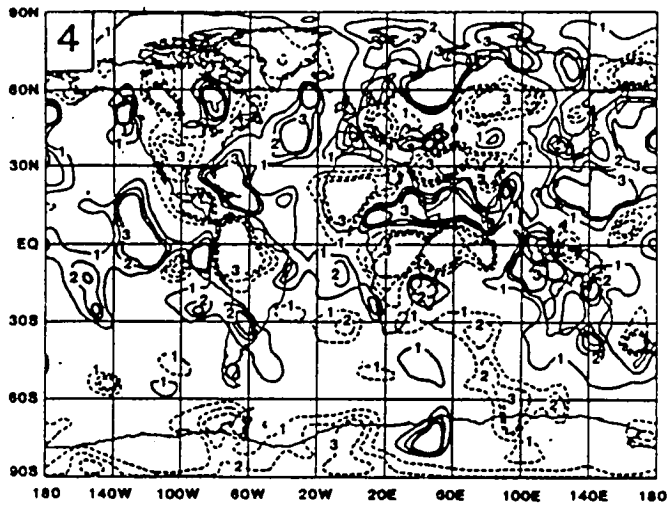

Fig. 4 Statistical significance of rainfall differences: (∇ precip/$\nabla\sigma$ model). Negative contours are dashed.

Our study suggests that land-surface roughness is an important parameter. In nature, land surface roughness, surface albedo and evapotranspiration are strongly influenced by vegetation. Therefore, it is vital that future simulations of weather and climate are made with GCMs that include a suitable parameterization of the vegetation on land. Recently, Anthes (1984) has examined the possibility of enhancement of convective precipitation by employing mesoscale variation in vegetation. Based on our studies on the large scale, we infer that vegetation induced surface roughness too can support such a design.

References

Anthes, R. A., 1984: Enhancement of convective Precipitation by Mesoscale Variations in Vegetative Covering in Semiarid Regions. J. of Climate and Appl. Meteor., 23, pp 541-554.

Deardorff, J. W., 1972: Parameterization of the planetary boundary layer for use in general circulation models. Mon Wea. Rev., 100, 93-106.

Mintz, Y. 1984: The sensitivity of Numerically Simulated Climate to Land-Surface Boundary Conditions Chapter 6, The Global Climate (editor: J. T. Houghton) Cambridge University press 79-105.

Randall, D. A., 1982: Monthly and Seasonal Simulations with the GLAS Climate Model. Proceedings of the Workshop on Intercomparison of Large-Scale Models Used for Extended Range Forecasts of the European Center for Medium Range Weather Forecasts. Reading, England, 107-166.

Sud, Y. C. and W. E. Smith, 1984a: Ensemble formulation of surface fluxes and improvement in evapotranspiration and cloud parameterization in a GCM. Bound. Layer Meteor., 29, 185-210.

Sud, Y. C. and W. E. Smith, 1984b: The influence of surface roughness of Deserts on the July circulation - a numerical study. Bound. Layer Meteor. (Approved for publication).

III. SUMMER LECTURE SERIES

The Structure and Dynamics of an Observed Moist Front

by

I. Orlanski

Geophysical Fluid Dynamics Laboratory/NOAA
Princeton University
Princeton, New Jersey 08542

The structure and dynamics of the moist cold front of 25-26 April 1979, the third observing day of the SESAME Experiment, are investigated through the use of a three-dimensional mesoscale numerical model. This work is one of the first studies in which model results are compared, in a one-to-one manner, with a detailed observational analysis, namely that of Ogura and Portis (1982) as taken from the SESAME observations. In addition, frontogenetical effects, both adiabatic and diabatic, are studied on a vertical cross-section through the front; similarities and differences with the adiabatic analysis of Ogura and Portis are discussed.

The mesoscale model, which is described by Orlanski and Polinsky (1984), is initiated at 0000 GMT 25 April from the GFDL/FGGE global analysis and is integrated for 26 hours, using the same FGGE data at the synoptic times for boundary data, to produce the solution of 0200 GMT 26 April to be compared with the Ogura-Portis analysis.

Many similarities exist between the modeled and analyzed fields, although the analysis tends to have weaker horizontal gradients due to the coarseness of the observational network. Vorticity and convergence near the surface are found to have the same magnitude in both the model solution and the analysis, in contrast to idealized frontogenesis models which predict vorticity to be much larger than convergence. The model produces a strong low-level jet ahead

of the front, in agreement with observations, when moist convection is active but with only a simple planetary boundary later used. Finally, vertical penetration of the frontal zone, indicated by the line of maximum vorticity in a vertical plane through the front, is close to the slope analyzed by Ogura and Portis. In fact, an analogous solution run without moisture produced much shallower penetration, suggesting that fluid parcels in the moist environment follow the more steeply inclined lines of constant equivalent potential temperature just as parcels in the dry case follow constant-θ lines.

A study was also made of the frontogenetical terms which act to enhance and weaken the horizontal potential temperature gradients within the front. The adiabatic terms, namely, the convergence, deformation, and tilting terms, show good agreement, with regard to sign and vertical structure, with those analyzed by Ogura and Portis. The low-level structure of each of the moist fields is close to that shown in the dry solution, with convergence and deformation being frontogenetical and tilting frontolytical near the surface. However, moist terms exhibit a much deeper penetration with the tilting field dominant in both the simulation and the analysis of observations. On the other hand, when diabatic and diffusive terms are obtained from the numerical solution, one finds that the tilting field is largely canceled by diabatic heating effects (Figure 1a). Hence, the complete frontogenetical function (Figure 1b) consists of: frontogenesis ahead of the front at low levels, due to convergence and deformation, and at middle levels due to diabatic heating; and frontolysis at middle levels to the rear of the maximum vorticity line, due to tilting and diffusive effects.

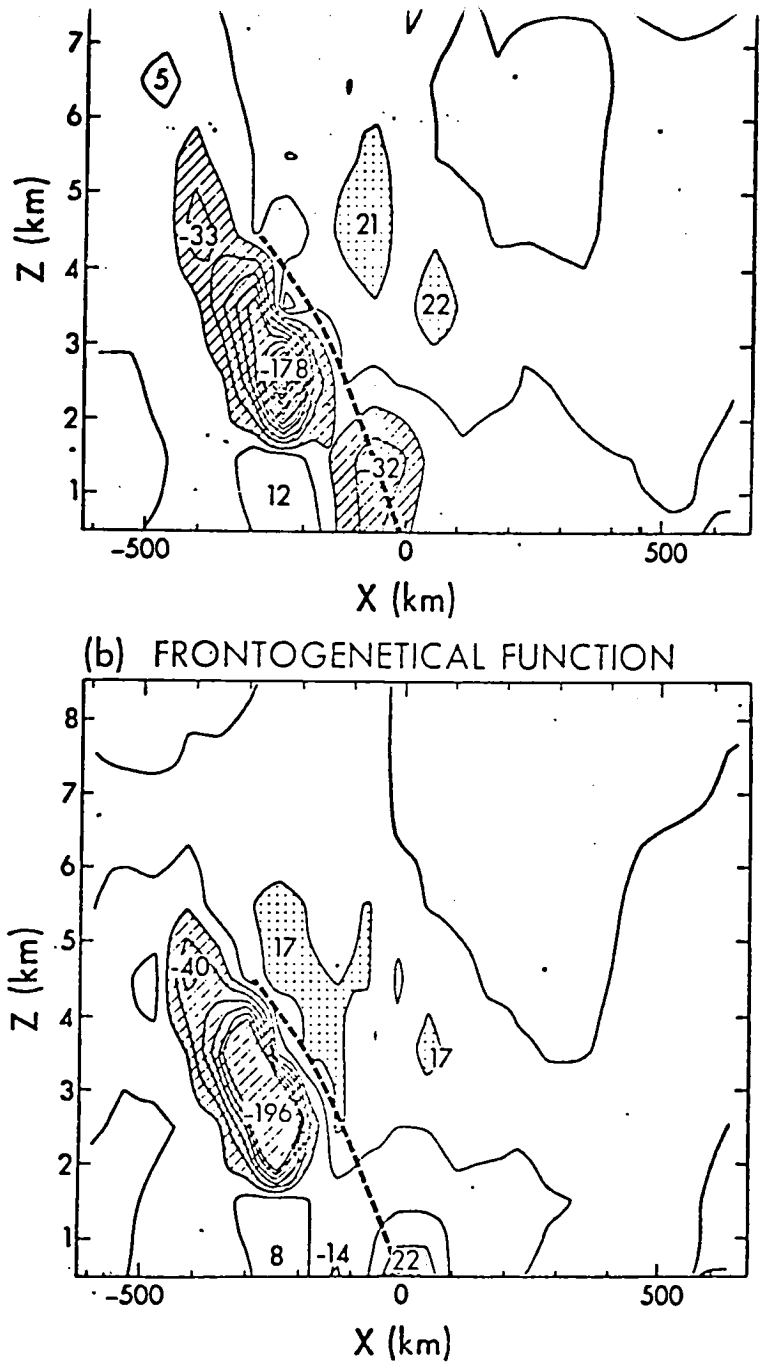

Figure 1 — Vertical cross-sections through the simulated cold front of 26 April 1979 showing (a) combined diabatic and tilting terms and (b) total frontogenetical function, both in units of 10^{-10} K $m^{-1}s^{-1}$. Frontogenetical effects (stippling) are shown at ground level and upper levels ahead of the front, whereas frontolytical effects (cross-hatching) are shown behind the front. The effects at the ground produced by adiabatic processes (convergence and deformation) and the frontolytical effects (tilting) had been speculated from idealized studies. The upper frontogenetical effects ahead of the front produced by latent heat release (diabatic processes) are shown for the first time by this study.

Some Recent Developments in Numerical Modelling at ECMWF

A.J. Simmons
European Centre for Medium Range Weather Forecasts,
Reading, Berks., U.K.

Extended Abstract

1. Introduction

A new atmospheric model was introduced into operational forecasting at ECMWF on 21 April 1983. The principal differences between this model and the Centre's first operational model were in the adiabatic formulation, which, in the new model, includes use of a spectral representation in the horizontal, a more general vertical coordinate, and a modified, more-efficient, time-stepping scheme. In addition, new programming techniques and standards were adopted to facilitate both the model's use as a research tool and its adaptation to make full use of the features of the recently-acquired CRAY X-MP computer. A number of revisions were also made in detailed aspects of the formulation of the parameterisation schemes. The operational change to this new model was accompanied by a second important change, namely the use of a higher 'envelope' orography in the lower boundary conditions of the model. An account of the design and early performance of the new model has been given by Simmons and Jarraud (1984).

Since its operational implementation, effort has continued to be directed towards the development of the new model. This effort can be divided into two categories. The first concerns development directly related to problems in the operational performance of the model. The second concerns the development preparatory to the future operational implementation of a high resolution version of the model on the CRAY X-MP.

2. Development of the Numerical Formulation of the Operational Model

(a) The representation of orography

In the version of the new model originally introduced into operational forecasting, the spectrally-fitted envelope orography was modified iteratively to reduce the height of the model orography in coastal areas, and thereby increase the use of synoptic observations from such areas in the data assimilation

Subsequent tests showed that any beneficial impact of such data was more than masked by the impact of an unrealistic model orography in near-coastal regions. It was thus decided to use an orography defined by a direct spectral fit of the envelope orography. In the construction of the latter, the standard-deviation of the sub grid-scale orography was not used to enhance the mean at model "sea" points (points for which more than 50% of the surrounding grid-square is in reality covered by sea). Improvements in local synoptic features were evident near regions of significant change in the orography, and some of the precipitation biases were reduced.

In addition to making the above operational changes, the overall performance of the envelope orography in routine prediction has been monitored. Comparing the results of objective verifications for the summers of 1982 and 1983 showed the improvement in quality in surface forecasts anticipated from previous comparisons of grid-point and spectral forecasts. However, a clear improvement at 500 mb of the type found previously to result from use of the envelope orography in winter forecasts was not evident. Although results for 1984 are substantially better and suggest that such interannual comparisons can be misleading due to variations in predictability in different synoptic situations, experimentation has indicated a small detrimental effect of the envelope orography in some summer forecasts. Some further investigation has been carried out, but it was decided to concentrate attention on co-ordinating this work with the experimental programme for the development of a higher resolution operational model.

(b) The semi-implicit gravity-wave treatment and the horizontal diffusion of divergence

Noise generated in the model vertical velocity field in conjunction with intense convection has been found to be a recurrent feature of forecasts, particularly in the short-range. In addition, noise has occasionally been found to develop in the data assimilation in association with anomalously strong mid-latitude jet streams, and a case of computational instability was encountered operationally when the problem was exacerbated by serious errors in satellite temperature data. Tests revealed sensitivity to the treatment of gravity waves by the semi-implicit time scheme. Pending a

fuller investigation of this problem, a solution has been adopted which involves a minor modification of the semi-implicit scheme, together with an enhanced (by a factor of 10) coefficient of horizontal diffusion for the divergence field. The position of this diffusion within the model code was also corrected so that it was executed after completion of the semi-implicit correction of the temperature and surface pressure. The overall impact on the accuracy of forecasts was extremely small, although some indication of excessive damping of tropical features has been found.

c) Other operational changes

Other minor changes in numerical formulation have been introduced in the light of operational experience. Horizontal diffusion is now applied not to temperature itself, but to the deviation of temperature from a reference profile in such a way as to approximate diffusion on surfaces of constant pressure. This acts to suppress excessive precipitation over mountainous areas in summer forecasts, which was formerly triggered by an erroneous warming of mountain tops associated with the diffusion of temperature along the terrain-following coordinate surfaces of the model. A small increase in the time-filter coefficient and a modification of the reference wind profile used for the semi-implicit treatment of vorticity and moisture advection have enhanced the computational stability of the model. These changes have had negligible impact on forecast quality.

3. Experimentation at High Resolution

Operational forecasting is currently carried out using triangular truncation at wavenumber 63 (T63) in the horizontal and a 16-level vertical representation. The acquisition of the CRAY X-MP computer allows use of a resolution up to about T106 using 16 levels, or about T95 if vertical resolution were to be increased to 20 levels. An experimental programme to assess the performance of the forecast model at higher horizontal and vertical resolution, and the sensitivity to orographic representation at such resolutions, has thus begun.

First results indicate little sensitivity to an increase in vertical resolution, but an overall improvement from an increase in horizontal resolution, at least in the extratropical Northern Hemisphere. Differences in conventional

objective verifications are not large in general but as no attempt was made in these first experiments to optimize initial and boundary conditions or model parameters, more substantial gains can be expected for the future. Improvement is more evident for the medium and smaller scales of motion, and can be clearly seen in the few precipitation forecasts that have been examined to date. Use of an envelope orography appears more beneficial at higher horizontal resolution, the small detrimental impact found in summer T63 forecasts disappearing at T106 resolution in the limited number of cases that have been completed. Further experimentation planned for the coming months should help quantify these conclusions and aid understanding of the sensitivity to orography.

LARGE-EDDY SIMULATION IN PLANETARY BOUNDARY-LAYER RESEARCH

J. C. Wyngaard
National Center for Atmospheric Research
Boulder, CO 80307

We do planetary boundary-layer research for the same reason we do research on any turbulent flow: to develop models (i.e., parameterizations) of its structure and dynamics. While the traditional approach is through experiments, two developments over the past decade bear on the continuance of this tradition.

The first is that progress in PBL research seems to have reached a plateau, in the view of a WMO working group (André et al., 1982). Experiments are very expensive (the 1968 Kansas program required three previous trials, 15 persons in the field, about 10 persons over the next 2-3 years in data analysis--all for measurements in the first 32 m!) and increasingly difficult to justify. Furthermore, inherent uncertainty--the inevitable difference between time-averaged and ensemble-averaged structure--becomes much more important higher in the PBL, causing severe data scatter problems. As a result, when we look at new experimental challenges, such as reliably parameterizing subgrid-scale transport through a cloud layer, we can easily become discouraged; such problems seem out of experimental reach!

The second development is the growing realization that large-eddy simulation, or LES, can provide data bases on PBL structure, and thereby supplement and extend the traditional direct measurements. LES refers to three-dimensional, fine-mesh, time-dependent turbulent flow simulation, with the spatial grid fine enough to resolve the energy-containing eddies. Deardorff (1970) demonstrated its potential first in turbulent channel flow, and then began his series of PBL simulations which produced, for example, a study of the evolution of day 33 in the Wangara experiment (Deardorff, 1974). LES is used rather widely today in fluid mechanics research problems ranging from engineering flows (Rogallo and Moin, 1984) to severe storms (Klemp and Rotunno, 1983). A recent working-group report (Wyngaard, 1984) examines LES in detail and recommends its wider use as a tool in PBL research.

In the Mesoscale Research Section of NCAR we are currently using LES to study the structure and dynamics of the convective boundary layer. In one study (Wyngaard and Brost, 1984) we simulated the vertical transport of a conservative, passive scalar. Because of the (mathematical) linearity of the governing transport equation for the scalar, we were able to represent the scalar field as the sum of "top-down" and "bottom-up" components. We isolated the statistical properties of these two processes and found them to be significantly different; "bottom-up" diffusion has a larger (by a factor of 2 - 4) eddy

diffusivity. We attributed this difference to the asymmetry in the vertical profile of buoyant production of turbulence, and to the difference in boundary conditions at bottom and top.

In a second study (Moeng and Wyngaard, 1984) we studied in more detail the statistics of top-down and bottom-up scalar fields. We found substantial differences between them, due again, presumably, to the asymmetry in the convective PBL. We developed a generalization of mixed-layer scaling which allows one to include the effects of top-down diffusion (i.e., the effects of entrainment).

Chin-Hoh Moeng is now extending this work to the study of cloud-topped boundary layers. We believe that LES has high potential for application to a very wide range of PBL problems, including turbulent dispersion, the stable PBL, and studies of mean wind profiles in baroclinic cases. Some of tomorrow's field programs might take place on the supercomputer!

References

André, J. C., K. Bernhardt, J. R. Garratt, G. A. McBean, H. Tennekes, and J. C. Wyngaard, 1982: Priorities in boundary-layer research--Thoughts from a working group of the World Meteorological Organization. Bound.-Layer Meteorol., 23, 125-128.

Deardorff, J. W., 1970: Numerical simulation of turbulent channel flow at large Reynolds number. J. Fluid Mech., 41, 452-480.

Deardorff, J. W., 1974: Three-dimensional numerical study of the height and mean structure of a heated planetary boundary layer. Bound. Layer Meteorol., 7, 81-106.

Klemp J. B., and R. Rotunno, 1983: A study of the tornadic region within a supercell thunderstorm. J. Atmos. Sci., 40, 359-377.

Moeng, C.-H., and J. C. Wyngaard, 1984: Statistics of conservative scalars in the convective boundary layer. To appear, J. Atmos. Sci.

Rogallo, R. S., and P. Moin, 1984: Numerical simulation of turbulent flows. Ann. Rev. Fluid Mech., 16, 99-137.

Wyngaard, J. C., and R. A. Brost, 1984: Top-down and bottom-up diffusion of a scalar in the convective boundary layer. J. Atmos. Sci., 41, 102-112.

Wyngaard, J. C., Editor, 1984: Large-Eddy Simulation: Guidelines for its Application to Planetary Boundary Layer Research. Available from U. S. Army Research Office, Research Triangle Park, N.C.

IV. RECENT PUBLICATIONS

Recent Publications:

Atlas, R., 1985: Large-scale numerical prediction of the President's Day cyclone. Accepted by Bull. Amer. Meteor. Soc.

Atlas, R., E. Kalnay, and M. Halem, 1984: Review of experiments on the impact of satellite data on numerical weather prediction. SPIE 481, 108-115.

Atlas, R., E. Kalnay, and M. Halem, 1985: The impact of satellite temperature sounding and wind data on numerical weather prediction. Optical Engineering. (In press).

Augenbaum, J., 1984: A Lagrangian Method for the shallow water equations based on a Voronoi Mesh - One Dimensional Results. Journal of Computational Physics, 53, 240-265.

Augenbaum, J. and C. Peskin, 1985: On the construction of the Voronoi Mesh on a sphere, Journal of Computational Physics, in press.

Augenbaum, J., S. Cohn, D. Dee, E. Isaacson and D. Marchesin, 1985: A factored implicit scheme for numerical weather prediction, Communications in Pure and Applied Mathematics, in press.

Baker, W. E., R. Atlas, M. Halem, and J. Susskind, 1984: A case study of forecast sensitivity to data and data analysis techniques. Mon. Wea. Rev., 112, 1544-1561.

Baker, W. E., R. Atlas, E. Kalnay, M. Halem, P. M. Woiceshyn, S. Peteherych, and D. Edelmann, 1984: Large-scale analysis and forecast experiments with wind data from the Seasat-A scatterometer. J. Geophys. Res., 89D, 4927-2936.

Baker, W. E., and Y. Brin, 1985: A comparison of observed and forecast energetics over North America. Quart. J. R. Meteor. Soc., 111, in press.

Baker, W. E. et. al., 1985: Experiments with a three-dimensional, statistical objective analysis scheme using FGGE data. Submitted to Mon. Wea. Rev.

Boers, R., E. W. Eloranta, R. L. Coulter, 1984: Lidar observations of mixed-layer dynamics: Tests of parameterized entrainment models of mixed-layer growth rate. J. Clim. Appl. Meteor., 23, 247-266.

Chen, T.-C. and W. E. Baker, 1985: Global diabatic heating during FGGE SOP-1 and SOP-2. Submitted to Mon. Wea. Rev.

Chou, S.-H.,D. Atlas, and E.-N. Yeh, 1985: Turbulence in a convective marine atmospheric boundary layer. Submitted to J. Atmos. Sci.

Daunt, S. J. A., T. Atakan, W. E. Blass, G. W. Halsey, D. E. Jennings, D. C. Reuter, J. Susskind, and J. W. Brault, 1984: The 12 m Band of Ethane: High Resolution Laboratory Analysis with candidate lines for infrared heterodyne searchers. Astrophys. J., 280, 921-936.

Duffy, D., R. Atlas, T. Rosmond, E. Barker and R. Rosenberg, 1984: The impact of SEASAT scatterometer winds on the Navy's operational model. J. Geophys. Res., 89, 7238-7244.

Duffy, D., 1985: The temperature distribution with a sphere placed in a directed uniform heat flux and allowed to radiatively cool. Journal of Heat Transfer, 107, 28-32.

Duffy, D. and R. Atlas, 1985: The impact of SEASAT-A scatterometer data on the numerical prediction of the QEII storm. Accepted in J. Geophys. Res.

Geller, M. A., K. Takano, W. I. Massman, J. Rosenfield, W. Chau, and E. Kalnay, 1985: General circulation model forecasting of the 1979 stratospheric warmings, submitted to Monthly Weather Review.

B. N. Goswami, J. Shukla, E. K. Schneider, and Y. C. Sud,1984: Study of the dynamics of the intertropical convergence zone with a symmetric version of the GLAS Climate model. Journ. Atmos. Sci., 41, 5-19.

Halem, M. and J. Susskind, 1985: Findings of a Joint NOAA/NASA Sounder Comparison: 1) AMTS vs HIRS2 2) Physical vs Statistical Retrieval. Advances in Remote Sensing Retrieval Methods, Williamsburg, VA, Oct 30 - Nov. 2, 1984. In press.

Harshvardhan, and D. A. Randall, 1985: "Comments on 'The parameterization of radiation for numerical weather prediction and climate models'". Monthly Weather Review, 113, (to appear).

Hoffman, R. N. and E. Kalnay, 1984: Lagged Average Forecasting, Some Operational Considerations. Predictability of Fluid Motions, G. Holloway and B. J. West, eds. American Institute of Physics, 106, 141-147.

Kalnay, E. and K. C. Mo, 1985: Mechanistic experiments to determine the origin of short scale Southern Hemisphere stationary Rossby waves. Accepted in forthcoming volume of Advances in Geophysics, R. Benzi and A. Wiin-Nielsen, editors.

Kalnay, E. and R. Atlas, 1985: Global Analysis of Ocean Surface Wind and Wind Stress Using the GLA GCM and Seasat Scatterometer Winds. Accepted in J. Geoph. Res.

Kalnay, E., J. Paegle, and K. C. Mo, 1985: Mechanistic experiments to determine the origin of SH stationary waves. Submitted to J. Atmos. Sci.

Kalnay, E., J. Paegle, and K. C. Mo, 1985: Large amplitude short-scale stationary waves in the Southern Hemisphere: Observations and their possible origin. Submitted to J. Atmos. Sci.

Kung, E. C. and W. E. Baker, 1985: Comparative energetics of the observed and simulated global circulation during the special observing periods of FGGE. Submitted to Quarterly J. Roy. Meteor. Soc.

Lau, 1985: Subseasonal oscillations, bimodal climate state and El Nino/Southern Oscillation. Coupled Ocean-Atmos. Models.

Lau, 1985: Elements of a stochastic-dynamical model of the El Nino/Southern Oscillation. J. Atmos. Sci.

Lau and Chan, 1985: Aspects of the 40-50 day oscillation during northern winter as inferred from outgoing longwave radiation. Mon. Wea. Rev.

Lau, K.-M. and N.-C. Lau, 1984: The structure and energetics of midlatitude disturbances accompanying cold-air outbreaks over East Asia. Mon. Wea. Rev., 112,1309-1327.

Lindzen, Richard S., David M. Straus, and Bert Katz, 1984: An Observational Study of Large Scale Atmospheric Rossby Waves During FGGE, Journal of the Atmospheric Sciences, 41, 1320-1335.

Livezey, R. E., 1985: Statistical Analysis of general circulation model climate simulation, sensitivity, and prediction experiments. To appear in May issue of Journ. Atmos. Sci., 42.

Melfi, S. H., J. D. Spinhirne, S.-H. Chou, and S. Palm, 1985: Lidar observations of vertically organized convection in the planetary boundary layer over the ocean. Accepted in J. Clim. Appl. Meteor.

Merkine, L. O., K. C. Mo and E. Kalnay, 1985: On Foffonoff's mode. Geophysical and Astrophysical Fluid Dynamics. In press.

Mo, K. C., 1985: Interhemispheric correlation statistics during the Northern Hemisphere Winter. J. Atmos. Sci., submitted for publication.

Mo, K. C. and Harry Van Loon, 1984: Some aspects of the interannual variation of mean monthly sea level pressure on the Southern Hemisphere. J. Geoph. Res., 89, 9541-9546.

Mo, K. C. and G. White, 1985: Teleconnection patterns in the Southern Hemisphere. Mon. Wea. Rev., 113, 22-37.

Mo, K. C. and H. Van Loon, 1985: Trends in the Southern Hemisphere. J. of Climate and Appli. Met, in press.

Mo, K. C., 1985: Quasi stationary states in the Southern Hemisphere. Mon. Wea. Rev., accepted for publication.

Moeng, C.-H., and D. A. Randall, 1984: "Problems in simulating the stratocumulus-topped boundary layer with a third-order closure model." Journal of the Atmospheric Sciences, 41, 1588-1600.

Munteanu, M. J., Westwater, R. E., and Grody, N. C., 1985: Improvement of MSU temperature retrievals by use of tropopause heights derived from TOMS ozone measurements (Submitted to J.C.A.M.).

Paegle, J., W. E. Baker, and J. N. Paegle, 1985: The forecast sensitivity to tropical winds in the global weather experiment. Submitted to Mon. Wea. Rev.

Peslen, C. A., S. E. Koch, and L. W. Uccellini, 1985: The effect of the arbitrary level assignment of satellite cloud motion wind vectors on wind analyses in the pre-thunderstorm environment. Accepted for publication in J. of Climate and Appl. Meteor.

Rambaldi, S. and K. C. Mo, 1984: Forced stationary solutions in a barotropic channel: Multiple equilibria and theory of non-linear resonance. J. Atmos. Sci., 41, 3135-3146.

Randall, D. A., J. A. Abeles, and T. G. Corsetti, 1985: "Seasonal simulations of the planetary boundary layer and boundary-layer stratocumulus clouds with a general circulation model." Journal of the Atmospheric Sciences, 42, (to appear).

Randall, D. A., and M. J. Suarez, 1984: "A note on the dynamics of stratocumulus formation and dissipation." Journal of the Atmospheric Sciences, 41, 3052-3057.

Randall, D. A., 1984: "Stratocumulus cloud deepening through entrainment." Tellus, 36A, 446-457.

Randall, D. A., J. Coakley, C. Fairall, R. Kropfli, and D. Lenschow, 1984: "Outlook for research on marine subtropical stratocumulus clouds." Bulletin of the American Meteorological Society, 65, 1290-1301.

Randall, D. A., 1984: "Buoyant production and consumption of turbulence kinetic energy in cloud-topped mixed layers." Journal of the Atmospheric Sciences, 41, 402-413.

Salstein, D. A., R. D. Rosen, W. E. Baker, and E. Kalnay, 1984: Impact of satellite-based data on general circulation statistics derived from GLAS FGGE analyses. Manuscript in preparation.

Schubert, S. D., 1985: A statistical-dynamical study of empirically determined modes of atmospheric variability. J. Atmos. Sci., 42, Jan. 1.

Sellers, P. J., Y. Mintz and Y. Sud, 1985: A simple biosphere for use in the General Circulation Model. (Approved for publication J. Climate and Appl. Meteor.)

Semazzi, F. H. M., 1985: An investigation of the equatorial orographic dynamic mechanism. Journ. Atmos. Sci., 42, 78-83.

Semazzi, F. H. M., 1985: A real data comparison between the bounded derivative and normal mode initialization methods. (Submitted to Mon. Wea. Rev.)

Sud, Y. and W. E. Smith, 1984: Ensemble formulation of surface fluxes and improvement in evapotranspiration and cloud parameterization in a GCM. Bound. Layer Meteor., 29, 185-210.

Sud, Y. and W. E. Smith, 1985: Influence of local land surface processes on the Indian Monsoon - A numerical study. (Approved for publication J. Climate and Appl. Meteor.)

Sud, Y. and M. J. Fennessy, 1984: A numerical study of the influence of evaporation in semi-arid regions on the July circulation. Journal of Climatology, 4,

Sud, Y. and W. E. Smith, 1985: The influence of surface roughness of deserts on the July circulation - A numerical study. Bound. Layer Meteor., 33, 135. Climate Model. J. Atmos. Sci., 41, 5-19.

Susskind, J., J. Rosenfield, D. Reuter, and M. T. Chahine, 1984: Remote Sensing of Weather and Climate parameters from HIRS2/MSU on TIROS-N. J. Geophys. Res., 89D, 4677-4697.

Susskind, J., J. Rosenfield, D. Reuter, and M. T. Chahine, 1984: Remote Sensing of Weather and Climate parameters from HIRS2/MSU on TIROS-N. J. Geophys. Res., 89D, 4677-4697.

Susskind, J. and D. Reuter, 1985: Retrieval of Sea-Surface Temperatures from HIRS2/MSU. Submitted to J. Geophys. Res.

Takacs, L. L., 1985: A two-step scheme for the advection equation with minimized dissipation and dispersion errors. Mon. Wea. Rev., 113.

Trenberth, K. E. and K. C. Mo, 1985: Blocking in the Southern Hemisphere. Mon. Wea. Rev., 113, 3-21.

Vergin, J., D. Johnson, and R. Atlas, 1984: A quasi-lagrangian diagnostic study of the effect of satellite sounding data assimilation on model cyclone prediction. Mon. Wea. Rev., 112, 725-739.

Wolfson, N. and R. Atlas, 1985: A diagnostic tool for investigation of heat waves. Submitted to Atmosphere-Oceans.

V. GMSB STAFF

Civil Service Staff

Atlas, R.
Baker, Wayman
Duffy, Dean
Helfand, Mark
Kalnay, Eugenia
Livezey, R.
Peslen, Cindy
Randall, Dave
Reuter, Dennis
Richardson, Benita
Straus, Dave
Suarez, Max
Sud, Yogesh
Susskind, Joel

FRAs, RRAs and University Consultants

Augenbaum, Jeff
Bloom, Steve
Ghil, Michael
Harrison, Ed
Massman, Bill
Mintz, Yale
Munteanu, M-J
Schubert, Siegfried
Semazzi, Fredrick

M/A-COM Sigma Data

Almeida, Manina
Ardizzone, Joe
Balgovind, Ramesh
Battle, Bill
Brin, Yevgenia
Carus, Herb
Corsetti, Tom
Dalcher, Amnon
Dazlich, Don
Dlouhy, John
Dlouhy, Ron
Edelmann, D. (Jim)
Friedeman, Heather
Grimball, Gilberta
Hamelink, Jane
Iredell, Dan
Iredell, Lena
Jackson, Sarah
Jusem, Carlos
Lamich, Dave
Lee, Sung-Yung
Mo, Kingtse
Molod, Andrea
Nestler, Mark
Pfaendtner, Jim
Phillips, Bill
Piraino, Paul
Place, Mike
Postman, Sandy
Pursch, Andy
Quick, Marlene
Rosenberg, Bob
Rosenberg, Jean
Rosenfield, Joan
Rumburg, Laura
Smith, Bill
Takacs, Lawrence
Terry, Joseph
Volk, Mike
Wallace, Dave
Wells, Mary Ann
Wobus, Richard
Woollen, Jack

VI. AUTHOR INDEX

AUTHOR INDEX: Authors only, alphabetical

AUTHOR AND TITLE INDEX: Alphabetical by primary author; then by title

VII. TITLE INDEX

Titles for the 1984 Annual Review

1. Report No.	2. Government Accession No.	3. Recipient's Catalog No.
NASA TM-86219		

4. Title and Subtitle	5. Report Date
Research Review - 1984	February 1986
	6. Performing Organization Code: Code 611
7. Author(s): Staff, Global Modeling and Simulation Branch, Laboratory for Atmospheres	8. Performing Organization Report No.: 85B0425
9. Performing Organization Name and Address: Goddard Space Flight Center, Greenbelt, Maryland 20771	10. Work Unit No.
	11. Contract or Grant No.
12. Sponsoring Agency Name and Address: National Aeronautics & Space Administration, Washington, DC 20546	13. Type of Report and Period Covered: Technical Memorandum
	14. Sponsoring Agency Code

15. Supplementary Notes

16. Abstract

The Research Review is a compilation of papers on the atmospheric, climatological, and oceanographic research performed during 1984 by the Global Modeling and Simulation Branch of the Goddard Laboratory for Atmospheres. The Review is divided into two areas of research: global weather/observing systems and climate/ocean-air interactions.

17. Key Words (Selected by Author(s))	18. Distribution Statement
atmospheric research oceanographic research climatological reasearch global weather ocean/air interactions	Unclassified - Unlimited Subject Category 47

19. Security Classif. (of this report)	20. Security Classif. (of this page)	21. No. of Pages	22. Price
Unclassified	Unclassified	168	A08

For sale by the National Technical Information Service, Springfield, Virginia 22161

NASA-Langley, 1986

National Aeronautics and
Space Administration
Code NIT-4

Washington, D.C.
20546-0001

Official Business
Penalty for Private Use, $300

SPECIAL FOURTH-CLASS RATE
POSTAGE & FEES PAID
NASA
Permit No. G-27

NASA

POSTMASTER: If Undeliverable (Section 158
Postal Manual) Do Not Return